MCAT Institute
Progress Report

CONTROL OF UNSTEADY SEPARATED FLOW ASSOCIATED WITH THE DYNAMIC PITCHING OF AIRFOILS

Dr. Sajeer Ahmed

December 1991

NCC2-637

MCAT Institute
3933 Blue Gum Drive
San Jose, CA 95127

CONTROL OF UNSTEADY SEPARATED FLOW ASSOCIATED WITH THE DYNAMIC PITCHING OF AIRFOILS

Dr. Sajeer Ahmed

Introduction

Research on unsteady airfoils has attracted the attention of many researchers from the point of utilization of aerodynamic lift generated for the maneuverability of the aircraft. Studies on oscillating airfoils have been performed to improve the performance of the retreating blade of a helicopter rotor, to understand the physics of dynamic stall and to delay the occurrence of dynamic stall. These studies have indicated the dependability of dynamic stall on parameters such as airfoil geometry, mean angle of attack, amplitude of oscillation and Mach number. Though these studies have established the qualitative and quantitative dependence of the dynamic stall, the physics of the flow responsible for the behavior is not yet clearly understood for its control.

In the early 1980's, studies on airfoils pitching in ramp motion were initiated to utilize the dynamic lift for supermaneuverability of fighter aircraft. Though these studies have been done to understand the dependence of parameters for the occurrence of deep stall, studies to control the flow for sustaining lift for a longer time has been little. To sustain the lift for a longer time, an understanding of the development of the flow over the airfoil is essential. Most of the work reported in literature was confined to low speeds, and studies at high speed are required to investigate how the flow behavior is dictated by the effects of compressibility. When the airfoil is pitched up in ramp motion or during the upstroke of an oscillatory cycle, the flow development on the upper surface of the airfoil and the formation of the vortex dictates the increase in lift behavior. Vortex shedding past the training edge decreases the lift. It is not clear what is the mechanism associated with the unsteady separation and vortex formation in the present unsteady environment. To develop any flow control device, to suppress the vortex formation or delay separation, it is important that this mechanism be properly understood. When the work was proposed, the idea was to achieve this goal. This report presents the research activities directed towards this effort and summarizes the results

obtained and highlights a new flow control device proposed for delaying the flow separation.

Objectives of the Research Efforts

1. To understand the compressibility effects on the flow development of a pitching airfoil through flow visualization.

2. Quantify the velocity field of an oscillating airfoil, for understanding the velocity field and for CFD code validation.

3. Quantify the density field through real time interferometry.

The above research efforts were carried out at the Compressible Dynamic Stall Facility located in the Fluid Mechanics Laboratory of NASA Ames Research Center. The experimental studies were conducted on a NACA 0012 airfoil of chord 3 in. in the Mach no. range of 0.2 to 0.45. Reynolds number variation in the test Mach number range was $2 \times 10^5 - 10^6$. The types of motion studied were 1) ramp motion where the airfoil is pitched up from 0 to 60^o and 2) oscillatory motion, where the airfoil is oscillated about 25% chord point in sinsusoidal motion, $a = 10^o\ 0\ 10^o \sin 2\pi ft$. The frequency of oscillation (f) was kept at 21.5 Hz and the corresponding reduced frequency (k) was 0.05. Flow visualization studies through Schlieren technique is limited for a ramp motion of the airfoil and velocity and density measurements were taken up on an oscillating airfoil. Results of these studies are summarized below. Details of these studies are published at various AIAA conferences and can be found in the papers appended at the end of this report.

Effect of Compressibility on Airfoils Undergoing Ramp Motion

Ramp rate and Mach number are chosen as two parameters to quantify their effects on the flow development of an airfoil undergoing a ramp motion from 0 to 60^o. Schlieren pictures of the flow field are taken in the Mach number range of 0.2 to 0.45 and reduced frequency range of 0.01 to 0.05. Schlieren pictures show the presence of multiple shocks at M=0.45 (Fig. 1). The vortex position is determined and its movement was studied with respect to the airfoil angular position. Vortex initiation and passage of vortex past the training edge appears to be dependent on the Mach

number and ramp rate; even at higher Mach numbers. With increase in ramp rate at a constant Mach number, the dynamic stall occurs at higher angle of attack. At a constant ramp rate, with increase in Mach number, the dynamic stall is accelerated to lower airfoil angles. Multiple vortices are observed at lower pitch rates and lower Mach numbers (Fig. 2). At a given chord location, a significant change in the position of vortex is observed for $M \geq 0.3$, indicating the effects of compressibility on the flow development (Fig. 3). This behavior warrants further studies; and quantification of the surface flow field near the leading edge is essential to understand the development of flow with various parameters. Such a study is planned through real time interferometry and experiments are about to begin. Results of this study are included in AIAA Paper no. 90-3038 and enclosed in Appendix A.

Velocity Measurements of Dynamic Stall Flow Field with LDV

Quantification of unsteady flow field is essential for developing and validating the CFD codes and to obtain a better understanding of the physics of dynamic stall. Towards this aim, velocity measurements of the unsteady flow field of an oscillating airfoil were taken up with the LDV. The components of velocity were measured with a two color, two component frequency shifted TSI LDV system. Measurements were restricted to the region above the airfoil surface and were carried out in a rectangular grid of size 33 x 13. The grid extends to a length of 3.0 in. in the streamwise direction starting from -0.75 in. from the leading edge and 0.75 in. in the vertical direction from the chord plane at zero degree angle of attack. Seeding of the flow was done by injecting PSL particles at the inlet of the tunnel. Velocity data for the upstroke portion of airfoil shows the formation of a separation bubble over the airfoil surface prior to the formation of vortex (Fig. 4) and flow experiences large velocity as high as 1.6 times the free stream velocity. As the airfoil angle of attack starts to exceed the static stall angle a wake-like profile develops near the wall as a result of bubble breakdown. For downstroke portion of the cycle, the velocity attained is comparatively lower, but still greater than the free stream velocity. A comparison of the velocity field at an angle of 10^{o} with the upstroke shows the extent of disturbed field is confined to a smaller region on the upper surface in the downstroke (Fig. 5). Details of the results are described in AIAA Paper no. 91-

1799 and AIAA Paper no. 91-3225 and enclosed in Appendix B, and Appendix C respectively.

Study of Dynamic Stall Using Real Time Interferometry

Measurements with Point Diffraction Interferometry (PDI) were undertaken to study the flow development through density fringe patterns and later to evaluate the Mach number field from the fringes and estimate the surface pressure distribution to investigate the changes in the flow development near the leading edge. In the first phase, studies were restricted to the global flow field and the flow pictures show evolution of a coherent vortical structure and not a tightly wound vortex as was thought earlier from the Schlieren studies. Using isentropic relations, the velocity field and pressure variations on the surface of airfoil were computed. A detailed pressure distribution near the leading edge of airfoil was obtained and as many as 13 pressure values were computed in the first 1% of chord (Fig. 6). PDI permits determination of detailed pressure distributions which is not possible with transducers on the airfoil of this scale. A comparison of the peak pressure with that of the steady case at an angle of attack of 10.8^{o} shows that the flow gradients in the unsteady case develop at a slower rate than in the steady case, thus contributing to the delay in the stall development. Results of this study are presented in AIAA Paper no. 91-0007 and included in Appendix D.

Detailed pressure distributions in the downward motion of an oscillatory airfoil show the reattachment of unsteady separated flow occurring through a bubble (Fig. 7). Using the surface pressure variations, at various angles, a schematic of the reattachment process is proposed (Fig. 8). Also, a comparison of LDV data which is a long time averaged point measurement shows a good agreement with the Mach number data evaluated from the interferogram at an angle of incidence of 10^{o} (Fig. 9). This enhanced the confidence in the measurements made with the LDV which is based on the assumption of statistical stationarity of the flow. Further, the agreement showed that the reattached flow field is two dimensional, a new finding. These results have been documented in AIAA Paper no. 91-3225.

Control of Dynamic Stall

Using the PDI technique, it is possible to quantitatively estimate the pressure distribution and identify the region of vorticity production and region where the pressure gradient promotes separation in the form of vortex. By possibly modifying this region of leading edge that is promoting separation, it is possible to control the vorticity distribution and modify the pressure distribution at the leading edge thus delaying the flow separation. Recently, NASA has developed a material which can be deformed rapidly with time and this material has been demonstrated successfully as a deicing device on a helicopter blade. It is proposed to use this as a material to vary the leading edge shape in a controlled way to produce a change in the pressure distribution to alleviate separation of flow. Initially, the shape of leading edge to an extent of 25% chord will be varied and there will be a provision to control the deformation of both the upper and lower surfaces independently. As the deformation required on an existing 3 in. chord is small, a 6 in. chord airfoil is chosen.

A fabrication scheme has been worked out in consultation with the Civil Technology Office and Model Development Branch for incorporating an adaptive geometry on a 6 in. chord airfoil. Design calculations have been performed to check the adaptability of a 6 in. chord airfoil in the present oscillatory test rig.

Concluding Remarks

Results of this investigation have shed some new light on the development of flow field on unsteady airfoils.

1 For the case of ramp motion, presence of multiple shocks at M = 0.45 and, multiple vortices at lower Mach numbers and lower pitch rates are seen.

2. Flow gradients in the unsteady case develops at a slower rate than in the steady case, thus contributing to the delay in the development of dynamic stall.

3. A separation bubble is seen prior to the formation of dynamic stall vortex and also during the reattachment of unsteady separated flow.

4. The partially reattached unsteady flow field is two dimensional.

5 Using PDI technique which permits detailed pressure distribution and identification of the gradients promoting separation, and using new material whose deformation can be varied with time, a new flow control device is designed. This device permits a variation in the leading edge geometry in a controlled way to delay unsteady separation.

Acknowledgements

The work was supported by the NASA Contract no. NCC2-637 through the funds from Navy-NASA Joint Institute of Aeronautics, AFOSR, ARO and NAVAIR. The discussions and the support provided by Dr. M. S. Chandrasekhara, Assistant Director, Navy-NASA Joint Institute of Aeronautics is gratefully acknowledged. The support of Dr. S. S. Davis, Chief, Fluid Dynamics Research Branch, and other staff members at FML, the discussions with Dr. L. W. Carr, U. S. Army AVSCOM at FML, the software development contributions of Mr. P. J. Trosin, and the image processing help rendered by Mr. C. Boswell of Sterling Federal Systems are all gratefully acknowledged.

Fig. 1. Schlieren Pictures of Multiple Shocks on a Rapidly Pitching Airfoil: M = 0.45, $\alpha^+ = 0.0313$, $\alpha = 12.6^0$.

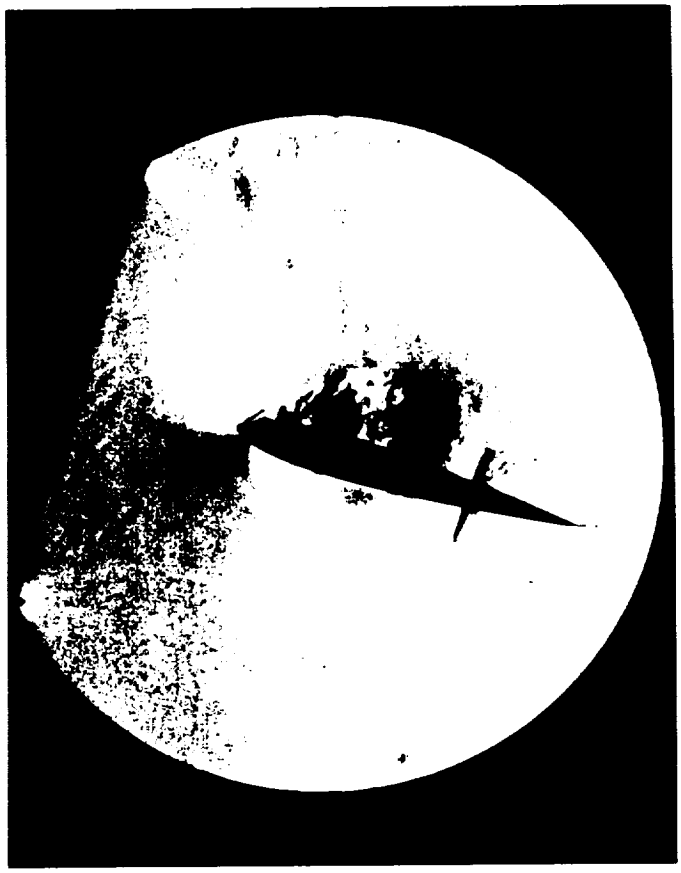

Fig. 2. Multiple Vortices on a Pitching Airfoil: M = 0.25, $\alpha^+ = 0.025$, $\alpha = 16.5^0$.

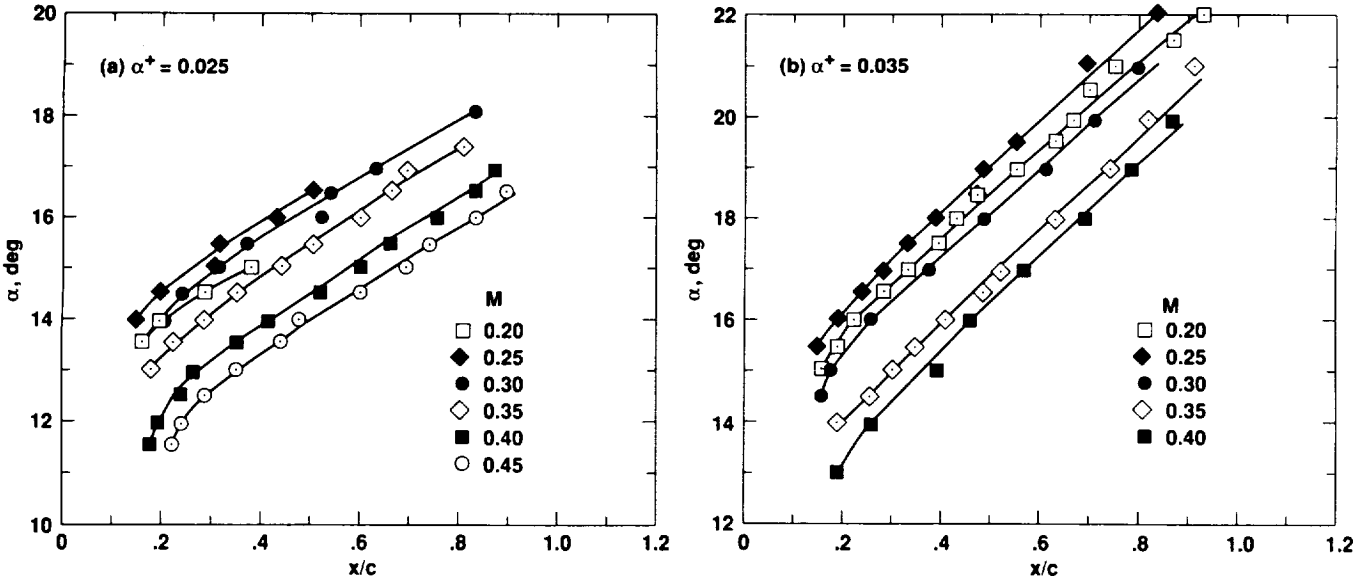

Fig. 3. Quantitative Effects of Mach Number on Dynamic Stall Vortex Location: (a)$\alpha^+ = 0.025$, (b) $\alpha^+ = 0.035$

APPENDIX A

AIAA-90-3038

Schlieren Studies of Compressibility Effects on Dynamic Stall of Airfoils in Transient Pitching Motion

M.. Chandrasekhara, Naval Postgraduate School, Monterey, CA;
S. Ahmed, MCAT Institute, San Jose, CA;
L. Carr, NASA-Ames, Moffett Field, CA

8th Applied Aerodynamics Conference
August 20-22, 1990/Portland, Oregon

Schlieren Studies of Compressibility Effects on Dynamic Stall of Airfoils in Transient Pitching Motion

M.S.Chandrasekhara [1]
Navy-NASA Joint Institute of Aeronautics
Department of Aeronautics and Astronautics
Naval Postgraduate School, Monterey, CA 93943

S.Ahmed [2]
Navy-NASA Joint Institute of Aeronuatics and
MCAT Institute, San Jose, CA

and

L.W.Carr [3]
Aeroflightdynamics Directorate, U.S.Army ARTA and,
Fluid Dynamics Research Branch
Fluid Mechanics Laboratory
NASA Ames Research Center, Moffett Field, CA 94035

Abstract

Compressibility effects on the flowfield of an airfoil executing rapid transient pitching motion from 0 - 60 degrees over a wide range of Mach numbers and pitching rates were studied using a stroboscopic schlieren flow visualization technique. The studies have led to the first direct experimental documentation of **multiple shocks** on the airfoil upper surface flow for certain conditions. Also, at low Mach numbers, additional coherent vortical structures were found to be present along with the dynamic stall vortex, whereas at higher Mach numbers, the flow was dominated by a single vortex. The delineating Mach number for significant compressibility effects was 0.3 and the dynamic stall process was accelerated by increasing the Mach number above that value. Increasing the pitch rate monotonically delayed stall to angles of attack as large as 27 degrees.

Nomenclature

c	airfoil chord
M	free stream Mach number
U_∞	free stream velocity
x	chordwise distance
α	angle of attack
$\dot{\alpha}$	pitch rate, degrees/sec
$\alpha^+ = \frac{\dot{\alpha}c}{U_\infty}$	nondimensional pitch rate

[1] **Assistant Director and Adjunct Research Professor, Assoc. Fellow AIAA.**

[2] **Research Scientist.**

[3] **Research Scientist and Group Leader, Unsteady Viscous Flows, Member AIAA.**

1. Introduction

There is considerable interest in the enhancement and sustenance of lift by dynamically pitching an airfoil in applications related to fixed wing aircraft supermaneuverability and enhanced agility. The production of dynamic lift by rapid unsteady motion such as oscillatory pitching or ramp type pitching is well known. Carr[1] provides a comprehensive review of the problem and related processes. Over the years, significant effort has been devoted to obtaining details of the process of dynamic lift generation over a rapidly pitching airfoil, quantify it and identify the parameters affecting it[2]. A survey of the available literature reveals that the process of dynamic stall is strongly dependent on the airfoil geometry (in particular the leading edge shape), Mach number, degree of unsteadiness or nondimensional pitch rate, Reynolds number, state of the airfoil boundary layer, airfoil initial angle of attack before pitching, three dimensionality, type of airfoil motion, location of pitch point, etc. The various aspects of the problem have been studied by several researchers. Freymuth[3] provides excellent flow visualization pictures at low speeds. Lorber and Carta[4], Albertson et al[5], Walker et al[6], among others have measured the surface pressure distributions. Francis and Keese[7] have found that the maximum lift coefficient increases monotonically till a nondimensional pitch rate of 0.025 and decreases therafter. Jumper et al[8] concluded from their studies that the pitch point has a large effect on dynamic stall. Harper and Flanigan[9] found that as the Mach number is increased, the dynamic lift steadily decreases and finally ceases at M $\approx$ 0.6 . Whereas these above mentioned studies are experimental, there are some computational studies (Ekaterinaris[10], Visbal[11], among others) that have produced good agreement with the available data.

The phenomenon of dynamic stall is characterized primarily by a clockwise vortex (for flow moving from left to right) that is produced by the large amount of coherent

vorticity that is created near the leading edge region of rapidly pitching airfoils by the unsteady motion. In fact, for certain flow conditions, Walker et al[6] observed that two vortices are present on the airfoil. During the early stages of the stall process the flow around the airfoil remains attached, with the vortex being surrounded by the outer stream. As the angle of attack is increased well past the static stall angle, the vortex begins to convect over the upper surface and grows. Eventually, when the vortex is shed into the wake, deep dynamic stall is said to occur. This sequence of events has been derived from flow visualization experiments at low Mach nmubers. Computations and surface presure measurements have shown that extremely large suction pressures develop in the region very close to the leading edge, pointing to formation of locally supersonic regions. In fact, even at the low free stream Mach number of 0.2, the local flow can attain sonic values[12]. It is then likely that a shock can form in the flow. If it does, it could have a dramatic effect on the dynamic stall process. However, till now there has been no direct experimental evidence of a shock, although its presence has been inferred from other measurements such as signatures of surface mounted hot film gages[4]. It is very clear that there is a strong need to obtain detailed experimental data about the influence of compressibility effects on dynamic stall before a full understanding of the dynamic stall process can be obtained. This paper presents some of the results of a visualization of the flow carried out using a stroboscopic schlieren method.

2. Description of the Experiment

A. Facility

The experiments were conducted in an in-draft wind tunnel of the Fluid Mechanics Laboratory (FML) at NASA Amers Research Center (ARC). It is one of the ongoing dynamic stall research projects of the Navy-NASA Joint Institute of Aeronautics between the Naval Postgraduate School and NASA ARC.

The details of the FML in-draft wind tunnel are given in Carr and Chandrasekhara [11]. The facility is one of a complex of four in-draft wind tunnels connected to an evacuation compressor. The test section size is 25cm X 35cm X 100cm. The flow in the tunnel is controlled by a variable cross section throat downstream diffuser. The throat is always kept choked so that no disturbances can propagate from the other tunnels or the compressor into the test section.

An NACA 0012 airfoil with a chord of 7.62cm is supported in a unique way by pins that are push fitted between two 2.54cm. thick optical quality glass windows. The pins are smaller than the local airfoil thickness and hence permit complete optical access to the airfoil surface. This makes detailed flow studies possible even at the surface. The airfoil motion is produced by a hydraulic drive located on top of the test section, which is connected to the window frames supporting the airfoil. Controlled movement of the hydraulic actuator provides the desired motion of the airfoil. Fig. 1 shows a schematic of the tunnel with the drive system.

B. Details of the Hydraulic Actuator System

The following were specified as the requirements on the airfoil motion:

angle of attack, α:	0-60°
pitch rate, $\dot{\alpha}$:	0-3600 °/sec
acceleration rate:	600,000 $°/sec^2$
change in α during acceleration:	$\leq$6° of pitch
acceleration time:	4 milliseconds
free stream Mach number:	0.1-0.5
airfoil chord:	7.62cm
Reynolds number:	2 x 10^5 - 10^6

It should be noted that at any Mach number, a 7.62cm chord airfoil pitching at 3600^0/sec. corresponds to a 3m chord wing pitching at 90^0/sec., which is beyond the range of present day aircraft. Thus, results obtained from this study will enable expanding the flight envelope of both current and future aircraft systems. The acceleration time was limited to 4 milliseconds and the change in angle of attack during this time was specified to be less than 6^0 so that the airfoil has reached a constant pitch rate well before the static angle is reached. To obtain reasonable experiment times, the system was also required to recycle 30 times a minute.

These exacting requirements meant that a powerful prime mover was necessary for this purpose. After considering several alternatives, a hydraulic drive system was found to be able to deliver the required performance. Such a system was designed taking into account the fact that the system characteristics are collectively determined by the interaction of the aerodynamic flow field, the mechanical system with its linkages and associated backlash, and the hydraulic system with its leakage and the nonlinearities in each of these systems. The details of the feed back system design can be found in Andrews[14]. Chandrasekhara and Carr[15] provide the other details of the final design, including those of the hydraulic circuit.

C. Instrumentation and Technique

The drive is equipped with its own instrumentation which is used by the feed back control system. These include a digital incremental position encoder (with a resolution of 0.03^0/count) to provide the instantaneous angle of attack, and a linear (analog) velocity transducer for maintaining the airfoil velocity constant. The airfoil motion is software controlled from an IBM PC, with a motion controller card installed in one of its slots.

As stated earlier, the airfoil pitches from 0 - 60^0 at pitch rates up to 3600^0/second and the motion is completed in 20 milliseconds. Records of individual pitch up motion were obtained using a MicroVAX II Work Station. The PC was linked to the MicroVAX with additional hardware to trigger data acquisition on the MicroVAX computer, using the third bit of the encoder providing the instantaneous angle of attack information. The third bit was chosen to prevent accidental triggering due to noise or such uncontrollable parameters. Simultaneously, the internal clock of the computer was started so that the time history of the motion could be documented. Fig. 2 shows typical plots of the variation of angle of attack with time for M = 0.45, a pitch rate $\dot{\alpha}$, of 3507^0/sec, and nondimensional pitch rate $\alpha^+ = 0.03$; M = 0.35, $\dot{\alpha} = 2256^0$/sec.,

$\alpha^+ = 0.025$; and M = 0.25, $\dot{\alpha} = 1263^0$/sec, $\alpha^+ = 0.02$. Similar plots were obtained for all cases.

The schlieren instrumentation used is standard and is shown in Fig. 3. It is also described in Carr and Chandrasekhara[13]. Flow visualization was obtained using the stroboscopic schlieren flow visualization technique. This involved triggering the schlieren light source at the desired instantaneous angle of attack by a specially designed electronic circuit. The encoder counts for the desired angle of attack was chosen as a BCD number by setting switches on the front panel of the hardware. The circuit includes a comparator which outputs a TTL pulse when a match occurs between the selected count and the constantly changing encoder count. This pulse triggers the strobe light source and also freezes the display of the encoder counter, thus permitting a check on and recording of the actual angle of attack at which the light flashed. No phase delays were found to be present in this process.

The experiment consisted of running the tunnel at Mach numbers ranging from 0.2 - 0.45, while pitching the airfoil at rates from 1200 - 3600 degrees/sec., and taking the schlieren pictures. The resulting Reynolds number range was 400,00 - 900,000. The matrix of experimental conditions is given in Table 1.

3. Results and Discussion

A. Stroboscopic Schlieren Flow Visualization Studies

Fig. 4 and 5 present two sequences of stroboscopic schlieren pictures obtained for the cases of M = 0.25, $\alpha^+ = 0.05$ and M = 0.45, $\alpha^+ = 0.03$. These pictures were obtained by pitching the airfoil once for each frame shown. They represent the density gradients at the instant the pictures were taken without any history effects - unlike most other flow visualization photographs. The knife edge of the schlieren system was kept vertical for all cases.

The dominant feature in these figures is the presence of the dynamic stall vortex that appears as a dark circular region over the airfoil and moves along the airfoil upper surface and eventually past the trailing edge.

The dark region near the leading edge of the airfoil on its lower surface indicates the density gradients in the stagnating flow. As the angle of attack increases (up to 30^0), the stagnation point moves downstream along the lower surface and stabilizes at $\approx$ 5% chord point. Also, as the angle of attack in increased, the dynamic stall vortex becomes distinct at $\alpha = 17^0$ in Fig. 4 at M = 0.25 and $\alpha^+ = 0.05$, and $\alpha = 13^0$ for the case of the higher Mach number of 0.45 and $\alpha^+ = 0.03$ in Fig. 5. In both cases, the vortex quickly grows into a large coherent structure. The boundary layer downstream of the vortex thickens with increasing angle of attack; at the same time, the leading edge shear layer appears as a thin streak (starting out initially as a dark layer and transforming into a lighter shade) and delineates the outer potential flow from the inner separated viscous layer. Ultimately, the vortex is bounded by the edge of the shear layer upstream and by the boundary layer downstream. The flow downstream of the dynamic stall vortex is still attached,as can be seen, for example, in Fig. 5, $\alpha = 14.5^0$. No trailing edge vortex was present for any of the cases studied. Walker et al[6] have pointed out that the trailing edge vortex is due to the separating shear layer on the upper surface and is absent at higher Reynolds numbers, which is perhaps the reason why it was not found in the cases studied.

The vortex itself appears as a dark region as in its formative stages, the flow gradients in it have not fully developed. But, when it grows and has acquired its terminal velocity, it appears as a partially bright and partially dark image, with a sharp transition line where the local density gradient changes sign from negative to positive (light to dark), as can be seen in Fig. 4 for $\alpha = 21.0^0$. For the case shown in Fig. 4, the flow stalls dynamically at $\alpha = 27^0$ (when the vortex has travelled past the trailing edge) and for M = 0.45, (Fig. 5), at $\alpha = 18^0$. Both these angles are substantially higher than the corresponding static angles. (See also Table 2).

As the airfoil pitches past this angle, the flow becomes largely separated and the separating leading edge shear layer grows unstable forming several vortices, as can be seen from the bottom row frames in both Fig. 4 and Fig. 5. The flow downstream of the trailing edge also shows several small organized vortical structures. Occasionally, (Fig. 4, $\alpha = 28^0$) a trailing vortex (much like the starting vortex) can be seen coming off the trailing edge of the airfoil during the deep stall phase of the flow.

Fig. 6 presents an enlarged schlieren picture for M = 0.25, $\alpha^+ = 0.025$, at $\alpha = 16.5^0$. At this condition, some interesting details are present in the flow. As already stated, the forward stagnation point is on the lower surface at about 5%chord point. On the upper surface, there is a large dynamic stall vortex at x/c $\approx$ 0.5. Along with it it is another structure, which appears to have the same sense of vorticity as the dynamic stall vortex. Downstream of the primary vortex, the flow is still attached. It is surprising to see two clockwise vortical structures at the same time. Chandrasekhara et al[18] have detected such structures in their computational studies of the flow over an oscillating airfoil under compressibility conditions. Mane et al[19] have also found such structures in their computational studies on pitching airfoils, but at a low Reynolds number of 50,000. At this stage, it is not known whether the multiple structures would influence dynamic lift generation in any way. However, these seem to appear mostly at low Mach numbers and only at low pitch rates.

Another noteworthy feature is the large vertical length scale of the flow. It appears that the vortex diffuses and rapidly becomes disorganized as it moves over the airfoil. In contrast, studies of the flow field over an oscillating airfoil by Chandrasekhara and Carr[16] have shown that the vortex was very tightly wound. Chandrasekhara et al[17] have compared the effect of motion history and found that in the range of parameters tested, the ramp type motion is not very effective in introducing the levels of vorticity that can be attained by the oscillating motion due to the fact that the integrated effect of pitch rate history on vorticity generation is larger in the oscillating case. This is a possible explanation for the observed structure of the dynamic stall vortex in this case.

B. Formation of Shocks over the Airfoil

Fig. 7 shows the details of the flow near the leading edge of the airfoil for M = 0.45, $\alpha^+ = 0.0313$, $\alpha = 12.6^0$.

The strong density gradient near the airfoil leading edge under these conditions are responsible for deflecting the light rays completely around the region, which results in a dark region seen on the upper surface in this figure. The most striking result seen in the figure is the presence of multiple shocks within the first 5 - 8% chord distance. The rapid acceleration of the flow around the leading edge for this case has caused the flow to go supersonic. Such a result has also been indicated in computational studies. The extent of the supersonic region depends upon the Mach number, nondimensional pitch rate and instantaneous angle of attack. For example, Visbal[11] found that a supersonic region originates very near the leading edge and extends till about 8 - 10% chord point for M = 0.3, and it grows to about 30% chord at M = 0.6. The results obtained from the present study offer the first definitive experimental documentation of the fact that shocks actually form on the airfoil for certain flow conditions and support the study by Visbal[11]. It is well known that once a flow attains supersonic values, a shock can form. In the present case, it is not known whether the shock is normal or oblique, but presence of multiple shocks indicates that if a normal shock orignally formed, there are additional mechanisms present in the flow that are responsible for accelerating the flow repeatedly to supersonic values and thus forming more shocks. A possible explanation is that the shock induces small scale separation in the boundary layer. The separating streamlines could take a wavy shape and thus locally induce a series of expansion and compression waves. Such a system of waves could form additional shock waves (or shocklets) in the flow. Eventually the series of interactions ceases via a 'strong' shock and the flow becomes subsonic. This explanation still needs to be verified, but such a situation seems possible in transonic flow. Meier[20] has observed multiple shocks in vortex-wing interaction studies in transonic flows.

The shocks discussed above were present over a range of angles of attack and flow conditions. A sequence of schlieren pictures for M = 0.45, at a pitch rate of 3600 degrees/sec. ($\alpha^+ = 0.0313$) is presented in Fig. 8. These were obtained at a very fine resolution over angles of attack ranging from 12.2^0 - 12.9^0. It can be seen that at $\alpha = 12.4^0$, shocks (the thin dark streaks in the figure) appear over the airfoil surface in the region x/c = 0 - 0.05. At $\alpha = 12.4^0$, several shocks form and extend 1 - 2% chord width into the upper surface flow. The shocks remain on the surface at $\alpha = 12.5^0$. At $\alpha = 12.7^0$, only a single "strong" shock remains at about 10% chord, just upstream of the dark region. The shock finally disappears at an angle of attack of 13^0. However, no large scale shock induced separation could be detected for the cases studied. In fact, the dynamic stall vortex still forms and eventually gets shed at $\alpha = 17^0$.

C. Effect of Mach Number

Fig. 9 compares the schlieren pictures at different Mach numbers for $\alpha^+ = 0.03$ and $\alpha = 17^0$. It can be seen that for the subsonic case ($M \leq 0.3$), the vortex is at about 50% chord location. In addition, the vertical extent of the flow is nearly the same for M = 0.2, 0.25 and 0.3. However, for $M \geq 0.3$, the dynamic stall vortex moves successively closer to the trailing edge and the flow scales have increased as well. Movement of the vortex downstream indicates flow approaching the deep stall state and thus, it is clear from the figure that as the Mach number is increased, deep stall occurs at progressively lower angles of attack.

Fig. 10a shows the effect of Mach number on the dynamic stall for the pitch rate $\alpha^+ = 0.025$, and the corresponding results for $\alpha^+ = 0.035$ are shown in Fig. 10b. Plotted in it are the successive locations of the center of the dynamic stall vortex as a function of the instantaneous angle of attack at different Mach numbers. It can be seen in both the figures that the vortex appears at lower angles of attack as the Mach number increases. This also leads to the result that the vortex moves past the trailing edge at lower angles of attack for higher Mach numbers, causing deep dynamic stall to occur earlier in the pitching cycle. Significant decreases in the angle of attack occur for the same x/c location for $M \geq 0.3$ and thus, M = 0.3 can be considered to be the limit when compressibility effects set in. Consider for example Fig. 10a, for x/c, ≈ 0.6, the center of the vortex is at $\alpha = 16.5^0$ for M = 0.3, and $\alpha = 14^0$ for M = 0.45. Similarly, in Fig. 10b, the vortex is at 60% chord location at $\alpha = 19^0$ for M = 0.3; at M = 0.4, the corresponding angle of attack = 17.2^0. Similar results were obtained at other pitch rates.

Table 2 shows the angle of attack at which deep dynamic stall occurs for the cases studied. As the Mach number is increased for a given pitch rate, the dynamic stall angle remains nearly the same up to M = 0.3. However, for $M \geq 0.3$, this angle decreases. The scatter that is present in the data is unavoidable, owing to the subjectiveness involved in determining these angles. Further, as already stated in Section 3.A, for some cases multiple structures were found to be present. This, along with the diffused vortex, made the task of tracking the vortex movement more complex. Nevertheless, the data shows definitive trends that reflect the compressibility effects.

D. Effect of Pitch Rate

Fig. 11a through 11d show the vortex center locations over the airfoil plotted as a function of the angle of attack at different pitch rates for M = 0.2, 0.35, 0.4 and 0.45 respectively. It can be seen in all the figures that the vortex is retained on the surface of the airfoil to higher angles of attack as the pitch rate is increased. The trend is monotonic with increasing pitch rate. For example at M = 0.45, the vortex is on the surface even at $\alpha = 18^0$ at $\alpha^+ = 0.03$, whereas the static stall angle for this case is $\approx 9.5^0$ as determined from the schlieren images. For $\alpha^+ = 0.020$, deep dynamic stall occurs at $\alpha = 15.5^0$. For M = 0.35, the deep stall angle is $\approx 23^0$ for $\alpha^+ = 0.04$, and the static stall angle is 11.6^0. The figures show similar results for other Mach numbers. A summary of dynamic stall angles is presented in Table 2 at different pitch rates. A horizontal scan of the table shows stall delay till angles of attack significantly higher than the static stall angles can be achieved by simply increasing the nondimensional pitch rate, even at these higher Mach numbers. As indicated in the previous section, presence of multiple structures, especially at the low Mach number of 0.2, made following the primary vortex during its passage over the airfoil difficult. Hence, the plot for $\alpha^+ = 0.025$ in Fig. 11a does not extend till the deep stall angle of attack.

4. Concluding Remarks

Results obtained showing the global behavior of the dynamic stall vortex over an airfoil executing a rapid transient pitching motion are presented. These are the first pictures of the flowfield obtained at maneuver Mach number conditions and for conditions that are beyond the operational range of present day aircraft.

The following major conclusions could be drawn from the study.

1. Multiple shocks are present over the airfoil, at moderate free stream Mach numbers. The shocks do not seem to induce any large scale flow separation. Also, the global features of the dynamic stall process are not significantly affected by their presence. However, detailed studies are still needed to confirm local effects of the shocks.

2. At low Mach numbers, multiple vortices are present at low pitch rates. But, at higher Mach numbers, a single large dynamic stall vortex dominates the flow. Occasionally, a trailing vortex similar to the starting vortex is observed.

3. Compressibility effects are important for $M \geq 0.3$.

4. Stall delay is enhanced by increasing the pitch rate. Increasing Mach number accelerates dynamic stall by lowering the angle of attack at which dynamic stall occurs.

Acknowledgements

The project was supported by AFOSR-MIPR-87-0029 and 88-0010 (monitored by Capt. H.Helin) with additional support from NAVAIR (Mr. T. Momiyama) and ARO (Dr. T.L.Doligalski). The technical support of Mr. Michael J. Fidrich and the staff of the NASA Fluid Mechanics Laboratory is greatly appreciated.

5. References

[1] Carr,L.W., "Progress in Analysis and Prediction of Dynamic Stall", *Journal of Aircraft*, Vol.25, No.1, Jan. 1988, pp. 6-17.

[2] McCroskey, W.J., "The Phenomenon of Dynamic Stall", NASA TM 81264, March 1981.

[3] Freymuth, P., "Vortex Patterns of Dynamic Separation", *Encyclopedia of Fluid Mechanics*, Ed. N.P.Cheremisinoff, Gulf Publishing Corp., Vol. 8, 1989, Chapter 11.

[4] Lorber, P.F. and Carta, F.O., "Unsteady Stall Penetration Esperiments at High Reynolds Number", AFOSR-TR-87-1202, April 1987.

[5] Albertson, J.A., Troutt, T.R., and Kedzie, C.R., "Unsteady Aerodynamic Forces at Low Airfoil Pitching Rates", AIAA Paper No. 88-2579-CP.

[6] Walker, J.M., Helin, H.E., and Strickland, J.H., "An Experimental Investigation of an Airfoil Undergoing Large-Amplitude Pitching Motions", *Journal of Aircraft*, Vol. 23, No. 8, Aug. 1985, pp. 1141-1142.

[7] Francis, M.S., and Keese, J.E., "Airfoil Dynamic Stall Performance with Large-Amplitude Motions", *Journal of Aircraft*, Vol.23, No.11, Nov. 1985, pp. 1653-1659.

[8] Jumper, E.J., Dimmick, R.L., and Allaire, A.J.S., "The Effect of Pitch Location on Dynamic Stall", *Journal of Fluids Engineering, Trans. ASME*, Vol. 111, No. 3, Sep. 1989, pp. 256-262.

[9] Harper, P.W, and Flanigan, R.E. "The Effect of Rate of Change of Angle of Attack on the Maximum Lift of a Small Model", NACA TN 2061, March 1950.

[10] Ekaterinaris, J.A., "Compressible Studies of Dynamic Stall", AIAA Paper 89-0024, Jan. 1989.

[11] Visbal, M.R., "Effect of Compressibility on Dynamic Stall of a Pitching Airfoil", AIAA Paper No. 88-0132, Jan. 1988.

[12] McCroskey, W.J., McAlister, K.W., Carr, L.W., Pucci, S.L., Lambert, O., and Indergrand, R.F., "Dynamic Stall on Advanced Airfoil Sections", *Journal of American Helicopters Society*, Vol. 26, No. 3, pp. 40-50.

[13] Carr, L.W., and Chandrasekhara, M.S., "Design and Development of a Compressible Dynamic Stall Facility", AIAA Paper No. 89-0647, Jan. 1989.

[14] Andrews, D.R., "An Airfoil Pitching Apparatus: Modelling and Control Design", 35th ISA International Instrumentation Symposium, Orlando, Fl, May 1989.

[15] Chandrasekhara, M.S. and Carr, L.W, "Design and Development of a Facility for Compressible Dynamic Stall Studies of a Rapidly Pitching Airfoil", *Proceedings of the 15th ICIASF Conference*, Goettingen, West Germany, Sept. 18-21, 1989.

[16] Chandrasekhara, M.S., and Carr, L.W., "Flow Visualization Studies of the Mach Number Effects on the Dynamic Stall of an Oscillating Airfoil", AIAA Paper No. 89-0023, Jan. 1989. (also to appear in *Journal of Aircraft*, Vol. 28, No. 7, July 1990.)

[17] Chandrasekhara, M.S., Carr, L.W., and Ahmed, S. , "Comparison of Pitch Rate History Effects on Dynamic Stall", *Proceedings of NASA/AFOSR/ARO Workshop on Physics of Forced Unsteady Separation*, April 1990.

[18] Chandrasekhara, M.S., Ekaterinaris, J.A., and Carr, L.W., "Experimental and Computational Tracking of Dynamic Stall Vortex", *Bull. American Physical Society*, Vol. 33, No. 10, Nov. 1988, pp. 2251.

[19] Mane, L., Loc, T.P, and Werle, H., "Sur le Décollement Instationnaire Autour d'un Profil á Grands Nombres de Reynolds : Une Comparison Calcul Expérience", *Mécanique des Fluides*, Académie des Scinces, 305, Seires II, 1987, pp. 229-232.

[20] Meier, G.E.A., "Private Communications"

Table 1: Experimental Conditions

M	α^+						
	0.01	0.02	0.025	0.03	0.035	0.04	0.05
0.20			X	X	X	X	X
0.25		X	X	X	X	X	X
0.30		X	X	X	X	X	
0.35		X	X	X	X	X	
0.40		X	X	X	X		
0.45	X	X	X	X			

Table 2: Vortex Release Angle of Attack

M	α^+							
	0*	0.01	0.02	0.025	0.03	0.035	0.04	0.05
0.20				17.5		21.0	22.0	24.0
0.25				17.5	18.5	21.0	22.0	27.0
0.3	12.4		17.5	18.0	20.0	21.0	23.0	
0.35	11.6		16.0	17.5	19.0	20.0	23.0	
0.40	10.8		15.5	17.0	19.0	20.0		
0.45	9.5	12.0	15.5	17.0	18.0			

* Best estimate of static stall angle from schlieren pictures.

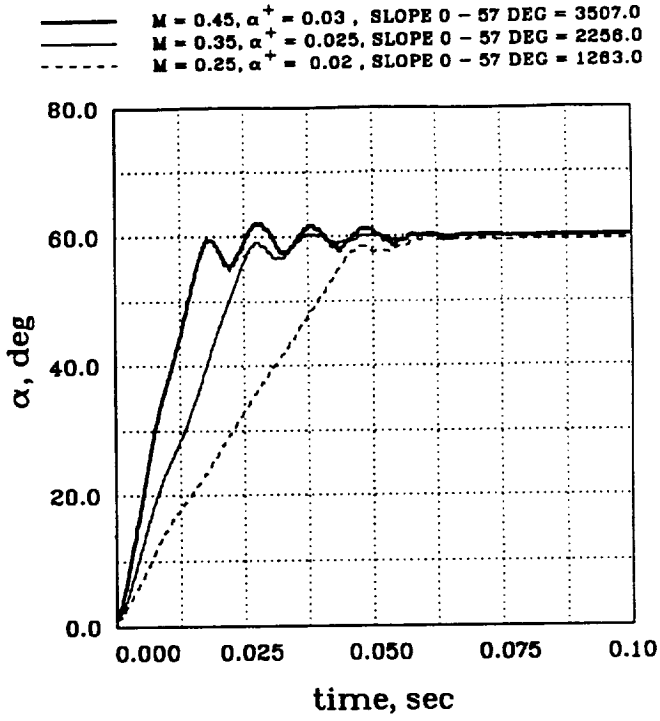

Fig. 2. Time History of Pitching Airfoil.

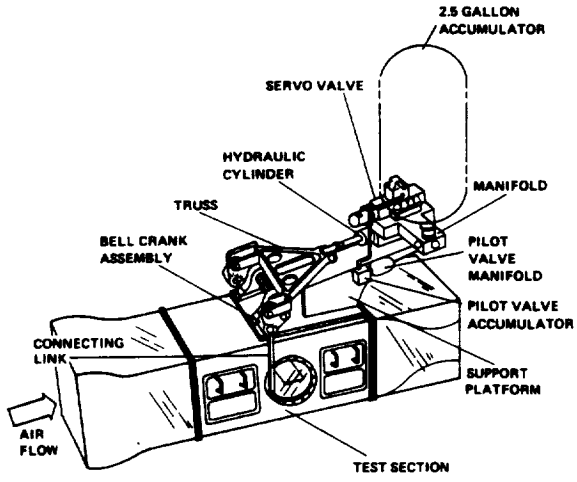

Fig. 1. Compressible Dynamic Stall Facility with a Hydraulic Drive.

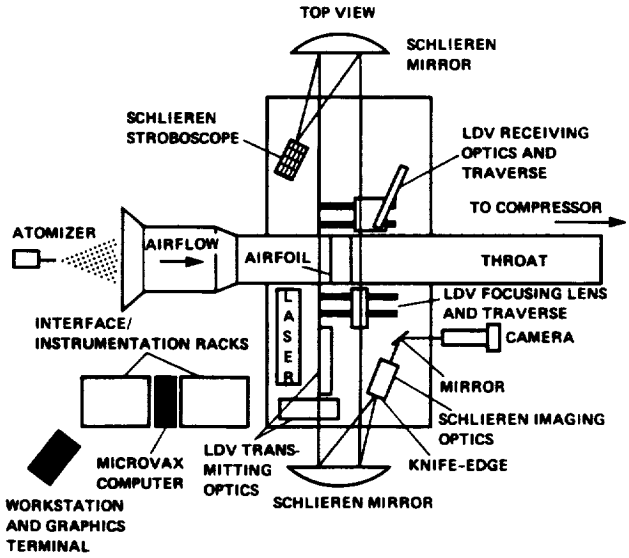

Fig. 3. Schematic of the CDSF Instrumentation.

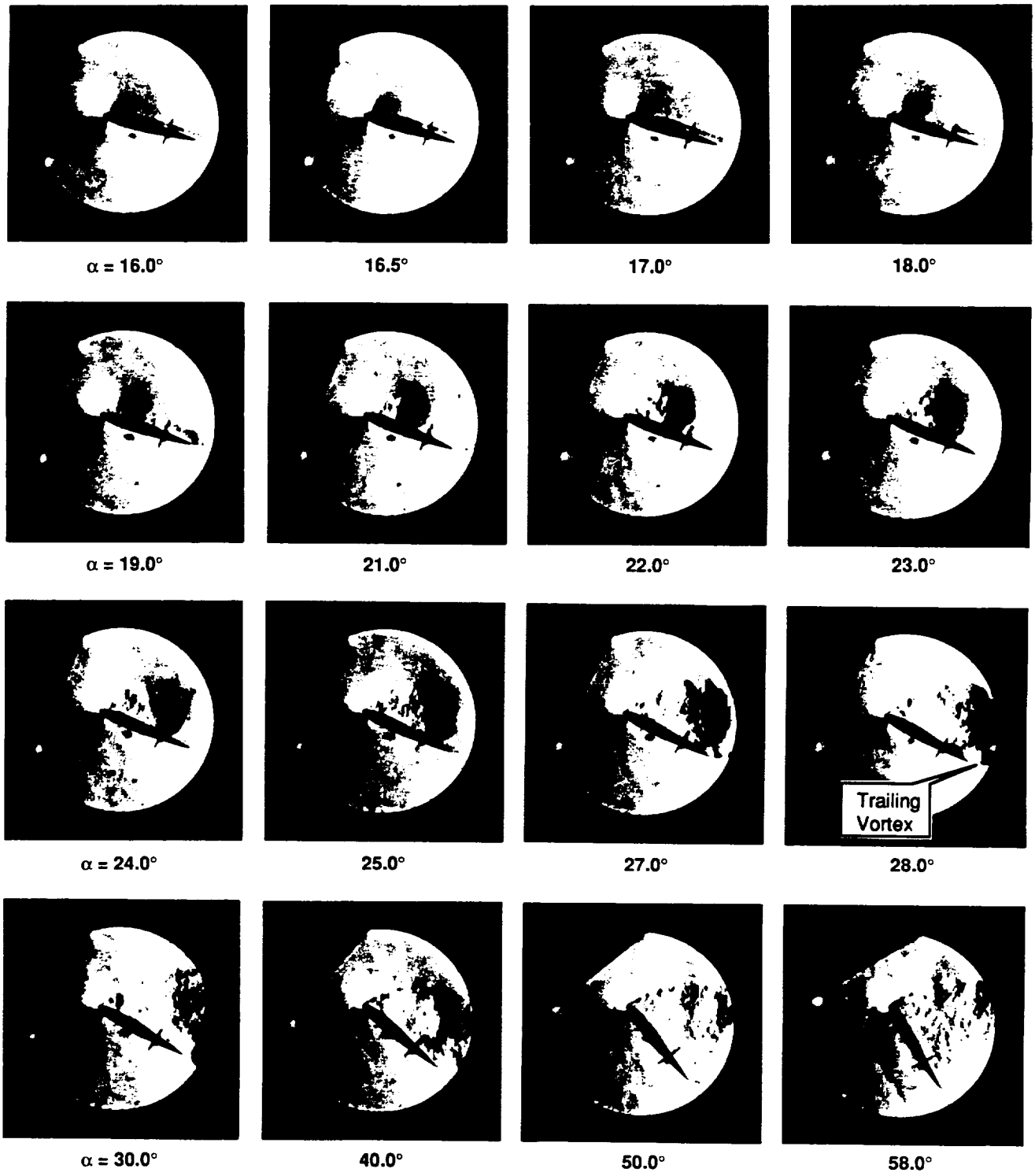

Fig. 4. Stroboscopic Schlieren Pictures of the Compressibility Effects on Dynamic Stall of a Rapidly Pitching Airfoil: M = 0.25, $\alpha^+ = 0.05$.

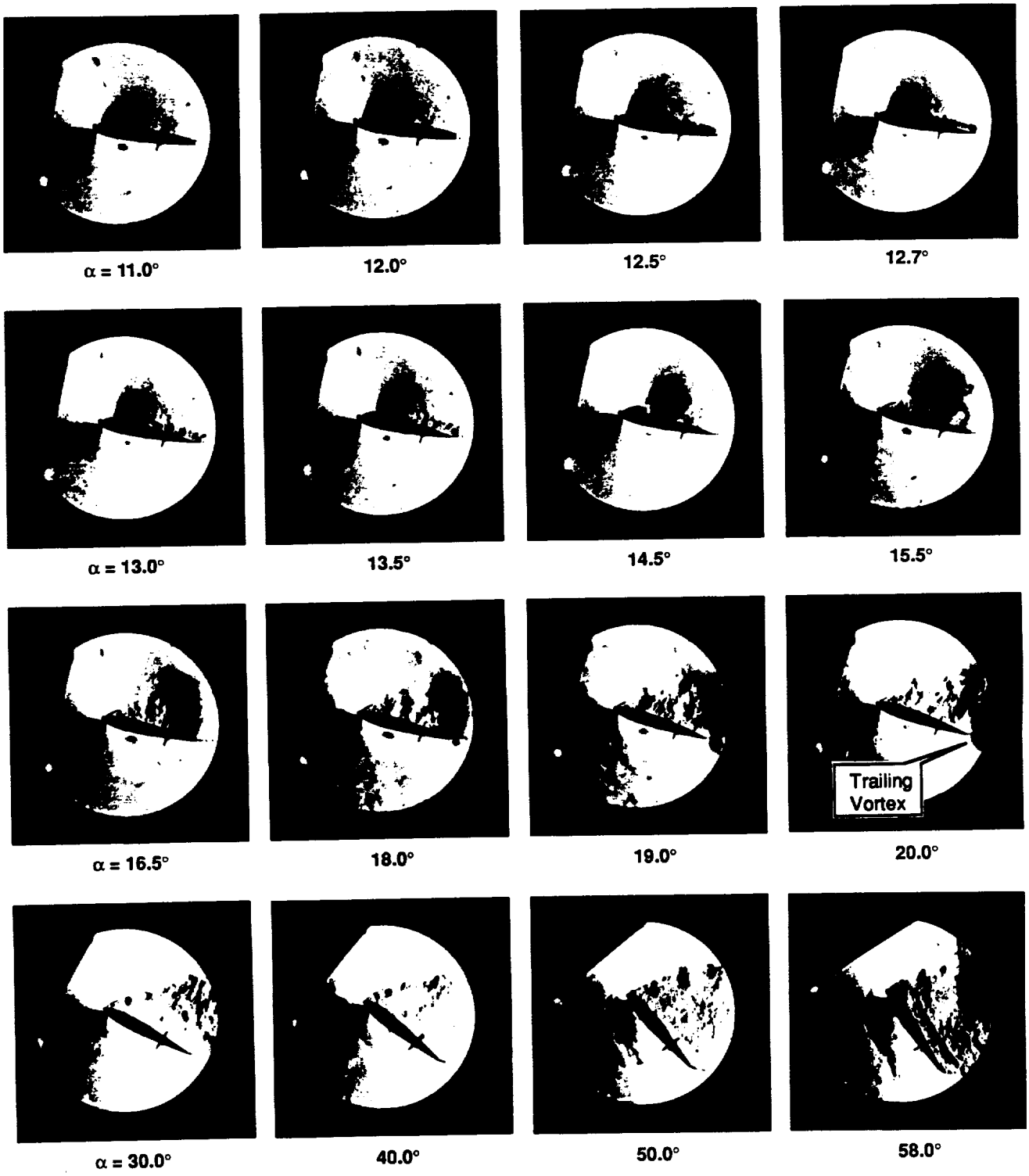

Fig. 5. Stroboscopic Schlieren Pictures of the Compressibility Effects on Dynamic Stall of a Rapidly Pitching Airfoil: M = 0.45, $\alpha^+ = 0.03$.

Fig. 6. Multiple Vortices on a Pitching Airfoil: M = 0.25, $\alpha^+ = 0.025$, $\alpha = 16.5^0$.

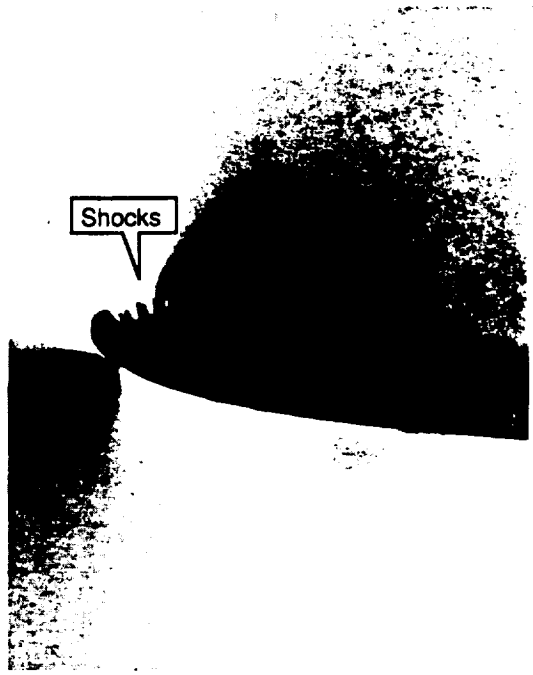

Fig. 7. Schlieren Pictures of Multiple Shocks on a Rapidly Pitching Airfoil: M = 0.45, $\alpha^+ = 0.0313$, $\alpha = 12.6^0$.

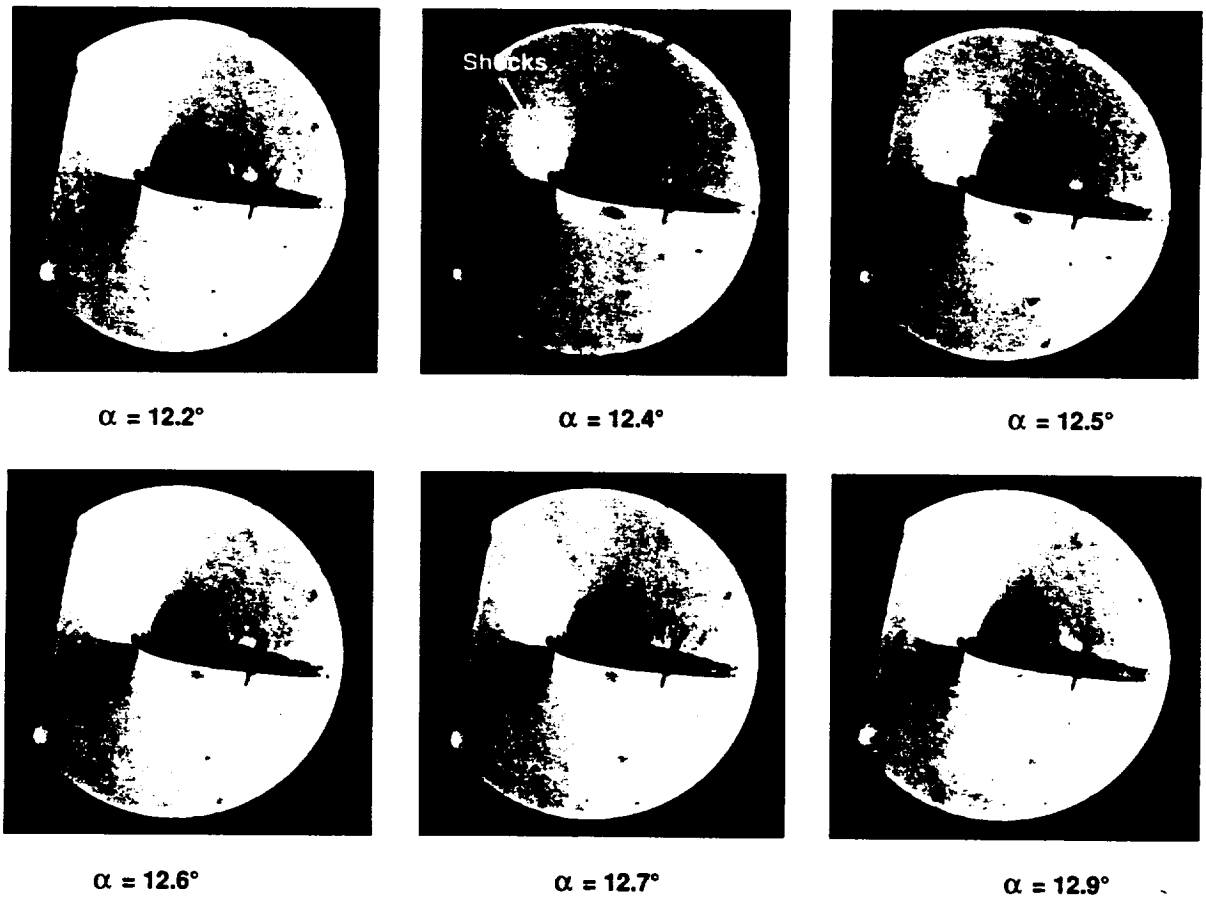

Fig. 8. A Sequence of Schlieren Pictures of Shocks on a Rapidly Pitching Airfoil: M = 0.45, $\alpha^+ = 0.0313$.

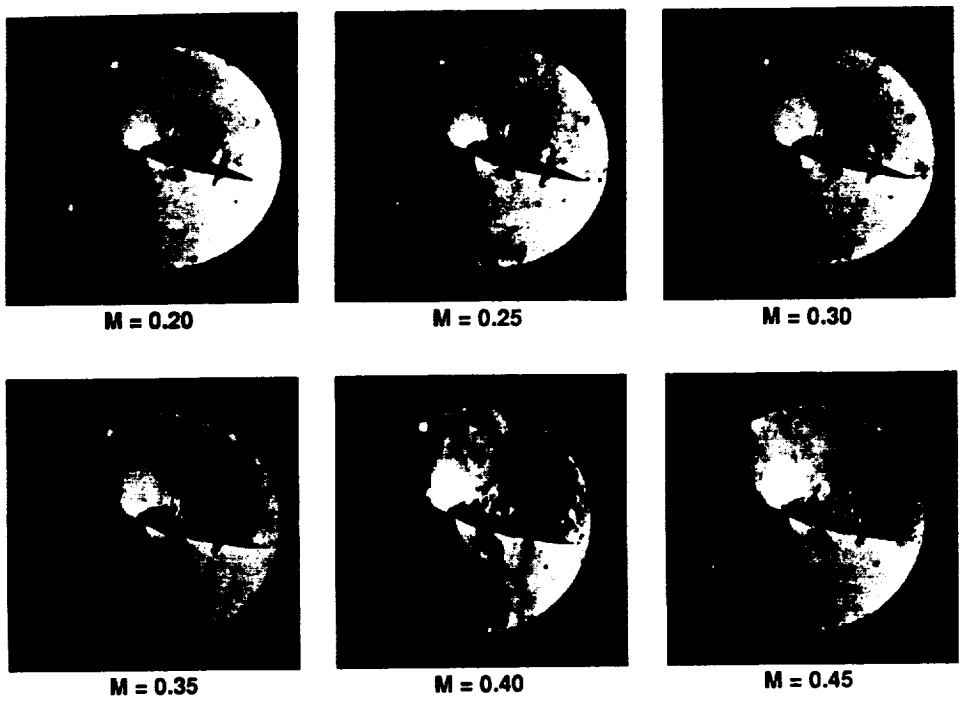

Fig. 9. Effect of Mach Number on Dynamic Stall of a Rapidly Pitching Airfoil, Schlieren Studies: $\alpha^+ = 0.03$, $\alpha = 17^0$.

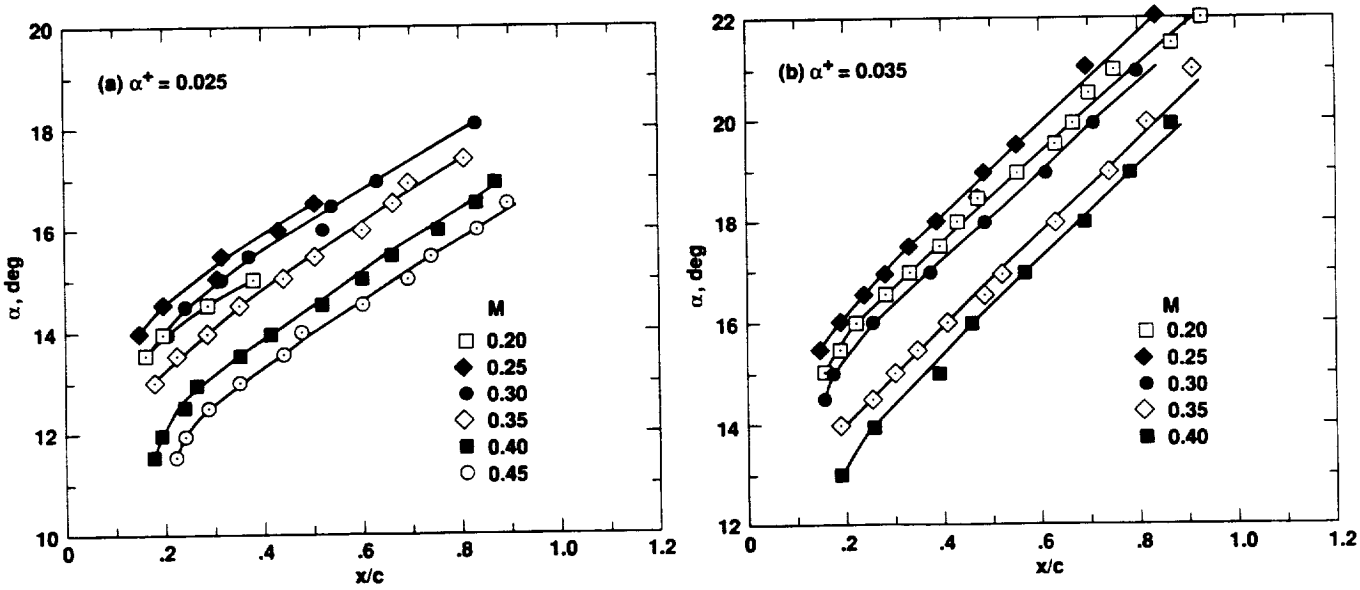

Fig. 10. Quantitative Effects of Mach Number on Dynamic Stall Vortex Location: (a) $\alpha^+ = 0.025$, (b) $\alpha^+ = 0.035$.

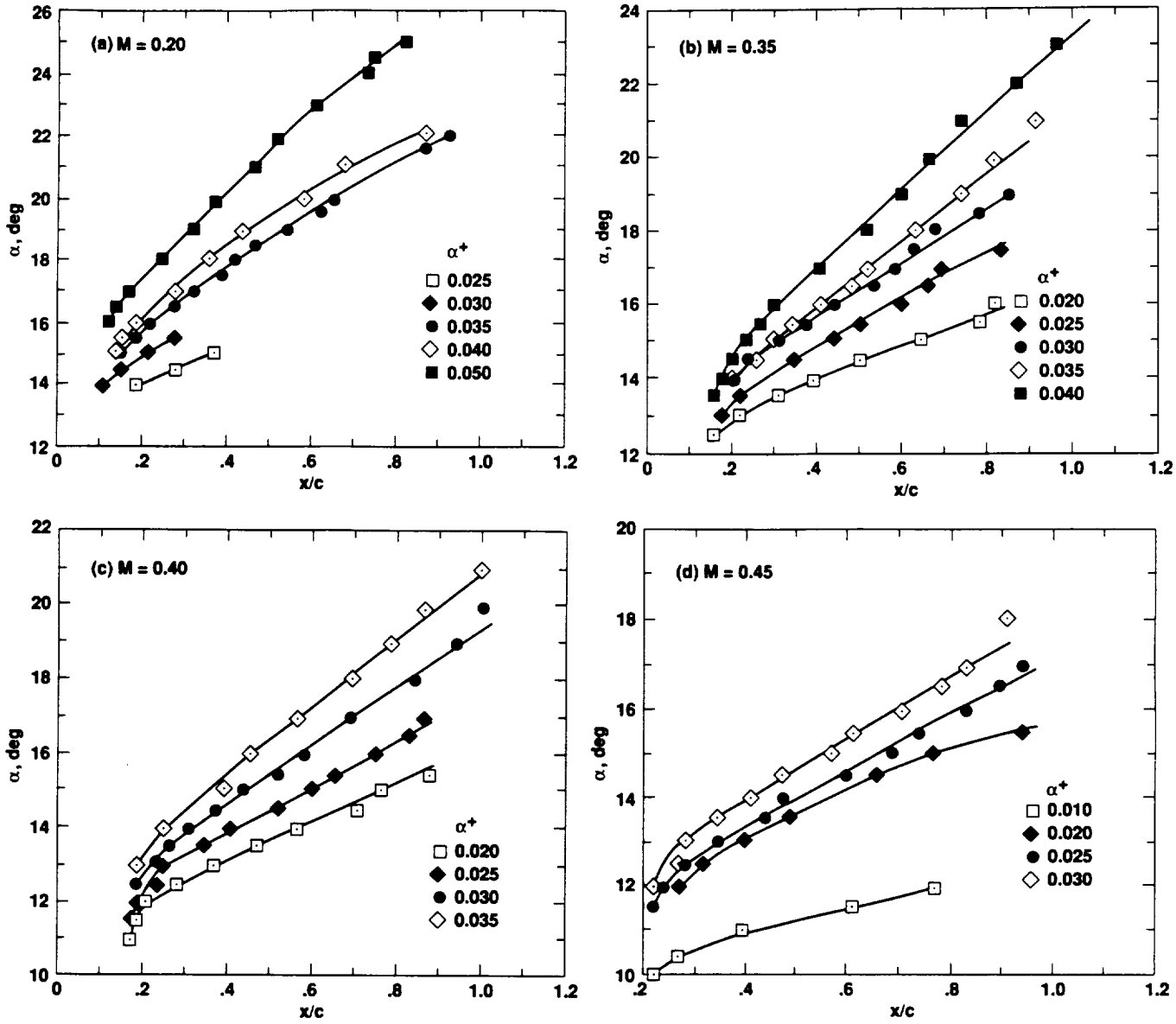

Fig. 11. Quantitative Effects of Pitch Rate on Dynamic Stall Vortex Location: (a) M = 0.2, (b) M = 0.35, (c) M = 0.40, (d) M = 0.45.

APPENDIX B

AIAA-91-1799

Laser Velocimetry Measurements of Oscillating Airfoil Dynamic Stall Flow Field

M. S. Chandrasekhara, Naval Postgraduate School and Navy-NASA Joint Institute of Aeronautics, Monterey, CA;
S. Ahmed, MCAT Institute, San Jose, CA.

AIAA 22nd Fluid Dynamics, Plasma Dynamics & Lasers Conference
June 24-26, 1991 / Honolulu, Hawaii

Laser Velocimetry Measurements of Oscillating Airfoil Dynamic Stall Flow Field

By

M.S.Chandrasekhara[1]
Navy-NASA Joint Institute of Aeronautics
and Fluid Mechanics Laboratory, NASA Ames Research Center
Department of Aeronautics and Astronautics
Naval Postgraduate School, Monterey, CA 93943

and

S.Ahmed[2]
MCAT Institute, San Jose, CA 95127

Abstract

Ensemble averaged two component velocity measurements over an airfoil experiencing oscillatory dynamic stall under compressibility conditions were obtained. The measurements show the formation of a separation bubble over the airfoil that persists till angles of attack close to when the dynamic stall vortex forms and convects. The fluid attains mean velocities as large as 1.6 times the free stream velocity(U_∞) with instantaneous values of $1.8U_\infty$. The airfoil motion induces these large velocities in regions that are far removed from its surface. Also, depending upon the behavior of the separation bubble, the *wall jet* profiles near the leading edge region could become *wake like* over the airfoil in a cycle at different phase angles. Vorticity contours indicate that the levels around the leading edge continuously increase till the vortex begins to convect. Some of the measurement difficulties, especially, particle behavior are discussed as well.

Nomenclature

c	airfoil chord
f	frequency of oscillation, Hz
k	reduced frequency = $\frac{\pi f c}{U_\infty}$
M	free stream Mach number
U,V	velocity components in the x and y directions
U_∞	free stream velocity
x,y	chordwise and vertical distance
α	angle of attack
α_0	mean angle of attack
α_m	amplitude of oscillation
ϕ	phase angle of oscillation
ω	circular frequency, radians/sec

1 *Assistant Director and Adjunct Research Professor; Associate Fellow, AIAA. Mailing Address: M.S. 260-1. NASA Ames Research Center, Moffett Field, CA 94035*

2 *Research Scientist; Member AIAA. On Leave from National Aeronautical Laboratory, Bangalore, India*

1. Introduction

The phenomenon of dynamic stall is an important case of forced unsteady separated flow and is of great importance to both helicopters and fixed wing aircraft. Dynamic stall relates to production of lift at angles of attack higher than the static stall angle by rapidly pitching an airfoil - a situation routinely encountered in helicopter blade motion. The major benefit of dynamic stall, namely, enhanced lift has remained unutilized because of the detrimental effects of the associated pitching moment fluctuations due to the convection of the dynamic stall vortex over the airfoil upper surface. A solution to the problem lies in controlling the process of flow separation and management of vorticity produced by the rapid pitching process. However, to accomplish this, a thorough understanding of the physics of the flow over the airfoil, especially around the leading edge is needed. The process of dynamic stall is very complex and Carr[1] provides a comprehensive review of the problem. The importance of compressibility, even at a low free stream Mach number of 0.2 has been established by the earlier work of McCroskey[2]. Harper and Flanigan[3] found that the benefits of dynamic stall, namely the production of enhanced lift, were negated by compressibility. Recently, Chandrasekhara and Carr[4], Chandrasekhara and Brydges[5], Chandrasekhara et al[6] have studied the global dynamic stall flow field by flow visualization, and found that compressibility effects set in at M = 0.3, and that the flow field is significantly affected, but the dynamic lift is still generated. Much of the earlier work referred to above is either globally qualitative or locally quantitative and limited to the

surface. About the only quantitative documentation of the flow field that exists was obtained by DeRuyck et al[7] at a very low flow velocity (O (10 m/s)). The low speed of the experiment and the use of hot wires in grossly separated flows severely limits the validity and usefulness of the data.

The dynamic stall flow field is a complicated combination of a multitude of fluid dynamic effects such as tremedous acceleration around the leading edge, formation of strong suction peaks, development of the local boundary layer under the strongly adverse pressure gradient following such acceleration, transition of the laminar boundary layer, separation of the boundary layer and its reattachment resulting in a separation bubble, its subsequent growth and eventual bursting just before the formation of the dynamic stall vortex, formation of shock(s) and the induced separation due to it, addition of large amounts of coherent vorticity into the flow and its coalescence into the dynamic stall vortex and so on. The interaction between the various phenomena and the trailing edge separated flow that propagates towards the leading edge only add to the flow complexity. For proper control schemes to be devised to manage this flow, it is obvious that a careful and thorough study of the basic fluid flow physics is needed to isolate the individual effects and the role of various parameters. A survey of the computational studies shows that Grohsmeyer et al[8], Ekaterinaris[9], Courier and Fung[10] have begun to address some of the above mentioned issues. However, there is no experimental data available for the comparison and validation of the computational results.

The present work is aimed at quantifying the velocity field with the hope that some progress can be made in understanding the flow physics, with which ideas of dynamic stall flow control can be developed, while at the same time the data base generated will serve to verify computational results and also enable development of new codes that incorporate appropriate flow physics.

2. Description of Facility

The experiments were conducted in the in-draft wind tunnel of the Fluid Mechanics Laboratory(FML) at NASA Ames Research Center (ARC). It is one of the ongoing dynamic stall research projects in the Navy-NASA Joint Institute of Aeronautcis between the Naval Postgraduate School and NASA ARC.

The details of the FML in-draft wind tunnel are given in Carr and Chandrasekhara[11]. The facility is one of a complex of four in-draft wind tunnels connected to a $108 m^3/sec$ (240,000 CFM), 9,000 hp evacuation compressor. The test section size is 25.4cm X 35cm X 100cm The flow in the tunnel is controlled by a variable cross section downstream diffuser. Its throat is always kept choked so that no disturbances can propagate upstream into the test section from the other tunnels or the compressor.

A unique mechansim was designed and built to produce the oscillatory motion of the airfoil. It is described in Ref. 11. The drive system is located on top of the test section. The test section windows are connected to the drive and the sinusoidal movement of the windows results in an identical movement of the airfoil which is supported by the windows. The airfoil is supported by pins push fitted between two 2.54cm thick optical quality glass windows. The airfoil supports are unique in that the pins carry the entire load. The pins are smaller than the local airfoil thickness and hence provide complete optical access to the airfoil surface. This makes detailed flow studies possible even at the surface.

The oscillating drive was designed to meet the following specifications:

$$\alpha = \alpha_0 + \alpha_m sin 2\pi f t = \alpha_0 + \alpha_m sin \omega t$$

$$0 \leq \alpha_0 \leq 15^0$$

$$2^0 \leq \alpha_m \leq 10^0$$

$$0 \leq f \leq 100 Hz$$

$$0 \leq M_\infty \leq 0.5$$

$$200,000 \leq Re \leq 10^6$$

$$\text{airfoil chord} = 7.62\text{cm}$$

The flow conditions correspond to a helicopter in forward flight and the Reynolds number corresponds to that of a $\frac{1}{7}$th scale model rotor, whose test results are directly applicable to a helicopter rotor. The in-draft wind tunnel and the unsteady drive system is known as the *Compressible Dynamic Stall Facility (CDSF)*. Fig. 1 provides a schematic of the facility and its instrumentation.

3. Instrumentation and Measurement Technique

A. Phase Locking Instrumentation

The CDSF is instrumented with 3 digital encoders. Of these, one is an absolute position encoder providing 3600 counts per revolution and is used for the mean angle of attack information. The other two are incremental position encoders with a resolution of 800 counts per revolution. One of the incremental encoders is used for obtaining the frequency/phase angle information. The other could be used for the instantaneous angle of attack. But, for the series of experiments being reported, it was not used.

A two color, two component frequency shifted TSI LDV system was used to obtain the measurements. Traversing was accomplished by directing the 4 beams of the system by mirrors on to a 352 mm focal length lens mounted on a computer controlled traverse. The scattered light was collected 15 degrees off-axis from direct forward scatter, this provided a reduced probe volume length and thus, improved the measurement resolution. The receiving optics were on a different traverse mechanism, but this was driven as a slave traverse to that on the transmitting side, and the two sides were kept aligned throughout. Two TSI 1990 series counters were used to process the individual photomultiplier tube signals.

Unsteady flow studies using LDV require phase locking circuitry that are capable of handling the random nature of the LDV data. Since the LDV data

rate is dependent on particle arrival rate, which is in general random and a function of the local flow, there is a need to read the instantaneous phase angle each time an LDV data sample is validated. This requires latching circuits to freeze the continuous encoder data based on an event in the flow. In the present experiments, this event was specified to be the occurence of coincident LDV data i.e. simultaneous Doppler signals in both the U and V components. The coincidence window width was chosen to be $50\mu sec$. The LDV data was input to a NASA LDV multiplexer, to which the encoder outputs processed by the counting circuitry were also connected. The coincidence detection pulse (i.e. the data ready pulse) from the multiplexer was used to freeze the encoder data at that instant, until all the data was completely transferred to a microVAX II computer in the DMA mode. As soon as this was accomplished, the latches were released for fresh data. In view of the high oscillation frequencies encountered, changes in the instantaneous angle of attack would occur in the time it takes to freeze the encoders. This along with the general paucity of the LDV data and the time it takes to transfer it to the computer required high speed latches to be used. Fig. 2 presents a schematic of the method followed. This inverse method of data collection is considered superior to specifying the phase angle and waiting for a certain sample size to be collected.

B. The Technique

As mentioned above, velocity data was acquired each time both components were available simultaneously. Concurrently, the various encoders were also read. In general, 10,000 coincident samples of each of U and V velocity components were obtained along with the encoder information for each sample. The process was computer controlled by an extensive software package that was specially developed for the purpose. The software capabilities include checks for detecting the oscillating drive frequency variations beyond a pre-set tolerance, sorting the data into bins and plotting histograms and velocity *vs.* phase angle distributions. At any stage when the data appeared not to pass the standard tests of data validation, (for example a widely scattered histogram), the entire data set was rejected and new data was acquired. The data was sorted into 36 bins corresponding to different phase angles in a $\pm 5^0$ range. If the distributions indicated any irregularities, then the data was rejected and the experiment repeated. Since such irregularities could be due to improper setting of the gains and the filters (it should be noted that the flow has a very large dynamic range in this experiment through an oscillation cycle), the electronic components were very carefully set and the setting maintained. Since this often resulted in reduced data rates, the collection of samples took several minutes at each point, (as much as 30 min. at some locations). However, this was preferred to any other means of increasing the data rate because of the truly unsteady nature of the flow and the large dynamic range dictated by the fluid dynamics of the problem. This procedure was repeated at each measurement location. Typically, a vertical velocity traverse above the airfoil surface consisted of 40 stations, acquiring 10,000 samples per channel along with the three encoder outputs, namely, mean angle of attack, phase angle and frequency of oscillation, per sample - all measurements were stored on disk and archived on tape.

During the analysis stage of the experiment, the raw data files were processed by another package by sorting into 120 bins at a resolution of $\pm 1.5^0$ and the plots displayed on the screen. At this stage, a minimum number of samples could be set depending upon the demands of statistical stationarity. The results presented here were obtained by stipulating that each phase angle bin contained at least 50 samples. When ever the required number of samples was not present in any bin, that bin was said to contain a 'hole'. A monotonic spline curve fit was then used to interpolate the data to 'fill the hole' between valid data bins. This method worked successfully over most phase angles of interest for the problem.

Data was acquired in a rectangular x-y grid, with x and y measured from the leading edge of the airfoil when its angle of attack was zero degrees.

C. Seeding

The flow was seeded with 1 μm polystyrene latex particles(PSL) suspended in alchohol and dispersed by the TSI 9306 six-jet atomiser. The particles were injected from slightly behind the indraft tunnel inlet continuously and arrived at the probe volume after travelling a distance of over 3 meters, by which time the alchohol had evaporated and only the PSL remained. The location of the injector was adjusted to suit the streamline pattern at different measurement points.

D. Experimental Conditions

The flow Mach number was set to 0.3. The oscillation frequency was 21.6 Hz which corresponded to a reduced frequency of 0.05. The airfoil was NACA 0012 airfoil, oscillating about the 25% chord point, with its angle of attack varying as

$$\alpha = 10^0 - 10^0 sin\omega t$$

Thus, phase angle of 0^0 corresponded to $\alpha = 10^0$, 90^0 to $\alpha = 0^0$ on its downstroke, 180^0 to $\alpha = 10^0$ on the upstroke and 270^0 to the maximum angle of attack of 20^0. The LDV probe volume was traversed in the range $-0.25 \leq x/c \leq 0.75$, $0.0 \leq y/c \leq 0.67$. The resolution was 6.25mm in the x direction and 1.25mm in the y direction.

3. Results and Discussion

A summary of the data to be presented is shown in Fig. 3. Following a measurement of the two dimensionality of the flow along a spanwise line at location B, time-histories of streamwise velocity at positions A,B,C,D are compared and contrasted. The next data set will concentrate on details of the separation region enclosed in the box E. The final set of measurements will examine the velocity and vorticity fields in the larger region denoted by the box F.

A. Two-Dimensionality Surveys

The tunnel flow two dimensionality was studied with the airfoil oscillating for M = 0.3, k = 0.05, at location x/c = 0.0 (i.e. nominally the leading edge) and y/c = 0.167 for several spanwise locations. Distributions of the normalized streamwise velocity component are shown in Fig. 4 at five spanwise locations on an offset scale. As can be seen, the curves are parallel everywhere through the oscillation cycle to within 5%, except in the range $216^0 \leq \phi \leq 320^0$. Earlier schlieren flow visualization experiments by Chandrasekhara and Carr[4] have shown that for the experimental conditions of this graph, deep dynamic stall occurs at $\alpha = 15.9^0$ corresponding to $\phi = 216^0$ when the dynamic stall vortex is shed. The upstream effects of the large scale flow separation and the large vertical flow scales are responsible for the differences seen after stall. However, the flow can be treated as essentially two-dimensional over the phase angle range of interest through the central two-thirds of the test section. Measurements beyond these stations were either difficult due to seeding problems or the LDV probe volume was not 'visible' to the receiving optics because of the off-axis forward scatter arrangement used. All further measurements were hence restricted to the mid-span plane.

B. Selected Distribution of $\frac{U}{U_\infty}$ *vs* Phase Angle

Fig. 5 presents the phase variation of the normalized U and V velocity components at selected locations in the flow field. Dramatic variations are to be expected in a complex flow such as this and hence, the following discussion.

In Fig. 5a, at x/c = -0.25, y/c = 0.583, a location upstream of the airfoil leading edge, the flow almost follows the sinusoidal motion imposed by the oscillating airfoil. The most noteworthy feature at this station is that the peak velocity is $1.15U_\infty$ and occurs at a phase angle of about 216^0, which corresponds to the dynamic stall angle as already stated. Beyond this phase angle, the separated flow causes the velocity to drop as the streamlines are decelerated when the airfoil continues to pitch up and the flow gets blocked by the high angle of attack of the airfoil. In fact, the effects remain until the flow reattaches at around a phase angle of $\approx 330^0$. Only after the flow is fully reestablished, does the velocity increase again. The V velocity distribution in Fig. 5b shows a velocity of about 6-8% of the free stream value at $\phi = 0^0$, i.e. at $\alpha = 10^0$, which drops to about 2-3% at $\phi = 90^0$, $\alpha = 0^0$ and starts to increase as the airfoil pitches up, reaching a peak value of $0.12U_\infty$ at $\phi = 216^0$. Once again, the value remains high as the streamlines are deflected upward while being slowed down due to massive flow separation until reattachment[4] becomes complete.

At x/c = 0.0, (the leading edge at $\alpha = 0^0$), the fluid experiences much more dramatic accelerations and decelerations through the cycle. For example, during the pitch down cycle of the airfoil $0 \leq \phi \leq 90^0$, the fluid velocity decreases from $1.2U_\infty$ to about $0.9U_\infty$. As the airfoil pitches up, the fluid around the leading edge is drawn with it and is imparted the accelerations of the moving surface and eventually by $\phi = 216^0$, it has attained a velocity of $1.3U_\infty$. As deep dynamic stall occurs, the velocity drops significantly to $0.85U_\infty$ and remains low till reattachment. The corresponding V velocities have reached values as high as 30% of the free stream value at $\phi = 0^0, \alpha = 10^0$, but decrease to about $0.15U_\infty$ at $\phi = 90^0, \alpha = 0^0$, and increase to nearly $0.6U_\infty$ at $\phi = 216^0$. During the deep dynamic stall phase of the motion, the V component of velocity remains high.

A very interesting case of the U velocity field is seen in Fig. 5a for x/c = 0.083, y/c = 0.067. (At this location, no samples could be found for $0 \leq \phi \leq 30^0$ and the airfoil blocks the beams for $190^0 < \phi < 360^0$. The non zero values shown are an artifact of the data processing routine for such cases.) As the airfoil angle of attack decreases, the velocity drops from $1.35U_\infty$ (at $\phi = 30^0, \alpha = 5^0$) to $1.05U_\infty$ at $\phi = 90^0, \alpha = 0^0$ and increases as the upward motion of the airfoil begins. At $\phi \approx 160^0$, ($\alpha = 6^0$) the maximum velocity of $1.45U_\infty$ in the cycle is reached and suddenly, over a very short phase angle range, the velocity drops by 45% to $0.8U_\infty$ and picks up slightly, before the beams are blocked by the moving airfoil. The significance of the drop is that the probe volume is penetrated by the separation bubble on the airfoil surface which moves with the airfoil and grows with increasing angle of attack. It is worth mentioning here that a bubble was also detected at this phase angle for this flow conditions in a separate study using interferometry[12]. Inside the bubble, the velocities are smaller than around it. The V velocity component remains high at $0.2U_\infty$ for most part where measurements could be obtained, but shows a drop through the bubble. The measurement point is estimated to be about 1-2%chord above the airfoil surface at this phase angle, and measurements closer could not be obtained due to the airfoil blocking the laser beams.

At x/c = 0.75 and y/c = 0.133, a point downstream of the point of oscillation, the velocity through the first half of the oscillation cycle are lower than the free stream value. But, as before, it increases during the upward motion of the airfoil until the deep dynamic stall phase of the cycle. Interestingly, the magnitude is $\approx 1.1U_\infty$ at this point and it does not drop during this phase at all. The V component is negative everywhere with a maximum of $-0.2U_\infty$. The streamlines are curving towards the airfoil surface at this location throughout the cycle and the local flow is three dimensional and turbulent during deep stall.

The above discussion provides a glimpse into the complexity of the flow field and the variety of possibilities encountered in large amplitude dynamic stall flow.

C. Velocity *vs* Phase at Different Vertical Locations: Measurements in the Separation Bubble

Fig. 6 shows the distribution of the U and V velocities with phase at x/c = 0.083. At this particular location, a separation bubble was present. Thus, the distributions in Fig. 6a show some very interesting

features. For example, at y/c = 0.067, at $\phi = 160^0$, the velocity drops as already discussed in Sec. B above. It should be noted that in unsteady flows, separation does not necessarily imply reverse flows and thus, over most of the bubble, only lower than free stream velocities were encountered. Reverse flows are expected to be present only very close to the wall and as stated earlier, measurement access down to the wall was not possible due to the beam configuration used. At the higher y/c locations, the phase angles at which the dip in velocity occurs is progressively higher due to the shape of the separation bubble and the airfoil motion till y/c = 0.150. (The data for y/c = 0.1 showed holes for $180^0 \leq 345^0$) Beyond this point, the distributions are nearly parallel, indicating that these points are clearly outside the bubble. From this data and the airfoil profile at $\phi = 200^0$, it appears that the maximum bubble height is 3-4% chord above the airfoil surface.

A look at the V component of velocity shows a nearly constant velocity through the bubble, for y/c = 0.067, till $\phi = 186^0$ where a decrease is observed. For y/c = 0.117, a gradual increase occurs through the bubble. For y/c = 0.133 and 0.150, at $\phi \approx 200^0$, $\alpha = 13.4^0$, an abrupt increase in the V velocity develops. It is believed that this change is due to the bubble breaking up at $\phi \approx 200^0$. When this happens, the streamlines around it are pushed outward and thus, an increase is seen at higher locations as well. As the dynamic stall angle is approached, the outer deflection of the streamlines is even more pronounced and this translates to even higher V velocities.

Similar trends were also measured at x/c = 0.167, but the bubble was found only at y/c = 0.083. Very closely spaced surveys by Chandrasekhara and VanDyken[13] confirmed this to be the case and also showed that the extent of the bubble is approximately 0.15c covering the range $0.017 \leq x/c \leq 0.167$.

It is interesting to compare the picture of the development of the bubble with that obtained using point diffraction interferometry (PDI) (Carr et al[12]). The interferometry results show that the bubble forms at nearly the same angle as was seen in the LDV studies and grows till it breaks up. The PDI images show that the dynamic stall vortex forms during the breaking up process and the constant density contours develop appropriate curvature subsequently on its front side. On the back side, however, the flow is very turbulent and thus, only a few density contours could be seen. The LDV data of Chandrasekhara and VanDyken[13] shows that the velocities rise when the bubble breaks at around $\phi = 200^0$, indicating a fair degree of mixing between the ambient fluid and the bubble fluid. Thus the spanwise averaged instantaneous flow measurements and the long time averaged point measurements agree reasonably well. Finer details of the flow need more sophisticated methods of extracting the flow information.

D. Velocity Profiles at Different x/c Locations

The velocity profiles at different phase angles are shown in Fig. 7a for x/c = 0.0 and in Fig. 7b for x/c = 0.083 at selected phase angles ranging from before the bubble formation to after occurence of deep dynamic stall. It is clear that the range of the velocities is much larger at x/c = 0.083 than at x/c = 0.0. For example, at y/c = 0.1, the maximum velocity is $1.6U_\infty$ at $\phi = 150^0$ and $1.64U_\infty$ at $\phi = 171^0$. The corresponding values for x/c = 0.0 are $1.56U_\infty$ and $1.52U_\infty$ respectively. Regardless, it is much higher than the free stream value and is due to two factors: (1) airfoil angle of attack and (2) the airfoil motion. Ericsson[14] has referred to the latter as the 'moving wall effect' wherein the fluid in the boundary layer is energized by the rapidly moving airfoil, thus acquires the ability to resist the adverse pressure gradient and hence, separation is delayed. A quantitative documentation of this effect was hitherto not available. The present results show that the 'leading edge jet effect' resulting in the *wall jet* like velocity distribution actually is felt considerably into the outer flow and is not just confined to near the wall. Also, it extends sufficiently downstream over the airfoil. Despite the fact that the velocities decrease in the separation bubble, the velocity immediately outside of it is extremely large, about $1.6U_\infty$. The acceleration is being felt from very low angles of attack, in fact, even at $\alpha < 5^0$ and thus, is clearly due to the moving wall because, at low angles of attack, the velocity at the leading edge is not very large and also, the dynamic stall vortex has not yet formed and thus, the flow is still attached and follows the airfoil profile. It is also to be noted that the velocity of the airfoil leading edge is a maximum of $\approx 3\%$ of the free stream value, but still the effects of the airfoil pitching are very strong. This implies that the degree of unsteadiness, if measured as a ratio of the leading edge velocity to the free stream velocity, shows a large effect even at very low values.

As the airfoil angle of attack increases beyond the static stall angle (12.4^0), the fluid velocity closer to the surface decreases as can be seen in Fig. 7a and 7b. Also, in Fig. 7b, a *wake like* profile emerges for $\phi > 198^0$. This change is believed to be due to the opening out of the bubble and the gushing of the fluid surrounding it immediately following the event. Further, the location of the maximum defect moves closer to the surface as the angle of attack increases. Typical velocity defects measured were about $0.2U_\infty$.

Fig. 7c shows the velocity profiles at x/c = 0.583. At low phase angles, $\phi \leq 200^0$, the profiles are the same as the local boundary layer as at this location, it is about 4-5% chord thick depending upon the angle of attack. Thus, a few measurement points could be obtained. At larger phase angles, at this location, the effect of the dynamic stall vortex is felt strongly. The vortex increases the velocity in the outer flow and decreases in the inner flow. It appears that the flow is very turbulent and unsteady within the vortex. Thus, measurements during its passage through the measurement voulme, show the effects as wiggles in the velocity profiles. The effect propagates to larger y/c locations as the angle of attack increases and the vortex grows in size. No negative U velocities were measured anywhere in the measurement grid and thus, the vortex as such could not be identified. But, the large scale distortions in the profiles are indicative of the passage of the vortex. (see also Sec. G)

E. Global Distributions of Absolute Velocity

Fig. 8 shows the absolute velocity vectors plotted at the local flow angle in the flow field. Fig. 8a is drawn for $\phi = 90^0$, or $\alpha = 0^0$ and indicates that even though the airfoil is at zero degrees angle of attack, the velocities over the airfoil exceed the free stream slightly. The vertical velocities were found to be non zero for this condition even in the outer flow, a clear indication of the presence of hysterisis effects of oscillation. Closer to the airfoil leading edge, in addition, the fluid still has to negotiate the curvature and hence, a slight positive (upward) velocity is measured. The figure shows that the streamlines are nearly horizontal, except around the leading edge.

Fig. 8b shows the absolute veloity field at $\phi = 201^0, \alpha = 13.58^0$. The rapid flow accelerations are clearly seen well into the outer flow in it, as also, the wake like distributions discussed above at x/c = 0.083. The slowing down of the flow is also evident near the airfoil surface at larger x/c locations. From the orientation of the velocity vectors it can be inferred that the vertical velocities around the leading edge are large. In fact, the V velocity could reach a value of $0.5U_\infty$. The effects of the airfoil motion are seen once again at very large (0.5c) y/c values. The effects are the strongest at both upstream locations (x/c = -0.083 and x/c = 0.0) and at x/c = 0.083. By x/c = 0.25, the fluid is turning inward and as the fluid moves downstream, it turns even more. The schlieren studies of Chandrsaekhara and Carr[4] have shown that at this angle of attack, the dynamic stall vortex has just formed, and the measured behavior is consistent with that study. In general, the outer flow is only slightly turning, but the inner flow streamlines are curving strongly upward around the leading edge, but by x/c = 0.25, the flow is pointing downward. Also, the decreasing velocities closer to the surface at larger x/c distances are also clearly seen.

At $\phi = 216^0$, the airfoil is at the dynamic stall angle and the velocity profiles exhibit large changes at some locations, and the dynamic range is also large. Yet, no negative velocities are seen. Even in the region enveloped by the leading edge shear layer and the dynamic stall vortex, large velocities are seen. One of the reasons for this is that the reverse flow region is expected to be only about 2-3% chord thick at best and the negative velocities in it are likely to be small. Since the vortex is being convected at $0.3U_\infty$[4], it is unlikely that large reverse flow velocities will be encountered. Once again, the vectors show that at this angle of attack, the leading edge flow has been pushed away from the airfoil, an effect felt over wide distances.

Fig. 9a presents the contours of the absolute velocity for some of the above cases. It is seen that even at $\alpha = 0^0$, the velocity range is from 0.88 - $1.1U_\infty$. At $\alpha = 8.95^0$, Fig. 9b, the contour lines (12) show a maximum velocity of $1.45U_\infty$. It is found in a pocket of fluid above the airfoil surface. Between this fluid and the airfoil, lower velocities could be found. It should be recalled here that a separation bubble was detected here. In Fig. 9c, as the angle of attack increases to 14.07^0, the peak velocity reaches $1.55U_\infty$, but the fluid is at 0.1c above the surface, at x/c = 0.08 - 0.1. Also, the leading edge wall jet effect is seen clearly. Further, following contour line 15, the wake like profile could also be found between x/c = 0.16 - 0.2. Regions of low velocity are developing beyond x/c = 0.3, but near the leading edge, at y/c = 0.05, the velocity is still $1.15U_\infty$. This figure resembles the interferogram obtained for the same conditions(Carr et al[14]). Finally, in Fig. 9d, at $\phi = 216^0$, it is interesting to note that several pockets of high fluid velocity ($1.4U_\infty$, contour line 19) form in the shear layer extending to x/c = 0.45 and y/c = 0.25. The velocities around the leading edge are still large, even under this condition. But, the flow towards the trailing edge is moving very slowly at $0.5U_\infty$. Significant structure can also be seen in the flow.

F. Vorticity Distributions

The z-component of vorticity (normalized by $\frac{c}{U_\infty}$) was calculated from the measured U and V components of velocities by first fitting a cubic spline curve to the data and interpolating the velocities in a grid at a resolution of 1.25mm - using a second order central differencing scheme. Thus, the noise level in the distributions is expected to be high at about 20% of the local maximum vorticity values (in both the positive and negative quantities). The following discussion about the vorticity field should be still valid, especially before the dynamic stall vortex begins to convect (see also Sec. G), because no discontinuities such as shocks were encountered within the measurement grid. The picture of the flow field thus is also quantitatively valid up to the point where the particles were able to follow the flow adequately.

Fig. 10a shows that at $\phi = 171^0$ ($\alpha = 8.44^0$), a region of clockwise vorticity has developed over the airfoil, just around the location of the separation bubble, with a peak vorticity of -8 units in it. A region of counter clockwise vorticity could also be found above it, but the peak vorticity in it is only about 5 units. As the airfoil reaches an angle of attack of 10 degrees, Fig. 10b, the clockwise vorticity has increased to -11 units, whereas the anticlockwise vorticity is still at 5 units. The extent of the vortical region has grown to about 25%chord in both the x and y directions. As the airfoil pitches to higher angles of attack, the vorticity should steadily increase until stall occurs. Fig. 10c shows that at $\phi = 198^0$, this is the case as the clockwise vorticity has doubled to -22 units, but the anticlockwise vorticity has only increased to about 10 units. Earlier experiments[4] have shown that the vortex begins to convect at around this phase angle. The separation bubble also bursts around the same angle of attack. Thus, a combined effect is felt by the airfoil, which should be seen in its vorticity field. By the time dynamic stall occurs, at $\alpha = 15.9^0$, the clockwise vorticity has increased to about -31 units, but the counter clockwise vorticity is still small at 12 units. Beyond this angle, the vortex is shed and so the total circulation over the airfoil should decrease.

Fig. 11 presents a plot of the 'net circulation' over the measurement grid. The computed vorticities were integrated by including only the values that were above the noise level (arbitrarily chosen to be 25% of the local maximum) for vorticity of both signs

to get the circulation. This graph has the same limitations as the vorticity field. However, some clear trends are evident and hence, the results are presented. It can be seen that the 'net circulation' monotonically increases till phase angle of 200^0 is reached when the vortex convection starts. Nearly a 10 fold increase was obtained in the upstroke of the airfoil from $\alpha = 5^0$ to $\alpha = 13^0$. The changes seen between $\phi = 200^0 - 216^0$ are believed to be due to the inability of the LDV seed particles to follow the rapid changes in the flow. However, near the dynamic stall angle, a slowly decreasing trend is observed. Some of the discrepancies noted here are due to the fact that the entire upper surface data has not yet been obtained and also due to the approximations made in reaching this stage.

G. Discussions of the Measurement Challenges

The measurements reported in this paper were obtained after partially solving some of the formidable challenges posed by the flow, flow geometry and the measurement technique. It is worth stating before proceeding further that the mean velocity measurements repeat to within 5% at any given station over most of the oscillation cycle. The unsteady nature of the flow and the large amplitude of oscillation of the experiment required acquiring a very large amount of data over the cycle to realize low uncertainty levels. The 10,000 samples/per point collected in this experiment ensures that this can be achieved, but a better accuracy could be obtained if a much larger number of samples, say 50,000 could be obtained. However, the extent of the flow field surveyed would mean an experiment that runs for several months with the airfoil oscillating, leading to other difficulties. This would still not guarantee that adequate number of samples will be found in each phase angle bin of interest from 180^0 to 216^0 due to the randomness of the particle arrival rate in the probe volume. The problems of the particle arrival in the measurement volume and particle lag are especially accute after the vortex forms and convects because the particles have to follow the rapid accelerations experienced by the flow in the shear layer that envelops the vortex. Given that the frequency of oscillation is 21.6 Hz and hence that the vortex is shed about once every 50 milliseconds, this is a challenge. In addition, the formation, growth and movement of the vortex all occur in approximately 5 milliseconds. At M = 0.3, with the range of velocities encountered, the particles are subject to an acceleration of $O\ ((10^3 - 10^4) m/s^2)$. It is clear that most particles may not be following the flow under these conditions. The small particles that may follow the flow would not scatter sufficient light to provide a good signal to noise ratio. The large dynamic range of the flow also reduces the SNR (as SNR is inversely proportional to bandwidth). It may be recalled here that in the present measurements, the system gains were optimized to get good signals over the whole cycle, that is, the gains were set intentionally some what low so that these measurements could be obtained. Hence, low amplitude signals would not have been validated and thus, some of the signals from the backside of the vortex would have been lost. The smallest velocity measured anywhere was about $0.15U_\infty$ as seen in histograms at some locations. These are largely responsible for the vortex not being seen in the measurements. Special seeding methods may mitigate this problem slightly, as also, conducting the experiment with large gains in the system with a method that validates the data below a preset amplitude limit so that only signals from small particles are indeed picked up and validated. Limiting the measurement to the phase angle range of interest would help too as in this method of measurement, a required number of samples will be obtained at each phase angle, rather than a total number in the whole cycle (This would also increase the experiment time enormously). The blockage of the beams by the airfoil will only add to these difficulties. All in all, the measurements are extremely difficult and some success has been achieved in the present study. Not seeing the dynamic stall vortex does not limit the usefulness of the data in anyway because the goal is to understand its formation and possible prevention. The 'game' is already 'lost' when the vortex begins to move.

5. Concluding Remarks

1. Velocity data over an oscillating airfoil in dynamic stall have been obtained for the first time. The velocity field exhibits interesting features over the entire domain of measurement.

2. The data show the formation of a separation bubble over the airfoil surface and its bursting just around where the dynamic stall vortex forms.

3. The velocity profiles over the airfoil change from that of a leading edge wall jet to a wake like distribution in an oscillation cycle depending upon the flow in the bubble.

4. The velocity field shows that the flow experiences rapid accelerations over a large region of the airfoil with values as high as $1.6U_\infty$ at a free stream Mach number of 0.3 and a reduced frequency of 0.05. Instantaneously, the velocities reached magnitudes of $1.8U_\infty$, but, no supersonic velocities were observed. It is believed that the formation of the bubble has modified the local pressure distribution sufficiently to grossly alter the flow.

5. The extent of the moving wall effect has been quantified and it is found to be much greater than previously assumed as flow accelerations can be seen at large distances (y/c = 0.5) from the airfoil.

6. Circulation (estimated from vorticity) was shown to increase monotonically until the dynamic stall vortex begins to convect.

7. The fact that the dynamic stall vortex was not found distinctly has been attributed to the limitations of the measurement technique and some possible methods of capturing it are offered. Further studies using the alternate methods of measurements discussed are expected to provide a more comprehensive information of the flow field.

Acknowledgements

The work was supported by the Army Research Office grant (MIPR-ARO-132-90) to the Naval Post-

graduate School and was monitored by Dr. Thomas L. Doligalski. Additional support was provided by AFOSR (MIPR-91-0007) (monitored by Maj. D.Fant) and by NAVAIR (monitored by Mr. Thomas S. Momiyama). The support provided by Dr. S.S. Davis, Chief, Fluid Dynamics Research Branch and other staff members at FML and the software development contributions of Mr. P.J.Trosin, Sterling Software are all gratefully acknowledged.

6. References

[1]Carr, L.W.,"Progress in Analysis and Prediction of Dynamic Stall," *Jl. of Aircraft*, Vol. 25,No.1, Jan. 1988, pp. 6-17.

[2]McCroskey, W.J., "The Phenomenon of Dynamic Stall," NASA TM 81264, March 1981.

[3]Harper, P.W., and Flanigan, R.E., "The Effect of Change of Angle of Attack on the Maximum Lift of a Small Model," NACA TN 2061, March 1950.

[4]Chandrasekhara, M.S., and Carr, L.W., "Flow Visualization Studies of the Mach Number Effects on the Dynamic Stall of Oscillating Airfoils", *Jl. of Aircraft*, Vol. 27, No. 6, June 1990, pp. 516-522.

[5]Chandrasekhara, M.S., and Brydges, B.E., "Amplitude Effects on Dynamic Stall of an Oscillating Airfoil", *AIAA Paper No. 90-0575*, Jan. 1990.

[6]Chandrasekhara, M.S., Carr, L.W., and Ahmed, S., "Pitch Rate History Effects on Dynamic Stall", presented at the *NASA/AFOSR/ARO Workshop on Physics of Forced Unsteady Flow Separation*, April 1990.

[7]De Ruyck, J., Hazarika, B., and Hirsch, Ch., "Transition and Turbulence Structure in the Boundary Layers of an Oscillating Airfoil", *Final Technical Report*, VUB Report STR-16, Vrije Universiteit Brussel, Brussels.

[8]Grohsmeyer, S.P., Ekaterinaris, J.A., and Platzer, M.F., "Numerical Investigation of the Effect of Leading Edge Geometry on Dynamic Stall on Airfoils", *AIAA Paper No. 91-1798*, June 1991.

[9]Ekaterinaris, J.A., "Compressible Studies on Dynamic Stall", *AIAA Paper No. 89-0024*, Jan. 1989.

[10]Courier, J., and Fung, K.Y., "An Analysis of the Onset of Dynamic Stall", *AIAA Paper No. 91-0003*, Jan. 1991.

[11]Carr, L.W., and Chandrasekhara, M.S., "Design and Development of a Compressible Dynamic Stall Facility", *AIAA Paper No. 89-0647*, to appear in *Jl. of Airccraft*.

[12]Carr, L.W., Chandrasekhara, M.S., and Brock, N., "A Quantitative Visual Study of Unsteady Compressible Flow on an Oscillating Airfoil", *AIAA Paper No. 91-1683*, June 1991.

[13]Chandrasekhara, M.S., and VanDyken, R.D., "Oscillating Airfoil Velocity Field During Large Amplitude Dynamic Stall", *Proc. 8^{th} Symposium on Turbulent Shear Flows*, Sep. 8-11, 1991, Münich, West Germany.

[14]Ericsson, L.E., "Moving Wall Effects in Unsteady Flow", *Jl. of Aircraft*, Vol. 25, No. 11, Nov. 1988, pp. 977-990.

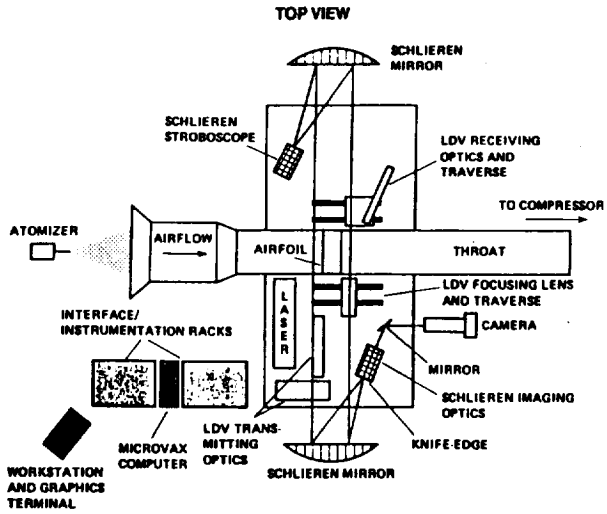

Fig. 1. Schematic of the CDSF Instrumentation.

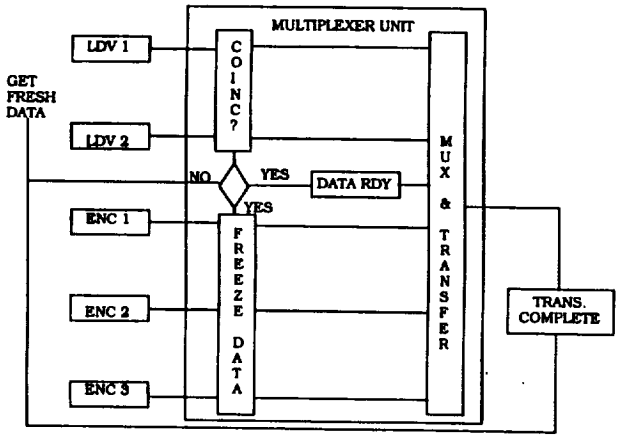

Fig. 2. Schematic of the LDV Data Acquisition Method.

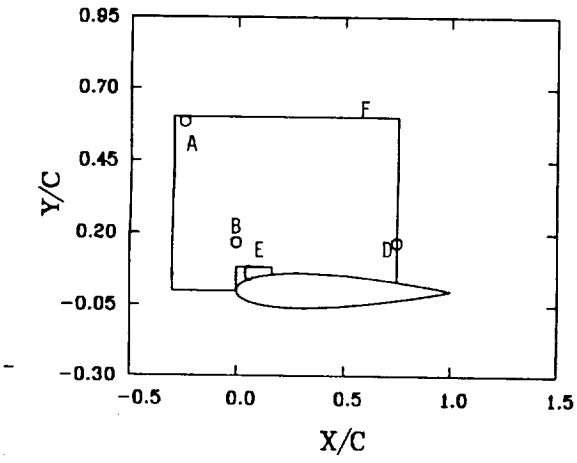

Fig. 3. Flow Domain for Discussion of Results.

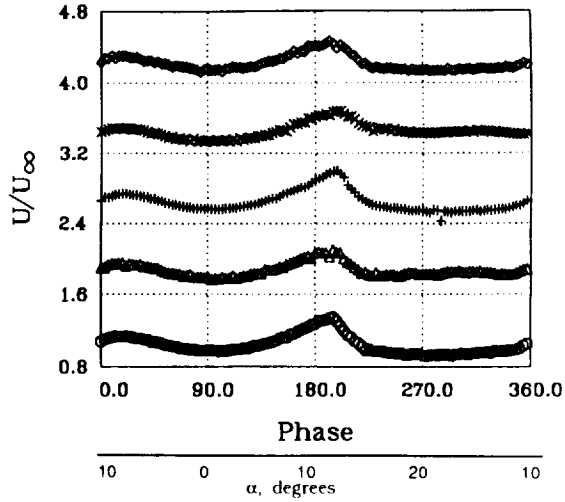

Fig. 4. Two Dimensionality Surveys: Normalized U Velocity Component, (Velocity Offset by $0.8\frac{U}{U_\infty}$), x/c = 0.0, y/c = 0.167.
o, z/c = -1.0; △, z/c = -0.5; +, z/c = 0.0; x, z/c = 0.5; ◇, z/c = 0.833.

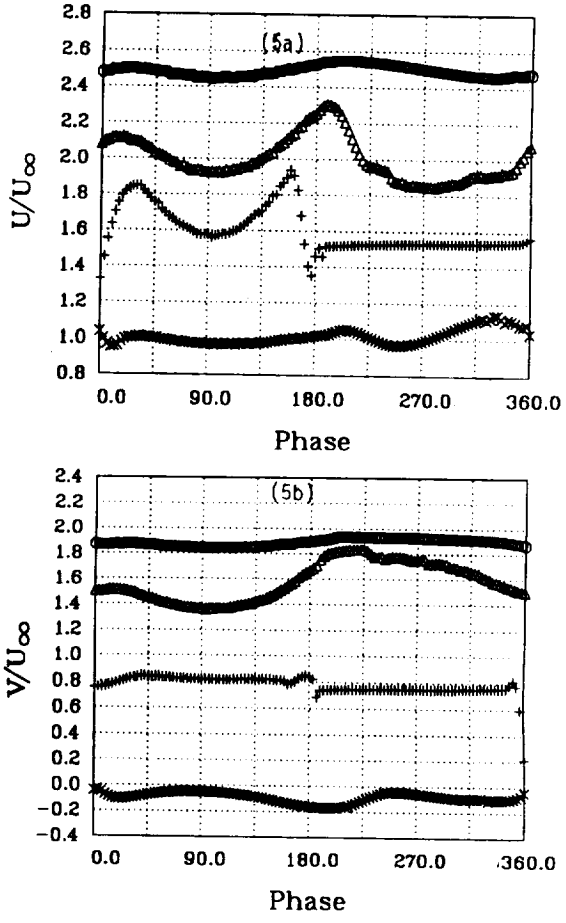

Fig. 5. Typical Velocity Distributions With Phase: (a) U Component (Velocity Offset by $0.5\frac{U}{U_\infty}$), (b) V Component (Velocity Offset by $0.6\frac{U}{U_\infty}$).
o, x/c = -0.25, y/c = 0.583; △, x/c = 0.0, y/c = 0.117; +, x/c = 0.083, y/c = 0.067; x, x/c = 0.750, y/c = 0.133.

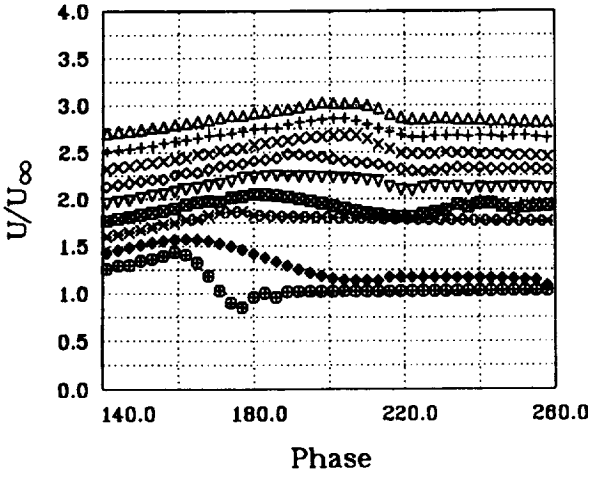

Fig. 6a.

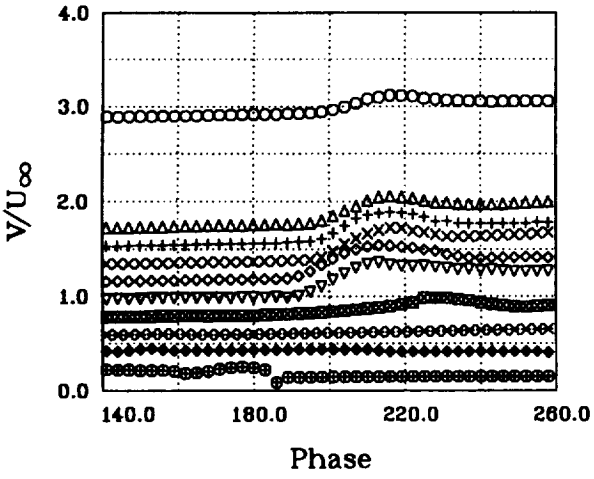

Fig. 6b.

Fig. 6. Measurements in the Separation Bubble: (a) U Component, (b) V Component, (Velocity Offset by $0.2\frac{U}{U_\infty}$), x/c = 0.083.

○	Y/C = 0.300	▽	Y/C = 0.133
△	Y/C = 0.200	⊠	Y/C = 0.117
+	Y/C = 0.183	×	Y/C = 0.100
×	Y/C = 0.167	◆	Y/C = 0.083
◇	Y/C = 0.150	⊕	Y/C = 0.067

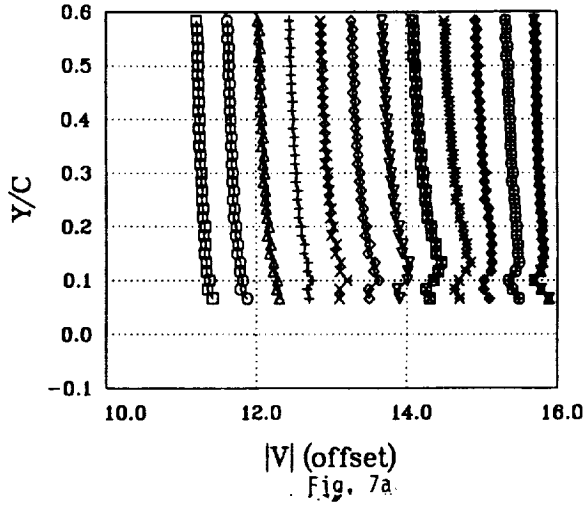

Fig. 7a.

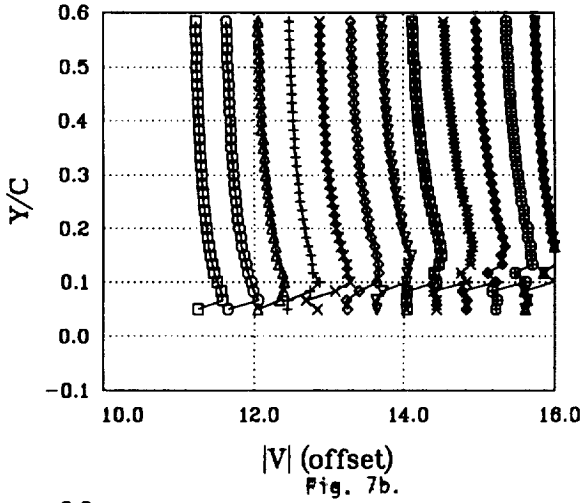

Fig. 7b.

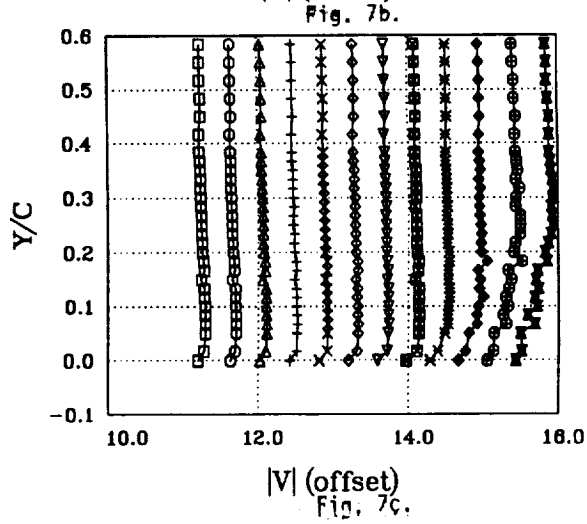

Fig. 7c.

Fig. 7. Absolute Velocity Distributions With Phase (Velocity Offset by $0.2\frac{U}{U_\infty}$ at Each Phase), (a) x/c = 0.0, (b) x/c = 0.083, (c) x/c = 0.583.

⊟	φ=153.0 ,SHIFT= 10.20	▽	φ=189.0, SHIFT= 12.60
⊖	φ=159.0, SHIFT= 10.60	■	φ=195.0, SHIFT= 13.00
△	φ=165.0, SHIFT= 11.00	×	φ=201.0, SHIFT= 13.40
+	φ=171.0, SHIFT= 11.40	◆	φ=207.0, SHIFT= 13.80
×	φ=177.0, SHIFT= 11.80	⊕	φ=213.0, SHIFT= 14.20
◆	φ=183.0, SHIFT= 12.20	■	φ=219.0, SHIFT= 14.60

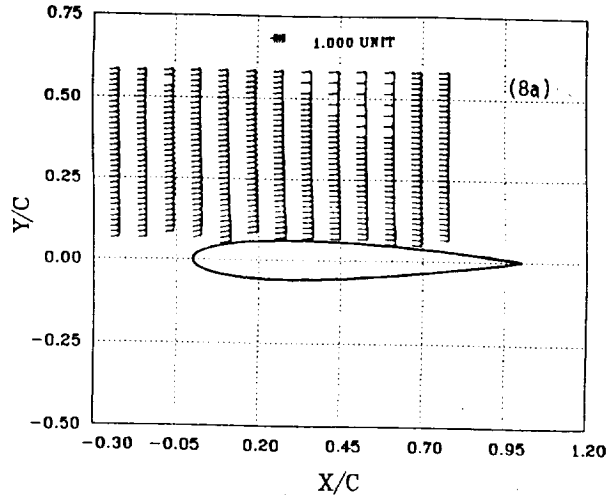

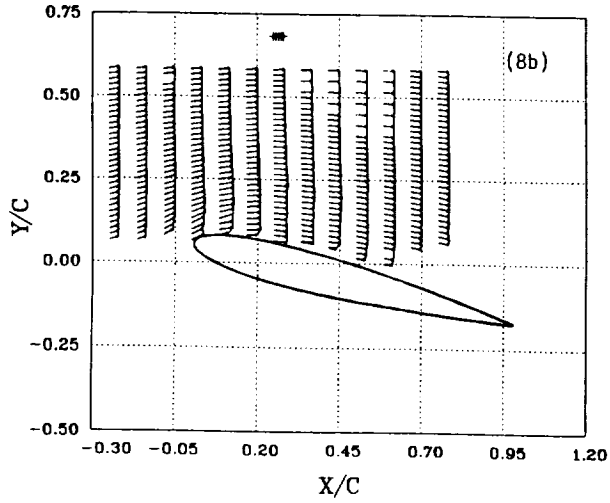

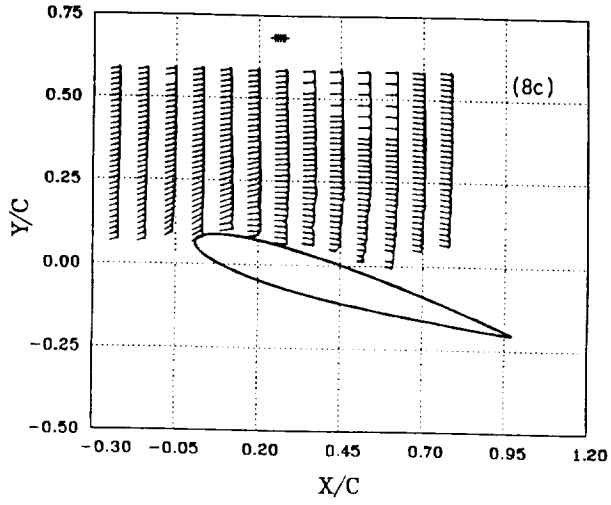

Fig. 8. Absolute Velocity Distribution: (a) $\phi = 90^0, \alpha = 0^0$, (b)$\phi = 201^0, \alpha = 13.6^0$, (c) $\phi = 216^0, \alpha = 15.9^0$.

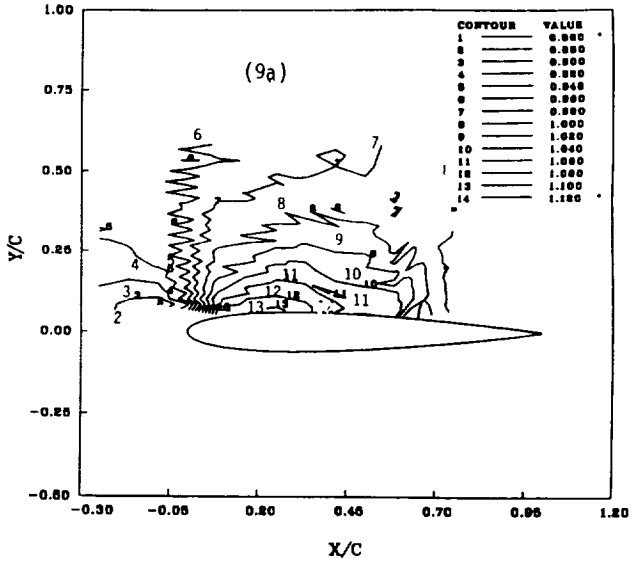

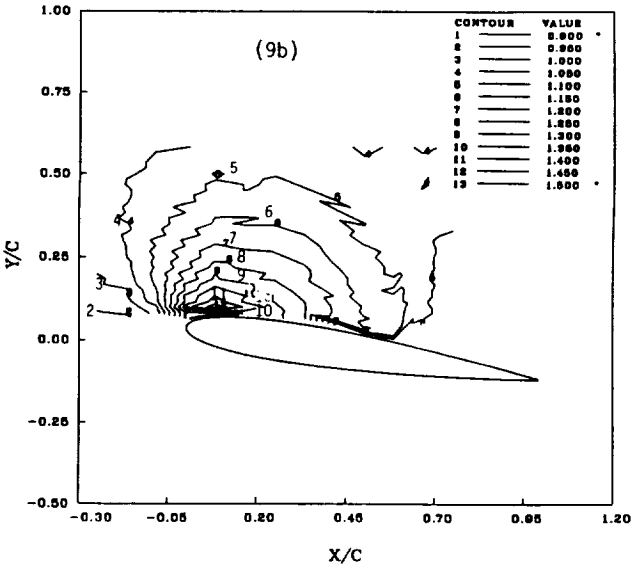

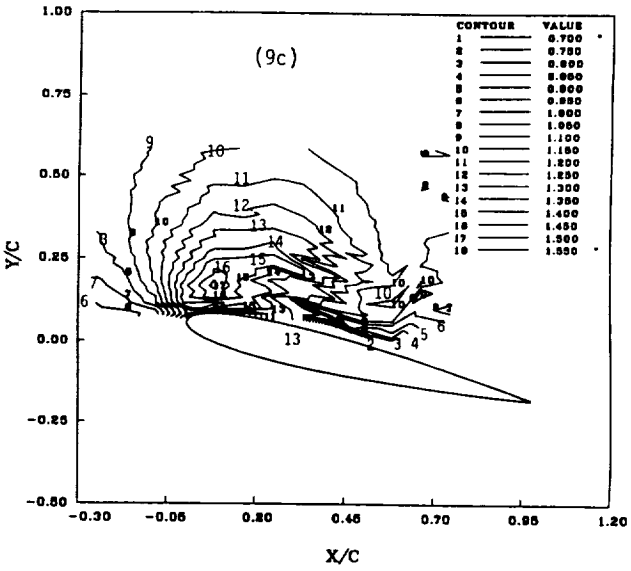

Fig. 9. Contours of Absolute Velocity: (a) $\phi = 90^0, \alpha = 0^0$, (b)$\phi = 174^0, \alpha = 8.95^0$, (c) $\phi = 204^0, \alpha = 14.07^0$ (Continued), *, No Contour Lines Found.

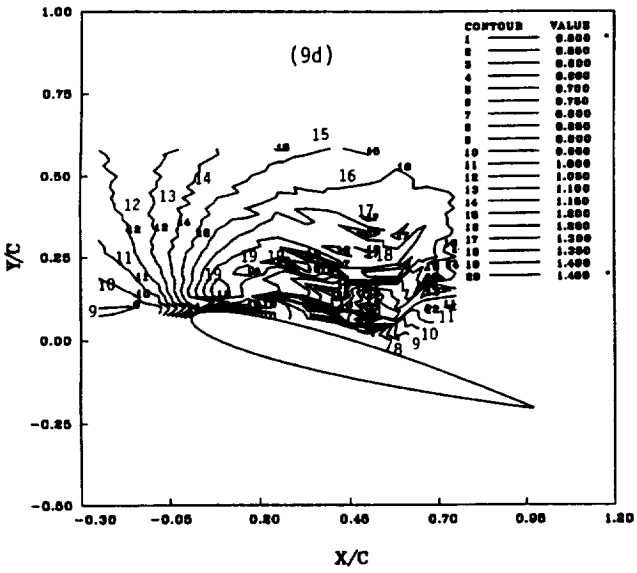

Fig. 9 (d) $\phi = 216^0, \alpha = 15.9^0$, (Concluded).

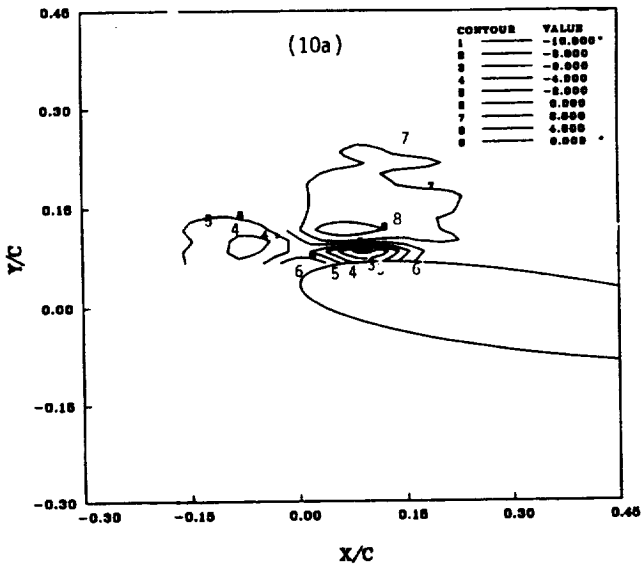

Fig. 10. Contours of Normalized z-Component of Vorticity: (a) $\phi = 171^0, \alpha = 8.44^0$, (Continued), *, No Contour Lines Found.

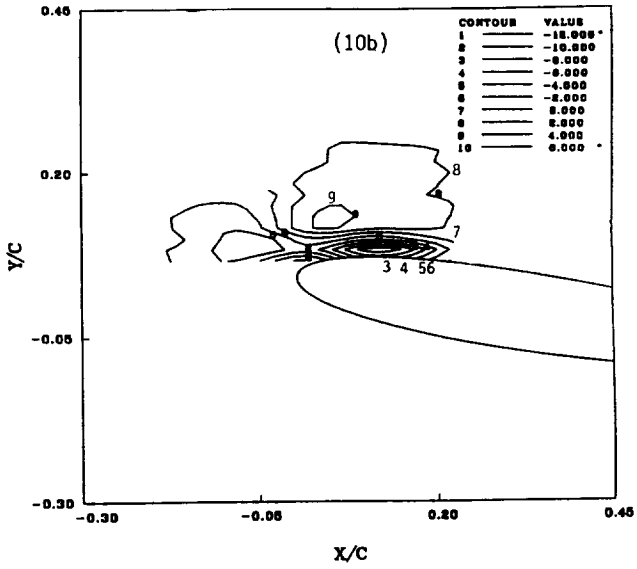

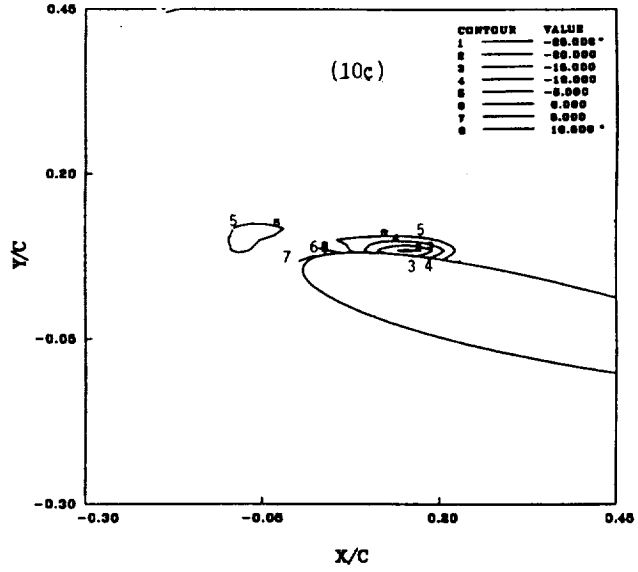

Fig. 10. (b)$\phi = 180^0, \alpha = 10.0^0$, (c) $\phi = 198^0, \alpha = 13.09^0$, (concluded).

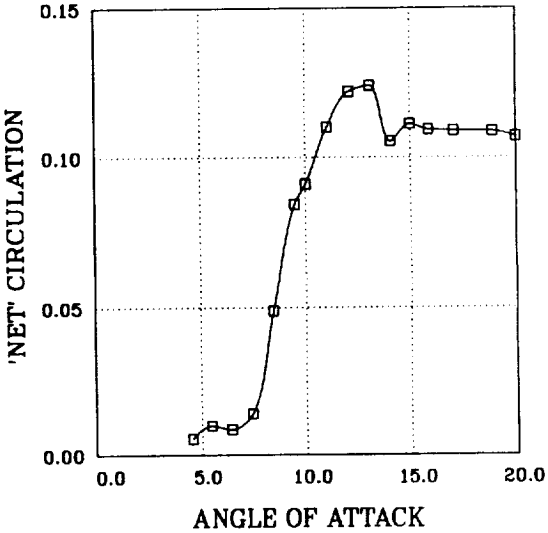

Fig. 11. Variation of 'Net Circulation' With Angle of Attack.

APPENDIX C

AIAA 91-3225

Reattachment Studies of an Oscillating Airfoil Dynamic Stall Flow Field

S. Ahmed, MCAT Institute, San Jose, CA;
M. S. Chandrasekhara, Naval Postgraduate School and Navy-NASA Joint Institute of Aeronautics, Monterey, CA.

AIAA 9th Applied Aerodynamics Conference
September 23-25, 1991 / Baltimore, MD

Reattachment Studies of an Oscillating Airfoil Dynamic Stall Flow Field

S.Ahmed[1,3]
MCAT Institute, San Jose, CA 95127

and

M.S.Chandrasekhara[2,3]
Navy-NASA Joint Institute of Aeronautics,
Fluid Mechanics Laboratory, NASA Ames Research Center,
Department of Aeronautics and Astronautics,
Naval Postgraduate School, Monterey, CA 93943

Abstract

The reattaching flow over an oscillating airfoil executing large amplitude sinusoidal motion around a mean angle of attack of 10 degrees has been studied using the techniques of stroboscopic schlieren, two component laser Doppler velocimetry and point diffraction interferometry, for a free stream Mach number of 0.3 and a reduced frequency of 0.05. The results show that the dynamically stalled flow reattaches in a process that begins when the airfoil is very close to the static stall angle on its downward stroke and progresses over the airfoil through a large range of angles of attack as the airfoil angle decreases to about 6 degrees. The airfoil suction peak shows a dramatic rise as the static stall angle is approached and the velocity profiles develop such that the flow near the surface is accelerated. The process completes through the disappearance of a separation bubble that forms over the airfoil.

Nomenclature

C_p	pressure coefficient
$C_{p_{max}}$	maximum pressure coefficient
c	airfoil chord
f	frequency of oscillation, Hz
k	reduced frequency = $\frac{\pi f c}{U_\infty}$
M	free stream Mach number
U,V	velocity components in the x and y directions
U_∞	free stream velocity
$\|V\|$	absolute velocity
x,y	chordwise and vertical distance
α	angle of attack
α_o	mean angle of attack
α_m	amplitude of oscillation
γ	ratio of specific heats
ϵ	fringe number
ρ	density
ρ_r	density at reference conditions
ϕ	phase angle of oscillation
ω	circular frequency, radians/sec

1. Introduction

Flows over oscillating airfoils have received considerable attention with a view to improve the performance of the retreating blade of a helicopter. The retreating blade performance is limited by flow separation leading to dynamic stall. A comprehensive review of dynamic stall and its events is given by Carr[1]. The flow eventually reattaches later in the cycle and depending upon the mean angle of attack, amplitude and frequency of oscillations, a hysteresis loop of varying size develops, McCroskey[2]. It is known that the hysteresis loop determines the aerodynamic damping. Whereas extensive studies have been carried out on oscillating airfoils to understand the dynamic stall process, the reattachment of the unsteady separated flows has received little attention. Reattachment of unsteady separated flows is a topic of basic research in itself, as several issues of flow separation and attachment are involved, such as the local pressure gradient, the state of the separated shear layer and its ability to overcome the adverse pressure gradient and so on. An understanding of the process may also help in modifying the flow. For example., if the process can be completed rapidly, the airfoil can generate more lift through the cycle, thus altering its performance. The changes in the pressure distribution that occur over the airfoil may for some conditions cause limit cycle oscillation. A parameter based on the pitching moment of the airfoil (which in turn is dictated by the hysteresis loop) was defined[2] to determine the aerodynamic damping over the cycle of oscillation. It was observed that the damping could become negative during certain parts of the cycle resulting in an increase in the amplitude of oscillations leading to

[1] *Research Scientist; Member AIAA. On Leave from National Aeronautical Laboratory, Bangalore, India*

[2] *Assistant Director and Adjunct Research Professor; Associate Fellow, AIAA.*

[3] **Mailing Address: M.S. 260-1. NASA Ames Research Center, Moffett Field, CA 94035**

stall flutter. An understanding of the reattachment process is therfore essential to alleviate the stall flutter and improve the dynamic lift characterisitics of an oscillating airfoil.

Niven et al[3] made the first and only attempt to analyze the reattachment of separated flow of a two dimensional wing undergoing ramp-down motion through surface pressure measurements. This study showed that the reattachment process occurs over a finite length of time and the airfoil incidence at reattachment was found to be close to the static stall angle. However, no flow field measurements were available to understand the physics involved in the process. The present study at the Navy - NASA Joint Institute of Aeronautics being conducted in the NASA Ames Research Center, Fluids Mechanics Laboratory(FML) is aimed at understanding the mechanisms involved in the separation and reattachment of flows associated with oscillating airfoils through flow field analysis using a variety of experimental techniques. The experimental techniques used included the schlieren method for qualitative analysis of the global flow field, laser Doppler velocimetry (LDV) for quantitative measurements of the velocity field, and point diffraction interferometry (PDI) for measurements of density and pressure distributions.The initial studies of the dynamic stall problem were confined to the upstroke of the oscillation cycle to understand the mechanism of separation leading to the dynamic stall and the effects of compressibility on dynamic stall. Results of schlieren studies by Chandrasekhara and Carr[4] on an oscillating airfoil have indicated that compressibility effects set in at M=0.3. Further studies by Chandrasekhara and Ahmed[5] using LDV have shown the formation of a separation bubble near the leading edge prior to the formation of a dynamic stall vortex. Studies with the PDI technique by Carr et al[6,7] have confirmed the presence of a separation bubble and shown that the flow gradients are slow to develop in the oscillatory case compared to the steady state resulting in the delay of stall known as dynamic stall.

In this paper, results obtained on an oscillating NACA 0012 airfoil as it executes the downward stroke are presented. Flow field data obtained using three different experimental techniques are discussed and an attempt is made to describe the reattachment process of the separated flow field.

2. Description of the Experiment

2.1. Facility

The experiments were conducted in the FML Compressible Dynamic Stall Facility (CDSF). The CDSF is an indraft wind tunnel with a 35cm. X 25cm. test section. The oscillatory motion is produced by a drive system located on top of the test section connected to the test section windows by connecting rods on either side. The windows are mounted in bearings and the airfoil is supported between the windows with pins smaller than the local airfoil thickness. This provides optical access to the airfoil surface as well. Sinusoidal motion of the windows results in a sinusoidal variation of the airfoil angle of attack.

The drive is equipped with incremental position encoders that provide the airfoil instantaneous angle of attack and frequency/phase angle of oscillation. An absolute position encoder indicates the angle of attack. The specifications of the tunnel and drive system are:

$$\alpha = \alpha_o + \alpha_m \sin 2\pi ft = \alpha_o + \alpha_m \sin \omega t$$

$$0 \leq \alpha_o \leq 15^\circ$$

$$2^\circ \leq \alpha_m \leq 10^\circ$$

$$0 \leq f \leq 100Hz$$

$$0 \leq M \leq 0.5$$

$$200,000 \leq Re \leq 10^6$$

airfoil chord = 7.62cm.

The airfoil angle, reduced frequency and Mach number correspond to those of a helicopter in forward flight and the Reynolds number corresponds to that of a $\frac{1}{7}$th scale model rotor, whose test results are directly applicable to a helicopter rotor.

The tunnel is connected to a 240,000 CFM, 9,000 HP evacuation compressor that allows continuous running at all flow speeds. All other details of the system could be found in Carr and Chandrasekhara[8].

2.2. Measurement Techniques

Three different nonintrusive optical diagnostic techniques were used in the study. These were (A) stroboscopic schlieren (B) two component, frequency shifted and phase averaged LDV (C) stroboscopic point diffraction interferometry(PDI) and are described below.

A. Stroboscopic schlieren studies

Fig. 1 shows the schematic of the schlieren and LDV system used. A standard 3m. focal length mirror based schlieren system was set up in a 'Z' type configuration with a Xenon arc lamp light source at the focal length of one of the mirrors. The beam passing through the test section was focused on to a vertical knife edge and then imaging optics. The light source was triggered externally at the desired phase angles by an electronic circuit which compared the chosen phase angle of oscillation and the encoder data from the drive system and produced a TTL pulse when a match occured. No delays were found to be present between the events of matching the phase angle and the light flashing.

B. Unsteady flow LDV studies

A two color, two component, frequency shifted Argon-Ion laser based TSI system was used for velocity measurements. The system was operated 15° off-axis, in the forward scatter mode. Traversing was accomplished by directing the 4 beams on to a 352mm. focal length lens mounted on a computer controlled

traverse. The signals were processed by TSI 1990 counters.

Phase locking circuitry specially built for handling the random LDV data and the unsteady position data were used as an integral part of the data acquisition instrumentation. The LDV data was acquired in the coincidence mode as determined by a NASA LDV multiplexer, with the coincidence window-width arbitrarily chosen as $50\mu sec$. The coincidence pulse was used to trigger data acquisition and freeze the rapidly changing encoder values till data transfer to the computer could be completed. The schematic of the method used is depicted in Fig. 2. The software for data acquisition and processing included the standard tests of data validation, phase averaging by binning the data appropriately, identifying gaps in the data if the number of samples in any bin was less than a preselected value (50 in this case) and providing phase distributions of the velocity components. Any time the standard criteria were not satisfied, the data set was rejected and new data was acquired. Seeding was accompished by injecting $1\mu m$ polystyrene latex particles suspended in alchohol into the tunnel inlet. A minimum of 10,000 samples were collected per channel at each measurement point. The complete details of the scheme can be found in Chandrasekhara and Ahmed[5].

C. PDI studies

PDI is a real-time interferometry technique that uses fluid density changes to produce flow interferograms. Fig. 3 shows the schematic of the optical arrangement used. The optical arrangement is based on a standard schlieren system, with a pulsed Nd-YAG laser serving as the light source and a predeveloped photographic plate being used at the knife edge plane. The principle has been detailed in Ref. 6 and 7 and is only briefly described here. A pinhole is created (burned) *in-situ* in the photographic plate by increasing the laser energy, with no flow in the wind tunnel. This serves to act as a point diffraction source, producing spherical reference waves. When the flow is turned on, the cylinder of light passing through the test section experiences phase shifting depending upon the local flow conditions and the beam exiting the tunnel window focuses to a slightly larger spot around the pinhole. The portion of the light that passes through the pinhole loses all the phase information introduced by the flow due to the spatial filtering characteristics of the pinhole and thus becomes the reference wave. This reference wave subsequently interferes with the light that was transmitted around the pinhole through the photographic plate, creating real time fringe patterns, at the image plane of the optics system. Ref. 9 describes the other details of the actual implementation of the technique in the CDSF. In operation, the laser was triggered stroboscopically, as was done in the schlieren studies; a pulse generated by a photo diode that responds to the actual laser light pulse was used to freeze the encoder display to record the actual phase angle at which an interferogram was obtained.

2.3. Experimental Conditions

The flow Mach number was set to 0.3; the corresponding Reynolds number was 540,000. The oscillation frequency was 21.6 Hz, which corresponded to a reduced frequency of 0.05. The airfoil was oscillated about the 25% chord point, with its angle of attack varying as

$$\alpha = 10^\circ - 10^\circ \sin \omega t$$

The LDV probe volume was traversed in the range $-0.25 \leq \frac{x}{c} \leq 0.75$, $0.0 \leq \frac{y}{c} \leq 0.58$. The data to be presented and discussed will pertain to the downstroke and envelope angles of attack ranging from 20° to 0°.

3. Results and Discussion

The results are discussed in three parts. The first part contains flow visualization pictures obtained using the schlieren technique; the second part presents the LDV data in the reattaching phase of the flow; the results of the PDI studies are discussed in the last part.

3.1. Schlieren Studies

A. Steady flow behavior

Fig. 4 shows schlieren pictures of steady attached and separated flow fields on the NACA 0012 airfoil at M = 0.3. Fig. 4a was obtained for $\alpha = 12.33^\circ$ and it is clear that the flow is completely attached. In the picture, the dark region near the leading edge on the lower side represents the flow at the stagnation point. The white region following it shows density gradients due to the the acceleration of the flow through the suction peak. The dark patch after this is the region where a laminar separation bubble forms[7]. At high angles of attack, the boundary layer thickens considerably near the trailing edge, as can be seen in the figure. At one encoder count higher, $\alpha = 12.41^\circ$, the flow separates and this state is shown in Fig. 4b. The flow could be brought back to the attached state by simply returning to the lower angle of attack of 12.33°, demonstrating the very small hysteresis that was present in steady flow. The two pictures clearly demonstrate the abruptness of flow separation and reattachment in steady flow.

B. Unsteady flow behavior

Contrary to steady flow, reattachment in unsteady flows is a process occuring over a range of angles of attack (time). Fig. 5 presents stroboscopic schlieren pictures as the airfoil executes the downstroke sinusoidally from $\alpha = 20^\circ$ to $\alpha = 0^\circ$. At $\alpha = 20^\circ$, the flow is completely separated from the leading edge as seen in Fig. 5a. The only flow features to be noted are the stagnation point, the separated shear layer emanating from the airfoil leading edge and the trailing edge shear layer. For $\alpha = 13.82^\circ$, in Fig. 5b, the flow has begun to reattach around the

leading edge, but over most of the upper surface, it is still separated. A trailing vortex can be seen in the wake at about 10-15% chord distance from the trailing edge, which could be the starting vortex related to partial reattachment. This suggests that the airfoil has already begun to generate lift. At $\alpha = 10°$, Fig. 5c, the reattachment has progressed to about 10% chord from the leading edge. A trailing vortex is also present. But, the significant point of interest is the appearance of a dark region near the leading edge in the reattached flow. A dark region in the schlieren image represents deceleration for the knife edge orientation used in the present schlieren arrangement. Hence, on either side of this region, the flow is accelerating. It is believed that a separation bubble forms in this region, in which the leading edge boundary layer separates and then reattaches. Studies by Carr et al [7] have shown that a bubble forms on the upstroke of the airfoil and is still present at $\alpha = 10°$. It is interesting to note that, even in the downstroke, a similar feature is present, (see also Sec. 3.3). Fig. 5d presents the result for $\alpha = 6.1°$ and it is clear that the flow has reattached over the entire airfoil. However, a slight imprint of the separation bubble can still be observed at $\frac{x}{c} \simeq 0.15$ as the flow is accelerating on either side of this point. It was found that only for $\alpha < 6°$ the separation bubble was not present. This confirms that flow reattachment after dynamic stall is a process over a long range of angles of attack, $14° \geq \alpha \geq 6°$. Whereas the flow on the upstroke was attached for all these angles of attack, at corresponding angles of attack on the downstroke, the flow was still separated, indicating the presence of strong hysteresis effects in the flow.

3.2. LDV Studies

As stated in Sec. 2.3, the LDV measurements were carried out over $-0.25 \leq \frac{x}{c} \leq 0.75$ and $0.0 \leq \frac{y}{c} \leq 0.58$. The distributions of the absolute velocity obtained from these measurements are discussed below. Due to limitation of space, only selected data are presented.

A. Global distributions

The absolute velocity vector field at two angles of attack corresponding to the schlieren pictures in Fig. 5 are presented in Fig. 6. Fig. 6a shows velocity field at $\alpha = 20°$, when the airfoil is in the deep dynamic stall state. Also shown the edge of the shear layer for direct comparison with the flow visualization studies. At $\frac{x}{c} = -0.25$, the approaching fluid is accelerated at higher $\frac{y}{c}$ locations (for ex., $\frac{y}{c} = 0.4$ and higher), and the airfoil slows down the velocities along a streamline in line with it. The most notable feature is the large variation between the shear layer and the airfoil upper surface. The velocity reaches $0.5U_\infty$ at $\frac{x}{c} = 0.42$ and $\frac{y}{c} = 0.05$, whereas far higher ($0 \leq \frac{x}{c} \leq 0.75$, $\frac{y}{c} = 0.58$), the magnitude is about 1.1 - $1.2U_\infty$. It is also interesting to note that despite the large scale separation, no reverse velocities could be measured, even though frequency shifting was used in the LDV system. As the airfoil angle of attack decreases to 10°, the flow becomes partially attached up to $\frac{x}{c} \simeq 0.10$ and beyond this, the flow is still separated as can be seen from the schlieren picture in Fig. 5c. The absolute velocity profiles in Fig. 6b are nearly flat with a ensemble means of $1.1U_\infty$, in the region $0.17 \leq \frac{x}{c} \leq 0.42$, and perhaps this is due to the mixing in the region. This emphasizes that in unsteady flow, even gross separation does not necessarily imply reverse flow. Part of this could also be due to particles not following the rapid flow changes during the cycle in this high speed, high frequency and large amplitude dynamic flow. The velocity vector field at $\frac{x}{c} = 0.083$, further shows acceleration of the flow near the surface, where velocities of up to $1.35U_\infty$ are encountered. From the schlieren picture (Fig. 5c), this is the region where the flow reattaches through the bubble and therefore the acceleration seen is due to the reattachment. This process where the velocity near the surface exceeds the free stream as the flow redevelops continues while the flow reattaches over the airfoil.

B. Progression of the reattachment process

Fig. 7a and 7b show the velocity profiles at different angles of attack from the top of the stroke when the flow is completely separated to when full reattachment occurs at $\frac{x}{c} = 0.083$ and $\frac{x}{c} = 0.25$ respectively. Of interest are the velocity defect seen closer to the airfoil for $0.1 \leq \frac{y}{c} \leq 0.15$ in Fig. 7a and for $0.067 \leq \frac{y}{c} \leq 0.25$ in Fig. 7b. As the shear layer is still detached from the surface at $\alpha = 20°$ (Fig. 7a), the defect in the velocity profiles seen is due to the shear layer itself, with the lowest velocity being nearest to the airfoil. There is waviness in the profiles even at $\alpha = 12.59°$. This is believed to be due to the unsteady shear layer and also possibly due to an insufficient number of samples at certain locations and phase angles. Below this angle of attack, the profiles become smoother and the fluid layers closer to the airfoil surface are accelerated relative to those away from it, which indicates local reattachment. At $\frac{x}{c} = 0.25$ (Fig. 7b), the velocity defect is seen to be larger ($\simeq 0.3U_\infty$). The defect extends over a larger height above the airfoil and over other angles of attack as well, including $\alpha = 12.59°$. At $\alpha = 10.52°$, the velocity profile looks smooth. However, at $\alpha = 8.44°$, the distribution shows larger velocities near the surface indicating that the reattachment has progressed to this location. Further decrease in the angle of attack to $\alpha = 7.41°$ results in the establishment of a flow where the local velocities near the surface increase above the free stream value. The velocity profiles over the airfoil change from those with a defect to those in which the fluid is increasingly accelerated as the surface is approached through the reattachment process. Data at other $\frac{x}{c}$ locations confirmed this observation.

C. Comparison of velocity distributions on the up and downstrokes

Fig. 8a compares the velocity distributions at $\frac{x}{c} = 0.083$ at $\alpha = 10°$ on the upstroke and downstroke.

It is clear that the velocities on the upstroke are significantly higher, by as much as 20%. At $\frac{y}{c} = 0.083$, the decrease in the value observed on the upstroke is due to the formation of a bubble and has been discussed in detail by Chandrasekhara and Ahmed[5]. Whereas a bubble formed on the downstroke as well, measurements could not be obtained in it due to seeding difficulties (discussed in Ref. 5). Fig. 8b which compares the profiles at $\alpha = 5.46°$, on the upstroke and on downstroke, shows no difference between the cases compared, indicating the absence of hysteresis at this location. A comparison of the upper surface flow field at $\alpha = 10°$ on the upstroke and downstroke is made in Fig. 9a and 9b. The peak velocity reached is about $1.45U_\infty$ during the upstroke, while during the downstroke it is $1.35U_\infty$. Also, the velocity data for the downstroke shows low velocities of the order of $0.7U_\infty$ beyond 30% chord and the extent of, for example, $|V|=1.1U_\infty$ (the solid line in the figure) is nearly half that during the upstroke. Some of the differences between the upstroke and downstroke occur because of the hysteresis effects (due to the large scale flow separation). At $\alpha = 10°$, the flow is partially attached in the downstroke and fully attached in the upstroke. Thus, the changes seen could also be attributed to the the pressure effects induced by the moving airfoil. This implies that the pressure distribution over the airfoil is also significantly modified at the same angle of attack, a factor that needs to be included in any calculations of the flow if the forces and moments through the cycle are to be satisfactorily computed.

3.3. PDI Studies

A. Interpretation of Interferograms

The fringes seen in the interferograms are contours of constant density. The quantitative nature of interferograms enables computation of the pressure distribution over the airfoil when the flow is attached, using isentropic flow relations. In the present study, this assumption is carried through the boundary layer fringes also. It is believed that the changes due to the vortical nature of the flow in the thin boundary layer that forms do not significantly affect the nature of the distributions. The density along any fringe can be calculated from the Gladstone - Dale equation[10] for the present wind tunnel and laser used as

$$\rho - \rho_r = .009421\epsilon$$

where ϵ the fringe number is $0, \pm1, \pm2, \ldots$ for the bright fringes and $\pm\frac{1}{2}, \pm\frac{3}{2}, \pm\frac{5}{2}, \ldots$ for the dark fringes. Fringes from the free stream to the stagnation point have positive values. Hence, by simply counting the fringes from the stagnation point, the flow quantities along any fringe can be determined. The corresponding C_p distributions can be computed from the relation

$$C_p = \frac{\left[\left(\frac{\rho}{\rho_r}\right)^\gamma - 1\right]}{\left[\frac{\gamma}{2}M^2\right]}$$

Knowing the local density values, the corresponding local Mach number can be determined. In all the interferograms shown, the triangular pointers seen are the registration markers used for scaling and obtaining the pressure distributions. The apex of the left side marker is aligned with the airfoil leading edge and the line joining vertical edges of the two markers above and below the airfoil passes through $\frac{x}{c} = 0.25$.

B. Interferograms of the reattachment process

Representative interferograms of the reattaching flow during the downward motion of the airfoil are shown in Fig. 10. Flow stagnation is indicated by the point on the airfoil lower surface near the leading edge where all fringes can be seen to converge. In some figures, the stagnation point appears to be a region because each fringe has a finite width. The fringes in the shear layer show that the flow is separated from the leading edge. The white and black patches seen between the separated shear layer and the airfoil surface in Fig. 10a at $\alpha = 12.27°$ indicate pockets of constant density fluid. Separation at this angle of attack occurs from very near the leading edge. It is clear that the velocity variation in the shear layer is that corresponding to two dark fringes, which is about $0.15U_\infty$ (as determined by fringe counting) for the present experiment. In Fig. 10b, at $\alpha = 10.69°$, the flow has partially reattached. One of the dark fringes in the shear layer after following the acceleration around the leading edge has turned down toward the airfoil and merged the local boundary layer. However, by $\frac{x}{c} = 0.2$, the fringe once again lifts off from the surface, indicating separated flow from there on. By this stage, a few more fringes appear around the leading edge indicating further establishment of the flow there.

As the angle of attack decreases to 9.84°, in Fig. 10c, the flow reattachment has progressed to about 35% chord, beyond which it is still separated. At the same time the fringe pattern on the upper surface around the leading edge shows that all outer fringes are smoothly shaped, but those closer to the airfoil (between $\frac{x}{c} = 0.02 - 0.1$) after coming out radially become nearly parallel to the upper surface and drop vertically before merging with the boundary layer. This is due to the formation of a laminar separation bubble, an event that was found to occur during the upward stroke as well, Carr et al[7]. This can also be seen from Fig. 10b, but it is less definitive. However, the pressure distributions (see next section) in fact indicate that a bubble is present at $\alpha = 10.69°$ also. Eventually, by $\alpha = 8.01°$, in Fig. 10d, the bubble almost disappears.

It is interesting to note that on the upstroke, the bubble forms at an angle of attack greater than 5° and remains on the surface till the dynamic stall vortex forms at around the static stall angle[7]. The overall flow is still attached till dynamic stall occurs at $\alpha = 15.9°$. However, on the downstroke, the flow is partially separated and the bubble is present only at certain lower angles of attack, $\alpha < 12°$. This once again demonstrates the hysteresis effects of the large amplitude oscillation of the airfoil.

C. Pressure distributions during reattachment

The variation of the maximum suction pressure coefficient as a function of angle of attack on the NACA 0012 airfoil during the downstroke is plotted in Fig. 11. It shows that as reattachment progresses, the airfoil redevelops suction steadily, during a *decrease* in angle of attack, till $\alpha = 8°$. Once the flow has fully established around the airfoil, the suction peak drops, as the angle of attack decreases further, as can be expected. Of particular interest and importance is the initial steep increase in the peak suction level at $\alpha \approx 12.6°$. It should be noted that this airfoil stalls at $\alpha = 12.41°$, at M = 0.3 in steady flow, (see sec. 3.1). The flow gradients seem to adjust such that as the static stall angle is approached during the downstroke, the leading edge shear layer begins to reattach and then flow reattachment begins. A similar observation has been made by Niven et al[3] also in their study of the reattachment process during ramp-down tests on dynamic stall at various pitch rates. The details of the pressure distribution can now be studied to see the salient features of the reattachment process.

Fig. 12 presents the pressure distributions at various angles of attack during the downstroke. For $\alpha = 12.27°$, only a few fringes could be counted in the accelerating region (up to $\frac{x}{c} = 0.017$ till flow separation); the graph shows that the local $\frac{dC_p}{dx} \approx 500$. For $\alpha = 11.15°$, fringes were present in the adverse pressure gradient region beyond $\frac{x}{c} = 0.02$ as well. In between, however, the fringes could not be detected clearly. It can be seen that the suction peak, C_p decreases to -1.0 and then a pressure plateau forms till $\frac{x}{c} = 0.083$, after which the pressure drops steeply. Such a behavior is indicative of the presence of a separation bubble, in which a constant pressure region followed by pressure recovery exists. The length of the bubble cannot be determined exactly as its edges could extend beyond this point of increasing pressure as has been pointed by Tani[11]. Though the pressure distribution gives approximately the length of the bubble, determination of its precise size requires quantification of the stall behavior by other surface flow measurement techniques. It appears that for $\alpha = 10.69°$ and $\alpha = 10.31°$, there is little change in the distributions through the bubble, although the suction peak seems to increase. As the angle of attack decreases, the bubble grows as the boundary layer reattaches further downstream of the leading edge as can be seen from the wider extent of the plateau, for example, at $\alpha = 9.84°$. At the same time, the $C_{p_{max}}$ also decreases as flow development continues around the leading edge. At $\alpha = 8.01°$, kinks are still present in the C_p distribution up to $\frac{x}{c} = 0.13$. Thus, it is possible that a separation bubble is still present till after this location. However, at $\alpha = 4.16°$, the distribution is smooth and the bubble has disappeared. The peak C_p estimated from these interferograms was -1.7, but the actual $C_{p_{max}}$ is expected to be slightly higher (due to the difficulty of resolving the fringes in this region), whereas the $C_{p_{max}}$ for attached flow on the upstroke is -1.43 and -2.12 for steady flow, at $\alpha = 4.25°$. This supports the conclusion that reattachment is a quantitatively different process from the separating flow on the upstroke, even though qualititative similarity exists in regard to the formation of the bubble. The differences in the angles of attack between the upstroke and downstrokes for the suction peak and the bubble development are due to the hysteresis effects that are always present in these unsteady flows.

D. Comparison of LDV and PDI studies

Since two different quantitative measurement techniques were used in the present study, it is instructive to make a direct comparison of the methods and the results obtained. PDI provides a spanwise averaged instantaneous quantitative flow field picture whereas LDV yields a long time averaged point measurement of the flow. The Mach numbers derived from both methods are compared in Fig. 13 at $\alpha = 10°$, when the airfoil is undergoing downward motion. The solid lines shown in it are the contours corresponding to midpoint of the dark fringes of the interferograms and the dashed lines are the Mach contours obtained from LDV (for the corresponding fringe numbers). The agreement is good, considering the vastly different nature of the techniques. The cylinder of light used in PDI provides more data points closer to the airfoil surface, which was not possible with LDV because of the blockage of the beams by the oscillating airfoil. However, the agreement for those data that are coincident demonstrates the statistically stationary nature of the flow field in the region compared. It should be noted that major differences could appear in separated flow regions or in three dimensional flows.

Since LDV is a point measurement whose resolution is controllable, very detailed surveys of the flow could be obtained. The resolution of PDI is limited to the number of fringes that naturally form based on the laser wavelength, wind tunnel span and flow density changes. But, PDI offers flow field information instantaneously, obtaining this information would be a very time consuming task with LDV, a major consideration in high speed, forced, unsteady flows. The agreement obtained in this study enhances the confidence level of the results presented.

3.4. A Global Picture of the Reattachment Process

Based on the study, a picture of reattachment emerges, which is represented in Fig. 14. During deep dynamic stall of rounded leading edge airfoils, the separated shear layer always appears to emanate from around the leading edge. However, the separation point cannot be precisely determined. As the airfoil angle of attack decreases, the shear layer starts moving towards the airfoil upper surface, without any significant reattachment until the static stall angle is approached. Reattachment begins near the static stall angle; the subsequent flow development around the leading edge causes the suction pressure to increase sharply. The adverse pressure gradient following the peak suction causes the boundary layer to separate slightly downstream of the suction peak and the separated shear layer has its origin now at this point of separation. There is a moderate angle of attack range in which the flow remains partly

separated. The shear layer attaches to the surface forming a bubble, only when the angle of attack falls below the static stall angle ($\simeq 11^0$), but it once again separates further downstream, depending on the local flow conditions. As the reattachment region proceeds towards the trailing edge, the suction pressures continues to increase with the bubble still present. Eventually, when the flow completely attaches itself over the airfoil, and the angle of attack falls to about 5 degrees, the bubble disappears and the pressures near the leading edge starts to decrease. Contrary to steady flow, where the suction pressure decreases as the angle of airfoil is lowered, in dynamic condition, there appears to be an interaction between the two mechanisms of flow reattachment and flow due to positive angle of attack. During the reattachment process, the suction pressure continues to increase till the reattachment is completed. Beyond this the pressure decrease is due to the decrease in angle of attack only. If a mechanism is created for the reattachment to occur earlier, it is possible to reduce the hysteresis loop, and thus increasing the usable lift in the cycle. Though, this study has shed some light on the physics of the reattachment process, more studies are required to identify the effect of other parameters such as airfoil geometry on the reattachment process.

4. Conclusions

A detailed study of the reattachment process of dynamic stall flow over an oscillating airfoil has been carried out using three different optical techniques. The major conclusions from the study are:

1. Reattachment of the dynamic stall flow is a process unlike that in a steady flow.
2. LDV studies show that the velocity profiles change shape; profiles with a defect change to those in which the fluid layers are accelerated steadily as the airfoil surface is approached, as the reattachment progresses.
3. The process includes development of larger than free stream velocities near the airfoil surface as the process advances over it.
4. Reattachment begins at or near the static stall angle even in unsteady flow. As flow begins to reattach, the suction pressure coefficient rises rapidly, but its values are different from that in steady flow and the unsteady flow during the upstroke.
5. For the Reynolds number of the experiment, reattachment progresses through a separation bubble, which changes size during the process and disappears at a low angle of attack.
6. Good agreement was found between LDV and PDI studies, enhancing the confidence level of the measurements.

Acknowledgements

The work was supported by the Army Research Office grant (MIPR-ARO-132-90) to the Naval Postgraduate School and monitored by Dr. T.L. Doligalski. Additional support was provided by AFOSR (MIPR-91-0007) monitored by Maj. D. Fant and also by NAVAIR (monitored by Mr. T.S. Momiyama). The support provided by Dr. S.S. Davis, Chief, Fluid Dynamics Research Branch, the discussions with Dr. L.W. Carr, U.S. Army AVSCOM at FML and the software development contributions of Mr. P.J. Trosin, and the image processing help rendered by Mr. C. Boswell of Sterling Federal Systems are all gratefully acknowledged.

5. References

[1] Carr, L.W., "Progress in Analysis and Prediction of Dynamic Stall", *Jl. of Aircraft*, Vol. 25, No.1, Jan. 1988, pp. 6-17.

[2] McCroskey, W.J., "The Phenomenon of Dynamic Stall", NASA TM 81264, March 1981.

[3] Niven,A.J., R.A.McD. Galbraith and David,G.F Herring., "Analysis of Reattachment during Ramp Down Tests", *Vertica*, Vol 13, No.2, pp. 187-196, 1989.

[4] Chandrasekhara, M.S. and Carr, L.W. "Flow Visualization Studies of the Mach Number Effects on the Dynamic Stall of Oscillating Airfoils", *Jl. of Aircraft*, Vol. 27, No. 6, June 1990, pp. 516-522.

[5] Chandrasekhara, M.S., and Ahmed, S., "Laser Velocimetry Measurements of Oscillating Airfoil Dynamic Stall Flow Field", *AIAA Paper No. 91-1799*, Presented at the 22nd Fluid Dynamics, Plasma Dynamics and Lasers Conference, Honolulu, HI, June 24-26, 1991.

[6] Carr, L.W., Chandrasekhara, M.S., Ahmed, S. , and Brock, N.J., "A Study of Dynamic Stall Using Real Time Interferometry", *AIAA Paper No. 91-0007*, Presented at 29th Aerospace Sciences Meeting, Reno, NV, Jan. 7-10, 1991.

[7] Carr, L.W., Chandrasekhara, M.S. and Brock, N.J., "A Quantitative Visual Study of Unsteady Compressible Flow on an Oscillating Airfoil", *AIAA Paper No. 91-1683*, Presented at the 22nd Fluid Dynamics, Plasma Dynamics and Lasers Conference, Honolulu, HI, June 24-26, 1991.

[8] Carr, L.W. and Chandrasekhara, M.S., "Design and Development of a Compressible Dynamic Stall Facility", *AIAA Paper No. 89-0647*, to appear in *Jl. of Aircraft*.

[9] Brock, N.J., Chandrasekhara, M.S., and Carr, L.W., "A Real Time Interferometry System for Unsteady Flow Measurements", To be presented at *The 14th ICIASF Conference*, Rockville, MD, Oct. 25-27, 1991.

[10] Goldstein, R.J., "Fluid mechanics Measurements", *Hemisphere Publishing Corp.*, 1983.

[11] Tani, I., "Low Speed Flows Involving Bubble Separations", *Progress in Aeronautical Sciences*, Vol. 5, 1964, pp. 70-103.

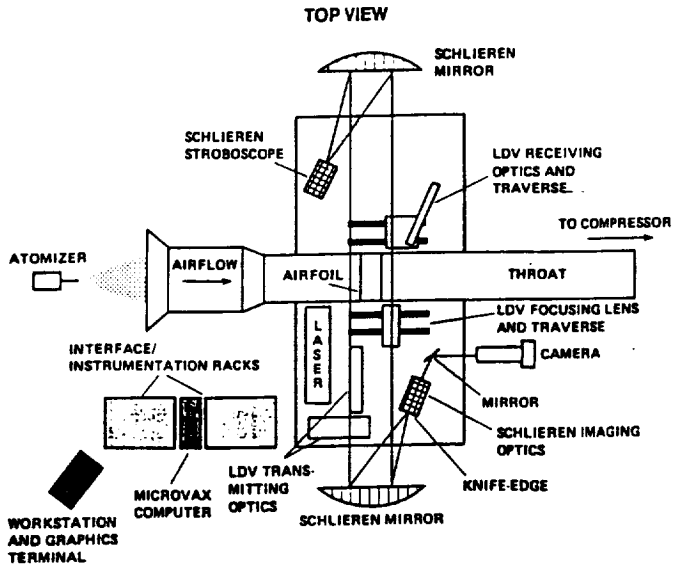

Fig. 1. Schematic of the CDSF Instrumentation.

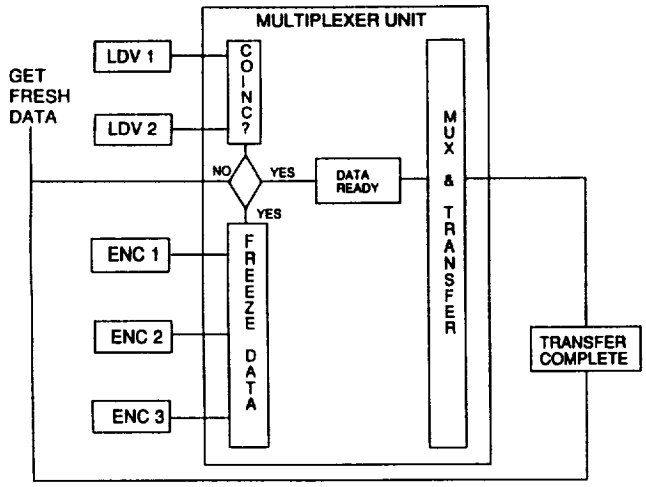

Fig. 2. Schematic of the LDV Data Acqusition Method.

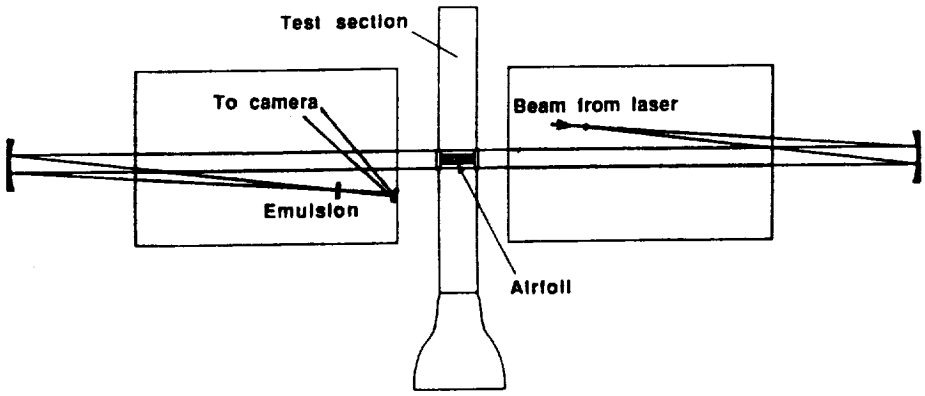

Fig. 3. Schematic of the Layout of Optics for Point Diffraction Interferometry.

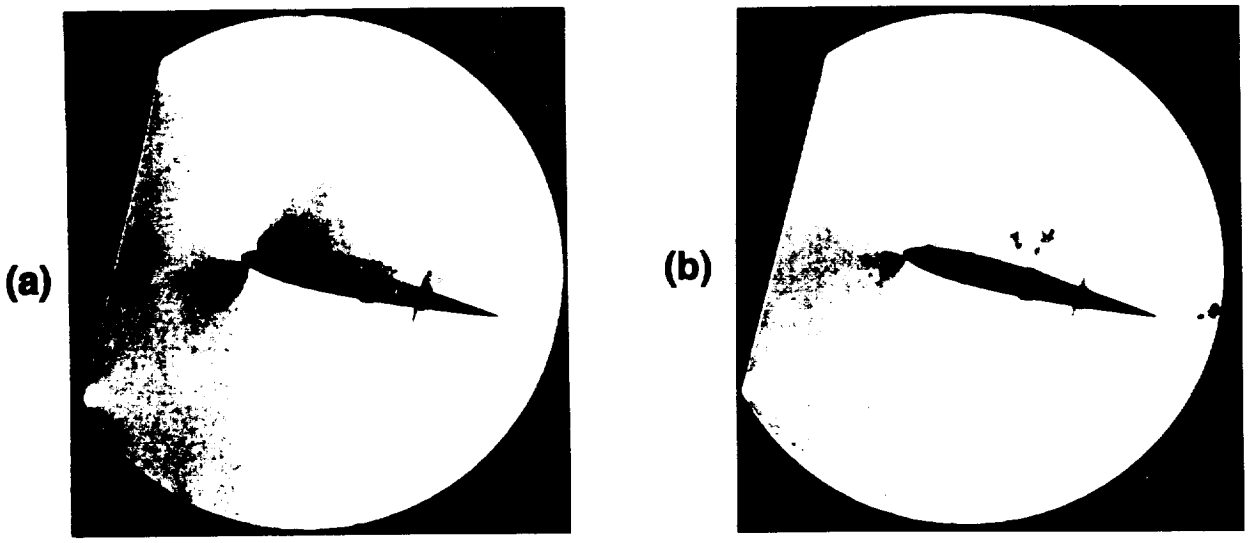

Fig. 4. Schlieren Photographs of the Steady Flow Behavior near stall: (a) $\alpha = 12.33°$, (b) $\alpha = 12.41°$.

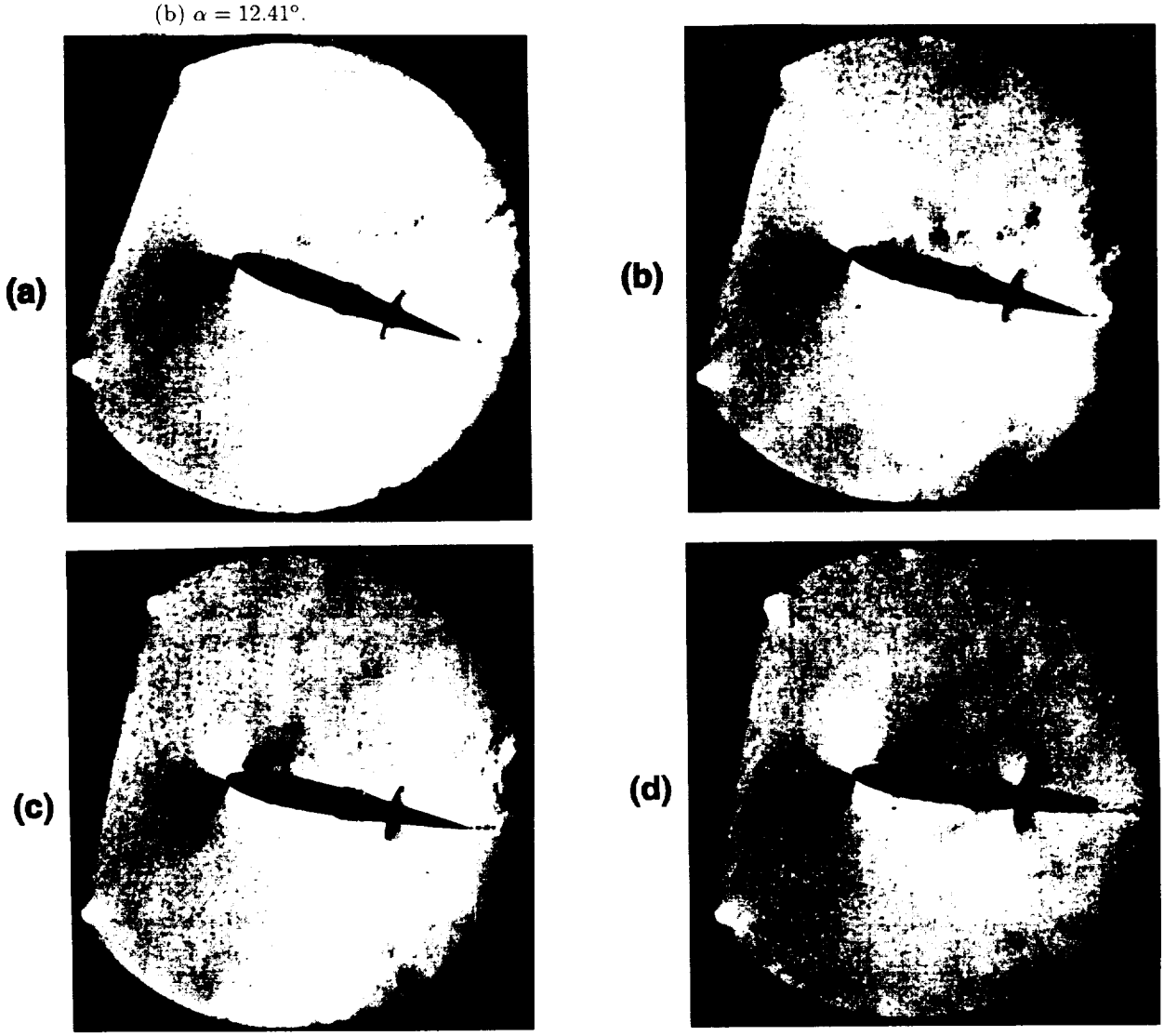

Fig. 5. Schlieren Photographs of Reattachment Process: (a) $\alpha = 20.0°$, (b) $\alpha = 13.82°$, (c) $\alpha = 10.0°$, (d) $\alpha = 6.17°$.

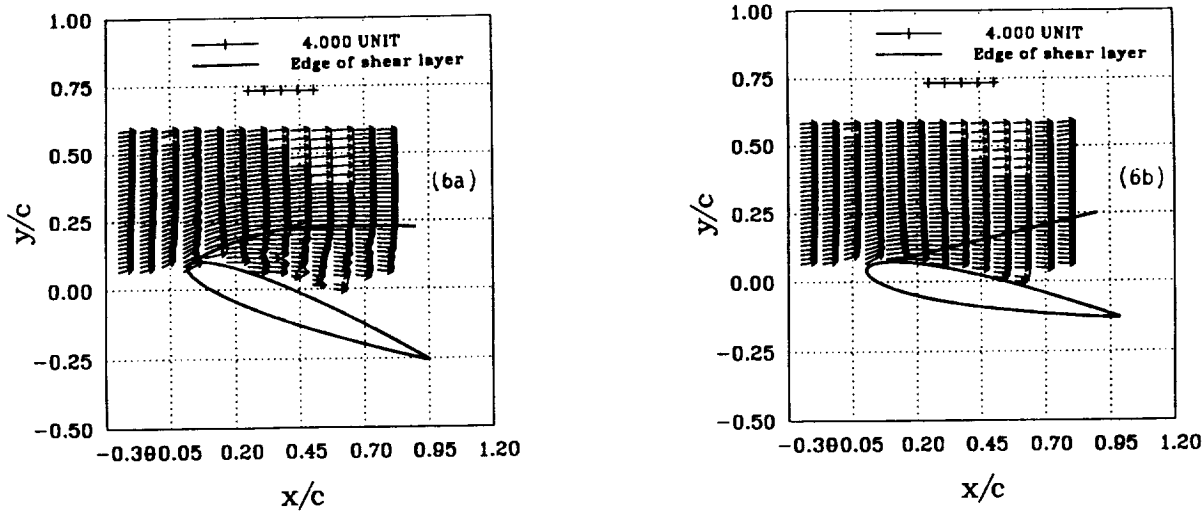

Fig. 6. Absolute Velocity Distribution: (a) $\alpha = 20.0°$, (b) $\alpha = 10.0°$.

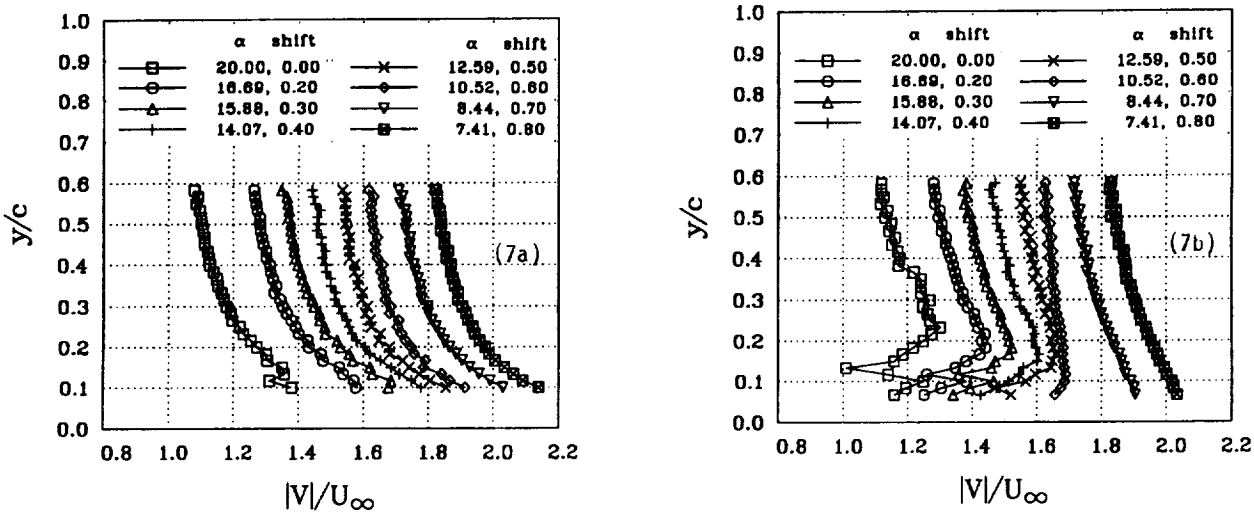

Fig. 7. Absolute Velocity Distributions with α : (a) x/c = 0.083, (b) x/c = 0.250.

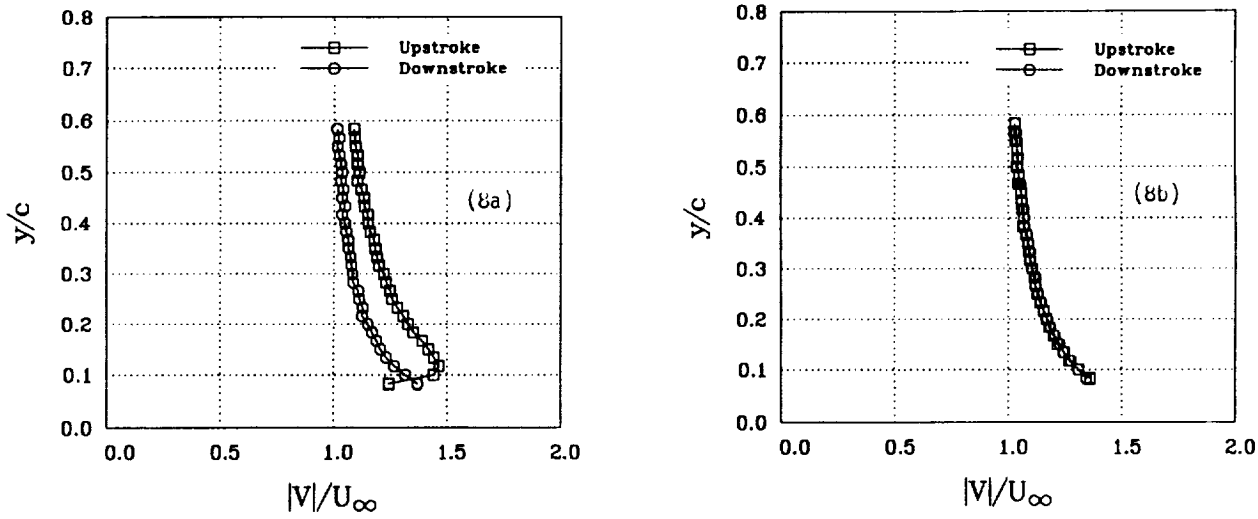

Fig. 8. Comparison of Absolute Velocity Distribution: (a) $\alpha = 10.0°$, (b) $\alpha = 5.46°$.

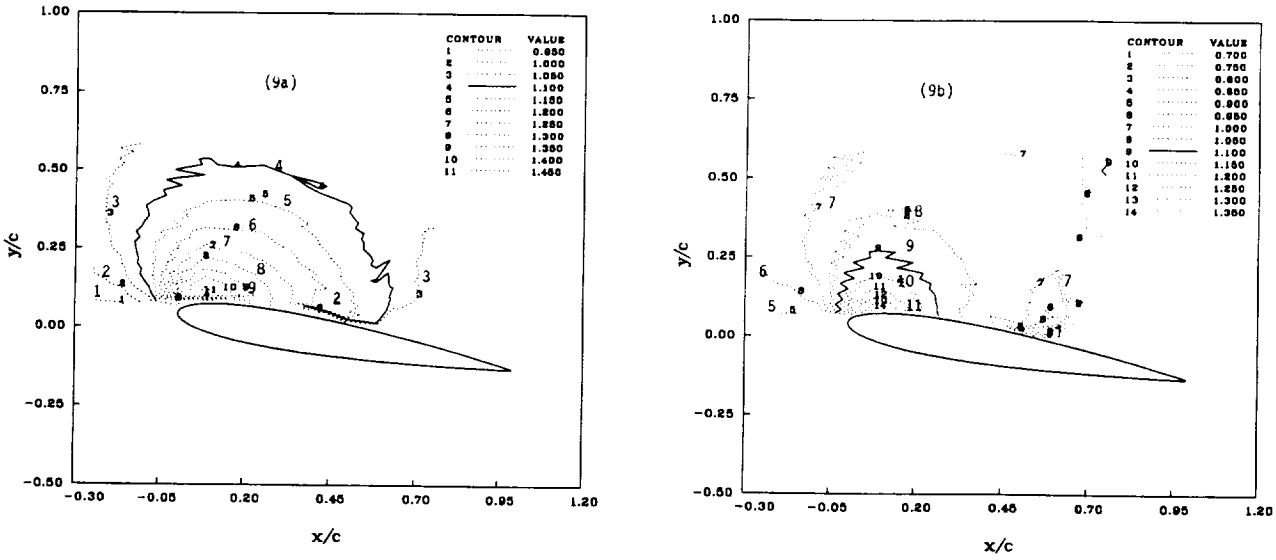

Fig. 9. Contours of Absolute Velocity at $\alpha = 10.0°$: (a) Upstroke, (b) Downstroke.

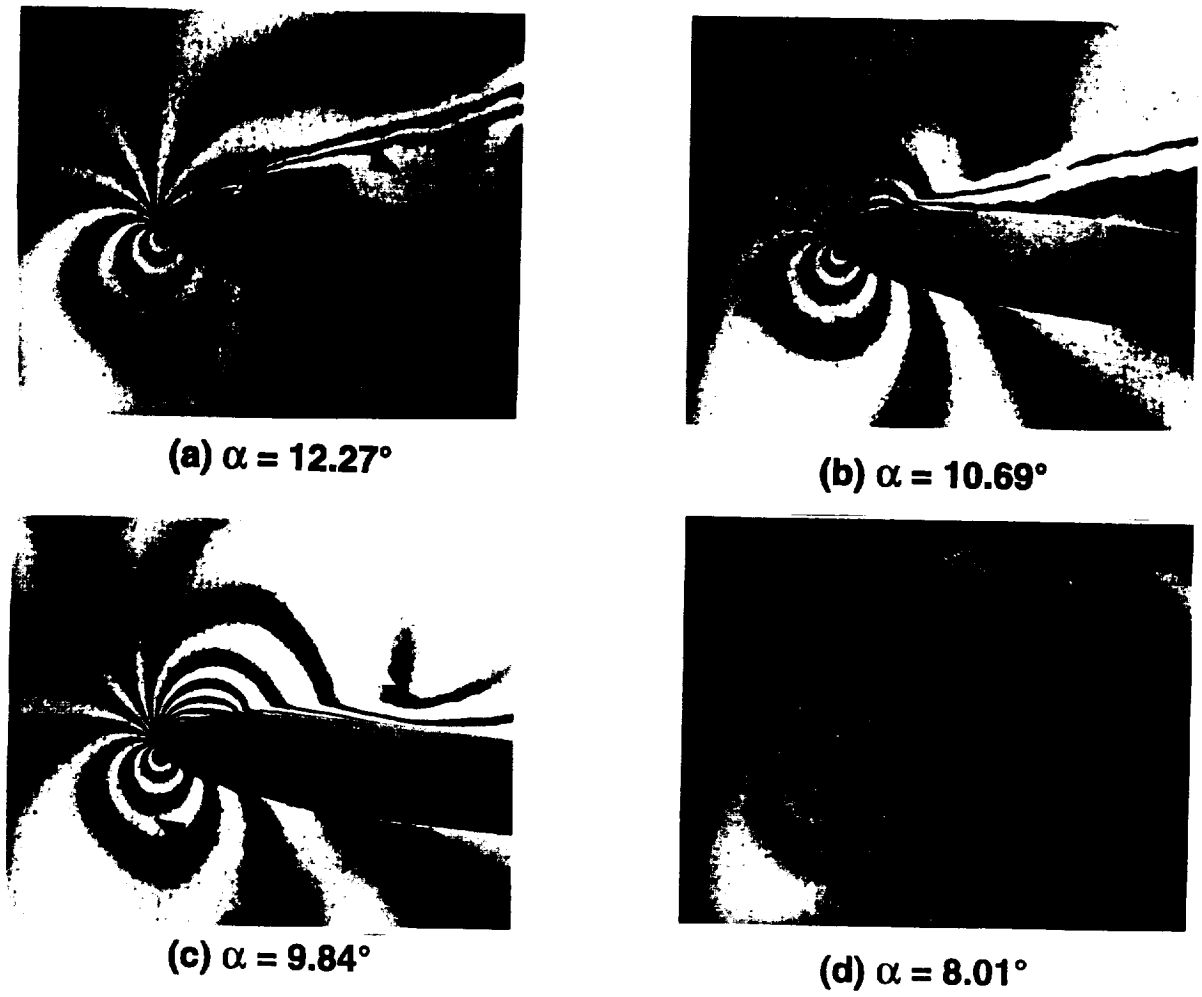

Fig. 10. Interferograms of Reattachment Process.

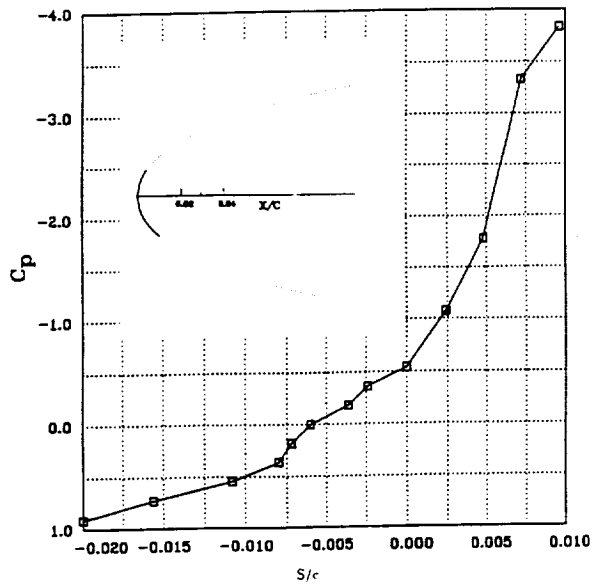

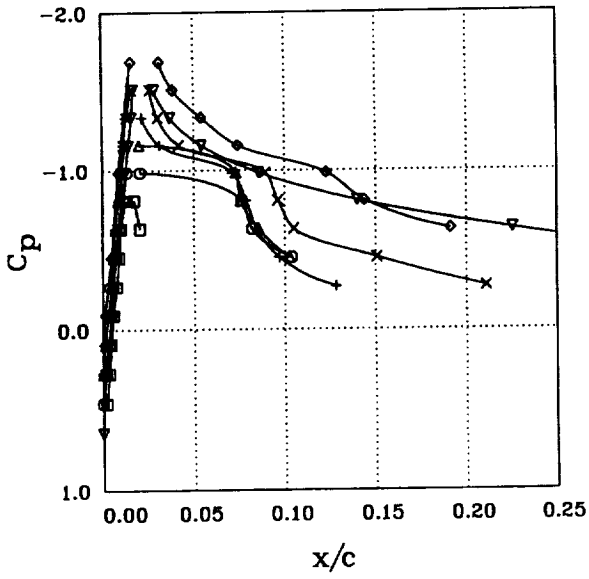

Fig. 12. Pressure Distribution During Reattachment Process.

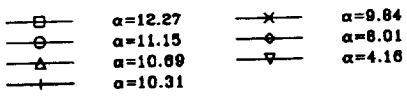

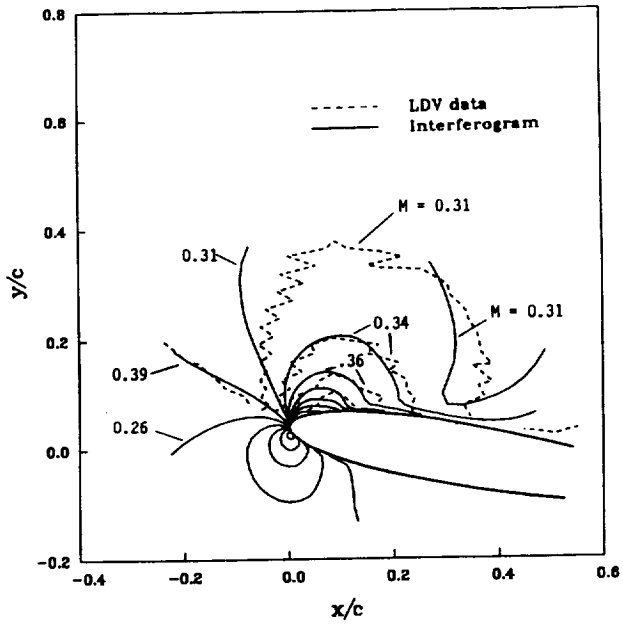

Fig. 13. Comparison of LDV Data with the Interferogram at $\alpha = 10.0°$.

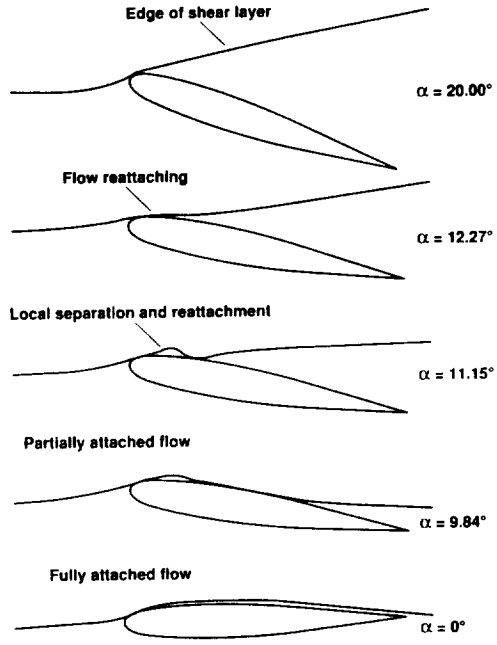

Fig. 14. Schematic of the Reattachment Process.

APPENDIX D

AIAA 91-0007
A Study of Dynamic Stall Using Real Time Interferometry

L.Carr, U.S.Army Aeroflightdynamics Directorate, NASA-Ames, Moffett Field, CA;

M.Chandrasekhara, Navy-NASA Joint Institute of Aeronautics, Naval Postgraduate School, Monterey, CA ;

S.Ahmed, MCAT Institute, San Jose, CA;

N.Brock, Aerometrics, Sunnyvale, CA

29th Aerospace Sciences Meeting

January 7-10, 1991/Reno, Nevada

A Study of Dynamic Stall Using Real Time Interferometry

L.W. Carr[1]
Aeroflightdynamics Directorate, U.S.Army AVSCOM
and Fluid Dynamics Research Branch
NASA Ames Research Center, Moffett Field, CA 94035

M.S. Chandrasekhara[2]
Navy-NASA Joint Institute of Aeronautics
Department of Aeronautics and Astronautics
Naval Postgraduate School, Monterey, CA 93943

S. Ahmed[3]
MCAT Institute, San Jose, CA 95127

and

N.J. Brock[4]
Aerometrics, Sunnyvale, CA 94086

Abstract

Dynamic stall over an oscillating airfoil in compressible flow was studied using a real-time interferometry technique. Instantaneous flow field data was obtained for various unsteady as well as steady flow conditions. The details of the dynamic stall vortex, including its formation and development have been revealed by the interferograms, resulting in the first documentation of the complete dynamic stall flow field under compressible flow conditions. Comparison of steady flow interferograms with those taken in unsteady flow reveal significant delay in development of leading edge suction peaks in the unsteady case. The interferograms permit detailed analysis of the leading edge pressure field; as many as as 13 pressure values have been obtained around the leading edge in the first 1% of the airfoil chord. The results offer significant new insight into the character of the dynamic stall vortex, and the stall delay that is observed during dynamic motions.

Nomenclature

C_p	pressure coefficient
c	airfoil chord
f	frequency of oscillation
k	reduced frequency $= \frac{\pi f c}{U_\infty}$
L	test section span
M	free stream Mach number
n	refractive index
n_r	refractive index at reference conditions
n_0	refractive index at atmospheric conditions
S	distance along airfoil surface
U_∞	free stream velocity
x	chordwise distance
z	spanwise distance
α	angle of attack
$\overline{\Delta PL}$	average path length difference
ϵ	fringe number
λ_0	wavelength of the laser
ρ	density
ρ_r	density at reference conditions
ρ_0	density at atmospheric conditions
ϕ	phase angle of oscillation
ω	circular frequency

1. Introduction

The control and utilization, or alleviation, of the dynamic-stall-induced aerodynamic loads which appear on helicopter rotor blades, and on rapidly moving conventional aircraft wings or control surfaces, will require a much greater understanding of the character of the unsteady flow field that occurs on these aerodynamic surfaces than is currently available. Significant study of the dynamic stall process has already been performed[1]. The effect of compressibility on dynamic stall airloads has been identified by a number of researchers[2-5]. However, experimental verification of the effects of the vortex on the compressible flow field have been limited so far to measurements on the airfoil surface[6] or qualitative imaging of the general flow field[7-9], with the exception of the work of Lee, et al[10], where much of the flow field was blocked by the system used to support the model. In the past, techniques for obtaining interferograms of compressible flows have required significant post-processing(e.g. holographic interferometry); real-time techniques such as Mach-Zender

---

1 Group Leader, Unsteady Viscous Flows; Member, AIAA.

2 Assistant Director and Adjunct Research Professor; Assoc. Fellow, AIAA.

3 Research Scientist; Member AIAA.

4 Research Scientist

interferometry systems [11] required expensive optics, and needed massive structure to reduce sensitivity to vibration. A new technique, based on the use of vibration-insensitive real-time interferometry known as point diffraction interferometry(PDI), has now been used to obtain results that reveal new details about the development of the dynamic stall vortex, and its effect on the flow over pitching airfoils.

The complexity and rapidity of the flow development during dynamic stall as well as the large pressure gradients that form near the leading edge make quantitative measurement very challenging and difficult. Better understanding of the stall process will be needed before any alleviation of the adverse effects of the dynamic stall event can be achieved; this will require careful study of the flow during the stall inception. However, physical space limitations greatly restrict the density of sensors that can be installed in this region of the airfoil, and the presence of these sensors can actually affect the flow being studied. Thus, issues about the origin of the dynamic stall vortex, and explanation of why and how stall delay occurs have remained very difficult to address experimentally; the technique used in the present study offers new opportunities for such a study. Some of the early results showing the flow development as obtained with this new technique are discussed in the present paper.

2. Description of the Facility

The present study was performed in the Compressible Dynamic Stall Facility(CDSF) at the NASA Ames Research Center Fluid Mechanics Laboratory(FML). The CDSF is specifically designed for study of dynamic stall over a range of Mach numbers, using non-intrusive optical flow diagnostic techniques. It is operated as a part of the in-draft tunnel complex at the FML(for details, see Carr and Chandrasekhara[12]). The CDSF is specially designed so that airfoil supports do not block the view of the airfoil. The airfoil is supported between two 2.54cm thick optical quality glass windows by pins that are smaller than the local airfoil thickness; thus the airfoil can be viewed unobstructed by any support mechanism(figure 1). The window/airfoil combination is driven in sinusoidal oscillation by a 4-bar, push-rod-flywheel system, about the 25% chord position. This permits study of the flow at the leading edge, where the dynamic stall vortex forms, as well as the flow field away from the airfoil. The drive motor is a variable speed a.c. motor with a controller to maintain speed to within 1%. The drive mechanism can oscillate the airfoil at frequencies up to 100 Hz, with oscillatory amplitudes ranging from 2° - 10°. The mean angle of attack can be varied from 0° - 15°. Phase angle in the cycle is determined by an optical encoder keyed to the flywheel. The present test conditions included M= 0.2-0.45, for k = 0.0 - 0.10, Reynolds number = 400,000- 900,000, with the airfoil oscillating at $\alpha = 10° - 10°\sin\omega t$. The airfoil was NACA 0012 with a 7.62cm chord.

The interferometric images were obtained by triggering a laser light source at defined phase angles through the oscillation cycle. The light source was a pulsed Nd:YAG laser with a frequency doubler, operating at a wavelength of 532nm. The phase angle for the interferogram was chosen by setting switches on a specially designed counter circuit box. Since the laser took a finite time to actually emit light, additional electronics were incorporated in the circuitry to display the phase angle when the laser actually fired. This was accomplished by sensing the light using a photo diode; when the laser fired, the output of the photo diode was used to freeze the angle of attack display so that the precise angle at which the image was taken could be recorded.

3. Point Diffraction Interferometry Technique

3.1 Principle

The point diffraction interferometry(PDI) technique used for the present test is based on the work of Smartt[13,14] as first applied to compressible flow by Bachalo and Houser[15]. The PDI technique utilizes the ability of a point discontinuity(in the form of a pin-hole) located at the image of a point source to diffract a portion of the incident light into a spherical reference wave front. In the Smartt interferometer, the light passing through the flow is used to produce the reference wave, by placing a sheet of partially-transmitting material containing the pin-hole at the focal plane of the point source(see Fig. 2). This reference wave front then interacts with light passing through the attenuating filter material surrounding the pin-hole, producing interference fringes dependent on the strength of aberration produced by the flow in question.

In a separate and unrelated effort, Anderson and Milton[16] developed an effective way to create a self-aligning spot as part of a study of dark-central-ground interferometry. In their approach, an exposed photographic plate was placed at the focus of the incident beam, and the focused energy of the light source was then used to char the photographic emulsion and thereby create a completely self-aligned point-diffraction spot. Since the point diffractor can be an aperture, or an opaque spot(the resultant wave fronts are mathematically related), this technique offers the same benefits as the Smartt interferometer. Since the mathematical derivations associated with point-diffraction interferometry are well documented in the referenced papers[13-16], the present paper will only address the physical implementation.

3.2 Implementation

In the present application, the primary optics of an existing schlieren system were used[12], with the pulsed Nd:YAG laser replacing the conventional spark as the light source, and a specially created point diffractor replacing the usual knife edge. Figure 3 shows a schematic of the arrangement. The laser light was expanded through a microscope objective to fill the schlieren mirror, transmitted through the test section, and refocused by another schlieren mirror. The exposed photographic plate used to create the point-diffraction spot was placed at the focus of this second mirror, and the laser was pulsed with enough energy to darken, or char the emulsion located at the focal plane of the second mirror. The spot was created *in-situ* by passing light through the test section at a no-flow condition, with the airfoil at 10° angle of attack(the Dark-Central Ground results were quite sensitive to the angle at which the spot was created; the PDI results were not). The spot was precisely tailored to the application under investigation, automatically correcting for nonuniformities

in the light source or optics. The tunnel was turned on and the real-time inteference fringes were recorded on Poloroid film(ASA 3000), and were available for immediate viewing. This was of great value for analysis of the dynamic flow field under investigation, since it permitted rapid review of the progress of the dynamic stall vortex, and on-line retaking of any photograph which was not of the quality required. This also permitted on-line study of the flow field as it developed, since any phase of the cycle could be accessed directly. This ability to actively search for the onset of dynamic stall using the PDI technique is in strong contrast to the more conventional holographic interferometer, which requires a major post-processing effort before the interferogram can even be verified, much less analyzed.

Although this technique is conceptually quite elegant, there were significant implementation difficulties, mostly related to the complexity of the flow field presently under investigation. For example, the PDI technique used light passing through the pin-hole located at the focus of the undisturbed light to create the spherical reference wave front. However, in several cases, particularly at high airfoil angles of attack, most of the flow field was disturbed by the dynamic stall process. This complication led to an investigation of a variety of spot configurations, and ultimately to an exploration of various alternative approaches for generation of the point diffractor. The photographs presented in the present study were obtained using a variation of the PDI technique where the photographic plate was replaced by a blue-line filter. The point diffraction source was then created by burning the filter coating until a *clear* aperture was created on it; this technique resulted in a greatly increased contrast in the interference fringes produced, and permitted full-flow field images to be made with no loss of detail anywhere in the image. The diffraction by the aperture was also insensitive to the angle of the airfoil at which the aperture was produced.

4. Results and Discussion

4.1 Qualitative Analysis of Interferograms

Figure 4a presents a point-diffraction-interferometer image of the NACA 0012 airfoil at 0° angle of attack, in steady flow at M = 0.40. The fringes seen are constant-density contours. The stagnation point is characterized by the convergence of circular fringes which appear at the leading edge. The fringe pattern is symmetrical on both the upper and lower surfaces, indicating the flow is symmetric(appropriate for this airfoil, at 0° angle of attack). The fringes generated at the leading edge terminate on the airfoil surface through an abrupt turning downstream due to the presence of the boundary layer. Since the fringe nearest to the leading edge encloses the stagnation point, correct Mach number values can be assigned to each of the fringes outside of the boundary layer(see Section 5.1).

Figure 4b shows the fringe pattern of an airfoil passing through 10.65° angle of attack, at M=0.40, k=0.05. Note that the circular fringes now appear on the lower surface of the airfoil, reflecting the movement of the stagnation point due to the increase in angle of attack. The concentration of fringes near the leading edge indicates strong acceleration in this region. The fringes originating near the leading edge curve back to the airfoil surface, indicating the presence of adverse pressure gradient on that part of the surface. The presence of the boundary layer can also be seen by the abrupt turning of fringes in the downstream direction as they approach the airfoil surface.

There is a region in the flow near the leading edge which is completely dark in this figure. The very high gradients in this region have so strongly bent the incident light that light from this area is no longer in the field of view by the time its image reaches the image plane(See Fig. 5). Thus, analysis of this region will require re-positioning of the schlieren mirror to a location much closer to the tunnel wall; this arrangement will be used for future study of the details of this critical area.

4.2 Dynamic Stall as Shown by PDI

Figure 6 presents images of the flow field for six angles during the upstroke for M = 0.35, k = 0.05. Figure 6a, taken at 10.65°, is similar to the image discussed above; figure 6b, taken at $\alpha = 12.11°$, shows similar characteristics, indicating that the flow is still attached. Figure 6c shows the character of the flow at $\alpha = 12.54°$. Although the outer flow field remains essentially unchanged, the fringes which rapidly curved back to the surface near the leading edge in figure 6a and 6b no longer do so. Instead, these are now displaced downstream, and show much less curvature until they again come close to the surface, where they abruptly turn normal to the surface. This is the first indication that dynamic stall *delay* (the static stall angle for M=0.35 is 11.6°) has ended, and that the dynamic stall process *itself* has begun. Figure 6d shows this flow for $\alpha = 12.83°$; here, the imprint of the dynamic stall vortex is more clearly delineated. The fringes near the leading edge terminate normal to the surface, and a few of them are curving against the direction of flow, showing the formation of a vortex-like structure. For this case, the outer flow field is still attached. In fact, the outer flow fringes pass smoothly around the dynamic stall vortex, and blend into the boundary layer from 40% chord to the trailing edge.

At $\alpha = 13.85°$, (Fig. 6e), the vortex has moved further down the airfoil, and has grown vertically. Further, although the interference fringes in the downstream part of the vortical region still show contours that might be expected from a classical vortex, the upstream part of the vortical region is much different from that which would be expected from such a vortex. Instead, all the fringes emanate from the leading edge, and enclose a fringe-free region above the airfoil surface. Since this region is vortical in nature, it is not clear that the fringes are still denoting constant velocity contours deep inside this region. It should be noted that the outer flow field was not changed significantly until the dynamic stall induced flow reached the trailing edge of the airfoil(shown in Fig. 6f, $\alpha = 16.02°$). This is in agreement with the lift calculated from integration of instantaneous pressure transducer readings obtained on the surface during related dynamic stall tests[2], which show the lift increasing until the dynamic stall vortex has left the trailing edge.

Although the images shown above were obtained at M = 0.35, the point diffraction technique is not limited to this relatively high Mach number. As can be seen in Fig. 7, the technique produces clear images of the stall process for a wide range of conditions. Figures 7a, 7c, and 7e show

the density field over the airfoil at $\alpha = 10.65°$, k=0.05, for M=0.20, 0.30, and 0.40, respectively. These photographs show the increase in number of density contours that are associated with the increase in speed from M=0.2 to 0.4 as can be seen by comparing these figures to figure 6a, taken at the same angle at M=0.35. Figure 7b, 7d, and 7f show the flow at $\alpha = 14.28°$, after the dynamic stall process has begun, for the same Mach numbers. This clearly shows that the stall vortex occurs earlier in the cycle as the Mach number is increased.

5. Quantitative Analysis of Interferograms

5.1 Determination of Mach Number by Fringe Counting

For a standard interferometer, the path length difference $\overline{\Delta PL}$ due to density (or phase) changes can be related to the fringe number ϵ as,

$$\epsilon = \frac{\overline{\Delta PL}}{\lambda_0} = \frac{1}{\lambda_0}\int (n - n_r)dz$$

For a two-dimensional flow, the above equation can be simplified to,

$$\epsilon = (n - n_r)\frac{L}{\lambda_0}$$

If ϵ is zero or an integer, then the fringe is bright and if it is a half integer, the fringe is dark. Using the Gladstone - Dale equation and the perfect gas equation, the above expression can be reduced to (Goldstein[17])

$$\rho - \rho_r = (\frac{\lambda_0}{n_0 - 1})(\frac{\epsilon\rho_0}{L}) = A\epsilon$$

Since λ_0 = 532 nm, L = 25cm, $(n_0 - 1) = 2.733 \times 10^{-4}$ (from Goldstein[17]), and $\rho_0 = 1.21 kg/m^3$, the constant A can be determined. For the specific case of the present experiments,

$$\rho - \rho_r = 0.009421\epsilon$$

or

$$\frac{\rho}{\rho_0} = \frac{\rho_r}{\rho_0} + \frac{A\epsilon}{\rho_0}$$

Since $\frac{\rho_r}{\rho_0}$ is a function of the free stream Mach number only, $\frac{\rho}{\rho_0}$ can be determined by knowing the fringe number. In this method, a positive fringe number represents deceleration and vice versa.

5.2 Comparison of the Steady and Unsteady Flow Interferograms

Figure 8 presents two interferograms of the airfoil flow at M = 0.3 for an angle of attack of 10.78°. Figure 8a was taken in steady flow; the concentration of fringes near the leading edge shows that the local flow around the leading edge on the upper surface has experienced very strong accelerations as a consequence of the suction that naturally develops at such an angle of attack. The peak local Mach number for this case (corresponding to a fringe number of -14) is $\approx$ 0.61. Also, the airfoil boundary layer thickness at the trailing edge is quite large, of the order of 10% of the airfoil chord. For comparison, Figure 8b shows the flow field for the case where the airfoil passes 10.78° during the upstroke of an oscillation cycle at k=0.05. Although the outer flow does not show much change, the flow near the surface is quite different. For example, only 10 fringes could be detected over it near the leading edge region, corresponding to a peak Mach number of 0.52. It appears that the flow gradients in the unsteady case develop at a slower rate than in the steady case, thus contributing to the delay of stall that is induced by the rapid unsteady motion. Also, the boundary layer thickness at the trailing edge is about half that of the steady case. Eventually, as the airfoil pitches to a higher angle of attack, the unsteady flow gradients attain values that indeed induce flow separation in the unsteady flow as well. The angle of attack at which this condition is reached is a strong function of the Mach number, degree of unsteadiness, amplitude of motion and other parameters. It is expected that further experimentation at a much closer resolution and covering a much broader range of experimental conditions will quantify this comparison. Once separation occurs, the vorticity input by the unsteady motion coelesces into a vortex whose ability to remain on the surface will determine the amount and duration of dynamic lift generation.

5.3. Estimation of Pressure Distribution Around the Leading Edge

As stated earlier, the interferograms represent constant density contours. From these contours, it is possible to compute the Mach number distribution and thus, the pressure distribution around the leading edge. To do this, an interferogram obtained at M = 0.3, k = 0.075 and $\alpha = 12.85^0$ was digitised and the region of interest was enlarged. This enlarged image was further 'cleaned up' by digital processing to enhance the contrast and brightness to sharpen the fringes. Because of the appearance of the dark region near the leading edge (see sec. 4.1), the definition of the leading edge itself was difficult. To properly define the leading edge, a picture of the airfoil without the flow was obtained, was digitized, and the resulting image was superimposed on the PDI image. The fringes in the PDI image were then extended backwards towards the leading edge, keeping their curvature continuous to intersect the airfoil surface. The Mach numbers for these fringes were computed as explained in sec. 5.2; the corresponding pressure coefficients were calculated and plotted as a function of the distance measured around the leading edge.

Figure 9 presents a portion of the instantaneous local C_p distribution and shows 13 pressure values in a region of 3% chord around the leading edge. The maximum $-C_p$(of 3.8) in the analyzed image occurs at x/c $\approx$ 0.4% for the conditions at which it was obtained. The flow accelerates slowly on the lower surface from the stagnation point and as it passes over the leading edge, the acceleration can be seen to be very rapid. The pressure variation near the leading edge dictates the vorticity production and hence,

its measurement at a fine resolution is critical. Interferometry appears to be the only technique that offers the capability of determining this distribution in such detail. Since it is a non-intrusive method, it offers significant benefits in comparison to other methods such as pressure transducers due to the absence of mechanical interference and the other inherent limitations of mechanical measurement of unsteady pressure(e.g. errors due to dynamic response of the cavities and tubing systems, dynamic calibration etc). Such measurements have been made[2], but the nearest location to the leading edge where the data was obtained in that earlier experiment was still at $x/c = 0.5\%$. To obtain the pressure distribution shown here using the transducers would require an extraordinary number of transducers; the costs concomitant with such a system and the need for a large model to house these and the associated large facility generally preclude such testing.

This result is presented to establish the capabilities of the PDI technique. Many such images are now available, which are being analyzed for quantification of the leading edge flow field so that further understanding of the physics of the flow in this critical region may be obtained.

5.4. Comparison of the Schlieren and PDI Images

Figure 10 compares the flow field pictures obtained with a stroboscopic schlieren technique[7] and the PDI technique. These pictures correspond to nearly identical nominal flow conditions of $M = 0.3$ and $k = 0.075$, at an angle of attack of 14.7^0. The knife edge for the schlieren picture was kept vertical and hence was perpendicular to the streamwise direction. The dark region in Fig. 10a represents an increase in the density gradient towards the knife edge associated with flow deceleration, and hence, the bright regions indicate flow accelerations. The stagnation point can be seen to be at $\approx 2\%$ chord from the leading edge on the pressure side. The same result is seen in Fig 10b, which is a PDI image, wherein the fringes converge towards the stagnation point at the same location. The strongly accelerating flow around the leading edge - the bright region in the schlieren picture - is seen in the PDI image as a large number of fringes (over 20) radiating from the region. The dynamic stall vortex is seen to be at about the 50% chord point in the schlieren picture. This picture also shows that the flow decelerates in the vortex towards the trailing edge. In the interferometry image, the dynamic stall vortex appears as a region with a system of fringes that are nearly concentric on the downstream side of the enclosed region(although they all originate in the leading edge region), and terminate over the airfoil suction side after they turn slightly upstream. A counting of the fringes shows that the PDI image confirms the deceleration of the flow in the vortex towards the trailing edge since the fringe number increases in this direction in the vortex. The two photographs also show a clear demarkation in the edge of the vortical layer. In the PDI image, the vortcial layer is seen to be filled with fringes whose curvature changes to accomodate the local flow conditions. In the schlieren image, this is simply the region where the black and white regions are present. Further downstream of the vortex, there are no significant flow density field changes that can be detected by either of the two techniques.

This strong agreement between the two independently obtained images is noteworthy, even though both are spanwise averaging techniques, use the same flow property - namely density - and also, share some of the optics. The two were obtained on different days, under nominally the same conditions. Despite the changes that could be expected to be present in the instantaneous pictures due to these differences, and from cycle to cycle variations, the two techniques give the same result, with the PDI being also quantitative.

The sharpness of the fringes through the vortical region during the formative stages of the vortex also suggests that the flow through the vortex is nearly two-dimensional. As the vortex grows, it continues to entrain fluid from the outer flow. Near the leading edge, the flow mixes rapidly, and the fringes are lost only in this region, as can be seen in Fig. 7f.

6. Conclusions

Real-time interferometry has now been demonstrated to offer significant benefits for analysis of unsteady compressible flow. In contrast to holographic interferometry, real time techniques permit immediate review and evaluation of the resultant interferograms. This capability is of major value in analysis of dynamic flow fields such as those created by dynamic oscillation of airfoils, and dramatically improves the continuity of analysis of the aerodynamic events; this continuity is critical to improved understanding of dynamic stall.

The interferograms obtained in the present experiment show that the dynamic stall vortex produced by airfoil oscillation in the range of conditions studied to date does not produce the symmetric imprint on the density field that would be expected from a classical vortex. Instead, these images imply that the dynamic stall develops as a region of strong gradients enclosing a region of low energy or weak structure, while still supporting the dynamically modified outer flow associated with the increase of lift that is typical of dynamic stall.

Analysis of interferograms obtained at steady and unsteady conditions show that dynamic motion inhibits the occurrence of the strong suction peaks that appear in steady flow at the same angle of attack. Interferometry permits detailed analysis of these pressure distributions; as many as 13 pressure values have been obtained in the first 1% of the chord, near the leading edge of the airfoil.

Acknowledgements

The project was supported by AFOSR-ISSA-89-0067 and AFOSR-MIPR-90-0012 (monitored by Capt. H. Helin and Dr. L. Sakell) with additional support from NAVAIR (Mr. T. Momiyama) and ARO MIPR-ARO-132-90 (Dr. T.L. Doligalski). We wish to thank Dr. Mark Loomis for introducing us to the dark-central-ground technique. The technical support of Mr. Christopher Boswell of Sterling Federal Systems, Mr. Michael J. Fidrich of the Naval Postgraduate School, and the staff of the NASA Fluid Mechanics Laboratory is greatly appreciated.

7. References

[1] Carr, L.W., "Progress in Analysis and Prediction of Dynamic Stall", *J. of Aircraft*, Vol 25, No. 1, January 1988, pp. 6-17.

[2] McCroskey, W.J., McAlister, K.W., Carr, L.W., Pucci, S.L., Lambert, O., and Indergand, R.F., "Dynamic Stall on Advanced Airfoil Sections", *J. of American Helicopter Society*, July 1981, pp. 40-50.

[3] Carr, L.W., Platzer, M.F., Chandrasekhara, M.S., and Ekaterinaris, J, "Experimental and Computational Studies of Dynamic Stall", *Numerical and Physical Aspects of Aerodynamic Flows IV*, Chapter 14, pp. 239-256, Springer-Verlag, 1990.

[4] Fung, K-Y, and Carr, L.W., "Effects of Compressibility on Dynamic Stall", to be published in *J. of Aircraft*.

[5] Visbal, M. ,"Effect of Compressibility on Dynamic Stall of a Pitching Airfoil", AIAA Paper No. 88-0132, Jan. 1988.

[6] Lorber,P.F., and Carta,F.O., "Airfoil Dynamic Stall at Constant Pitch Rate and High Reynolds Number", *J. of Aircraft*, Vol.25, No.6, pp. 548-556, June 1988.

[7] Chandrasekhara, M.S., and Carr, L.W., "Flow Visualisation Studies of the Mach Number Effects on the Dynamic Stall of an Oscillating Airfoil", J. of Aircraft, Vol. 27, No. 6, pp. 516-522, June 1990.

[8] Chandrasekhara, M.S., Carr, L.W., and Ahmed, S., "Comparison of Pitch Rate History on Dynamic Stall", Proc. NASA/AFOSR/ARO *Workshop on Physics of Forced Unsteady Separation*, April 17 - 19, 1990, Moffett Field, CA.

[9] Chandrasekhara, M.S., Carr, L.W., and Ahmed, S., "Schlieren Studies of Compressibility Effects on Dynamic Stall of Airfoils in Transient Pitching Motion", AIAA-90-3038, *Proc. AIAA 8th Applied Aerodynamics Conference*, pp. 346-356, Portland, OR 1990.

[10] Lee, G., Buell, D.A., Licursi, J.P., and Craig, J.E., "Laser Holographic Interferometry for an Unsteady Airfoil Undergoing Dynamic Stall, *AIAA Journal* ,Vol. 22, No.4, April 1984, pp. 504–511.

[11] Jaesohke, M., Hiller, W.J., and Meier, G.E.A., "Acoustic Damping in a Gas Mixture with Suspended Submicroscopic Droplets", *J. of Sound and Vibration*, Vol. 43, No. 3, pp. 467-481, 1975.

[12] Carr, L.W., and Chandrasekhara, M.S., "Design and Development of a Compressible Dynamic Stall Facility", AIAA Paper No. 89-0647, to appear in *J. of Aircraft*.

[13] Smartt, R.N., "Point-Diffraction Interferometry as a Diagnostic for Alignment", *SPIE Vol. 483, "Optical Alignment II"*,1984.

[14] Smartt, R.N., and Steel, W.H., "Theory and Application of Point-Diffraction Interferometers", *J. Appl. Phys.*, Vol 14, Suppl. 14-1, 1975, pp. 351-356.

[15] Bachalo, W.D., and Houser, M.J. , "Evaluation and Application of a New Interferometric Technique for Compressible Flow Research", NASA CR-177467, Oct. 1988.

[16] Anderson, R.C., and Milton, J.E., "A Large Aperture Inexpensive Interferometer for Routine Flow Measurements", *ICIASF'89 RECORD*, IEEE Publication 89CH2762-3, pp. 394-399.

[17] Goldstein, R.J., "Fluid Mechanics Measurements", Chapter 8, Hemisphere Publishing Corporation, 1983.

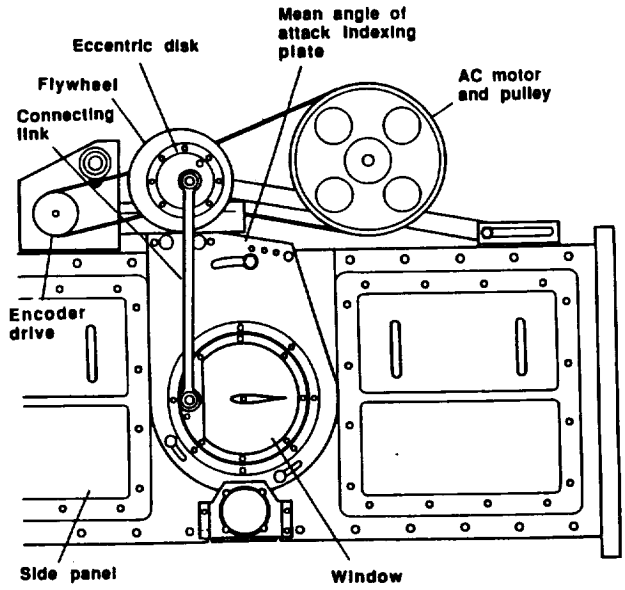

Fig. 1. Schematic of the Compressible Dynamic Stall Facility Test Section.

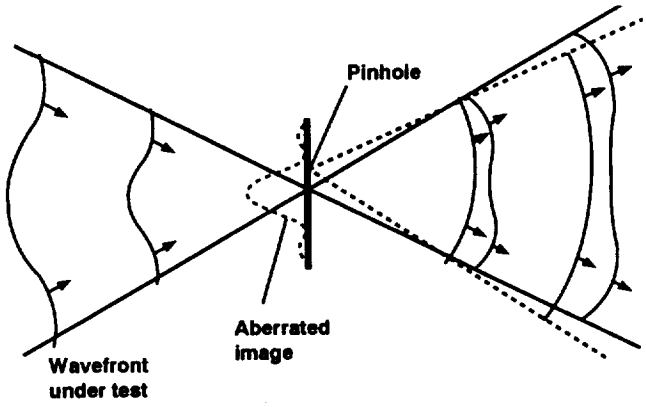

Fig. 2. Schematic of the Principle of Point-Diffraction Interferometry.

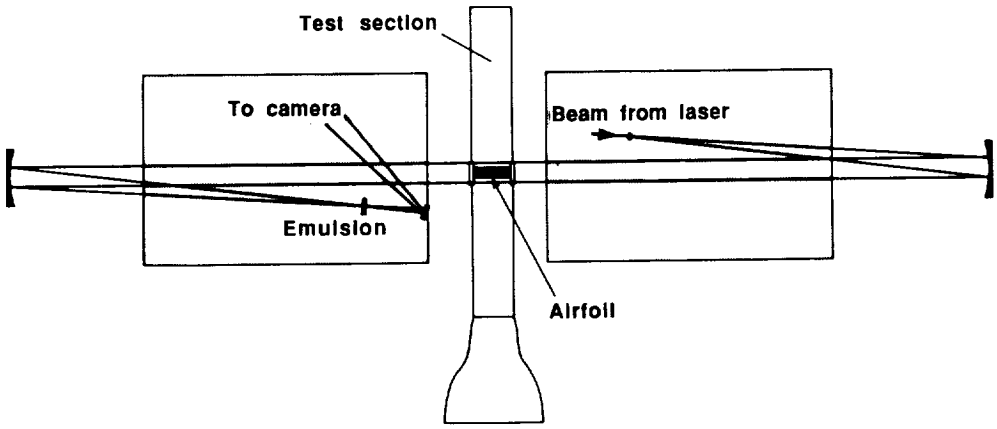

Fig. 3. Schematic of the Layout of Optics for Point-Diffraction Interferometry.

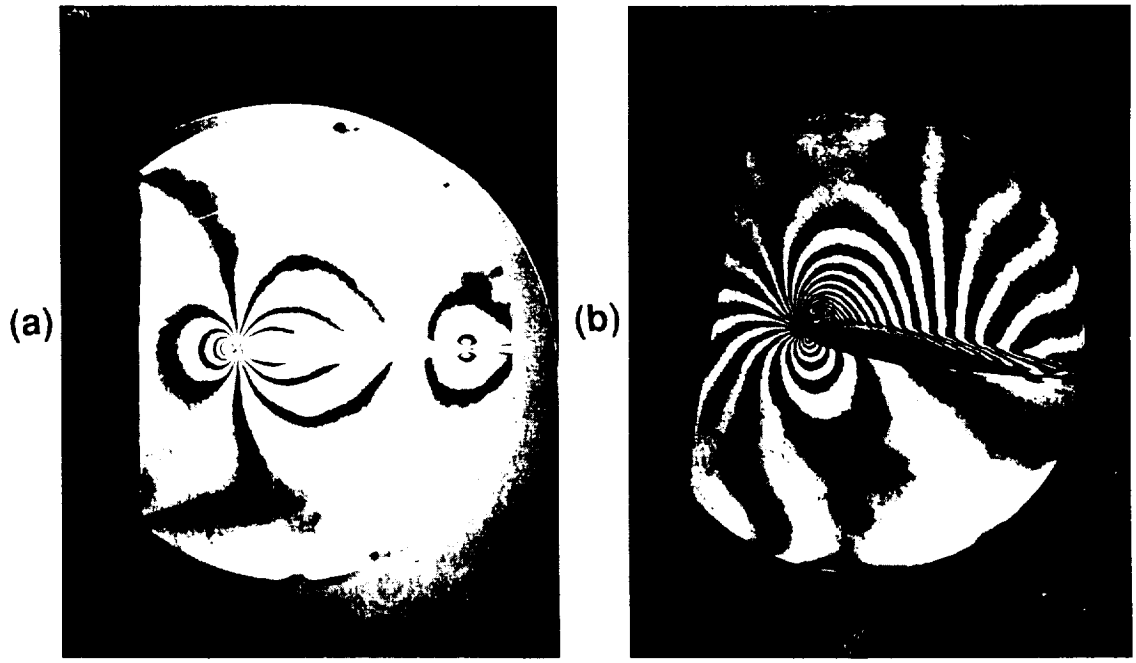

Fig. 4. Representative Interferograms for NACA 0012 airfoil, M=0.40, (a)α = 0°, k=0.0; (b) α = 10.65°, k=0.05.

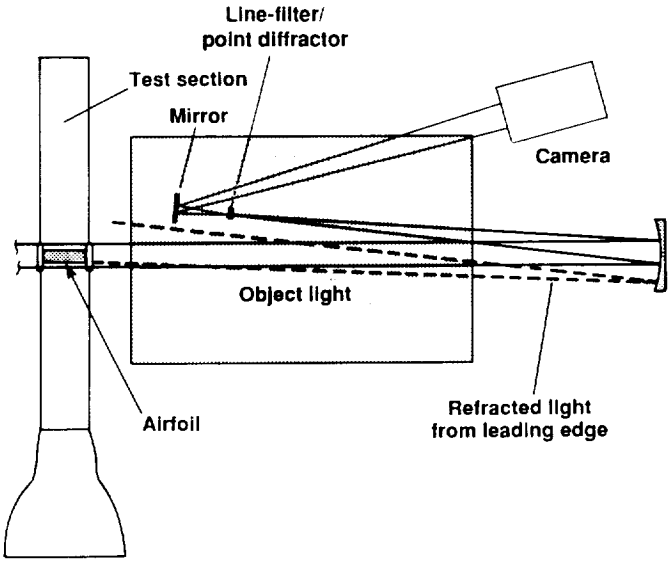

Fig. 5. Effect of Leading Edge Density Gradient on Light Refraction.

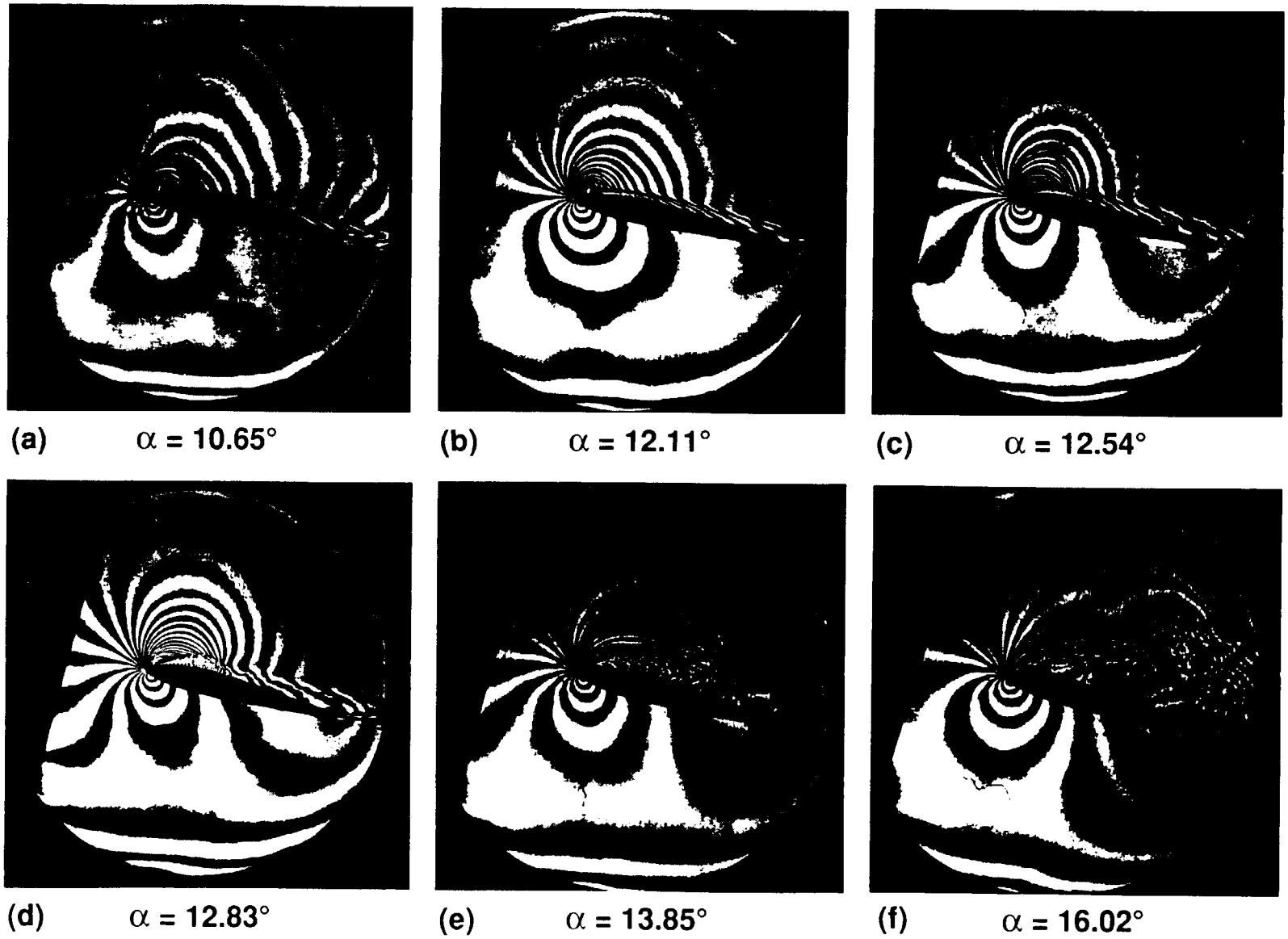

Fig. 6. Sequence of Interferograms Showing Development of Dynamic Stall on an Oscillating Airfoil; M=0.35, k=0.05.

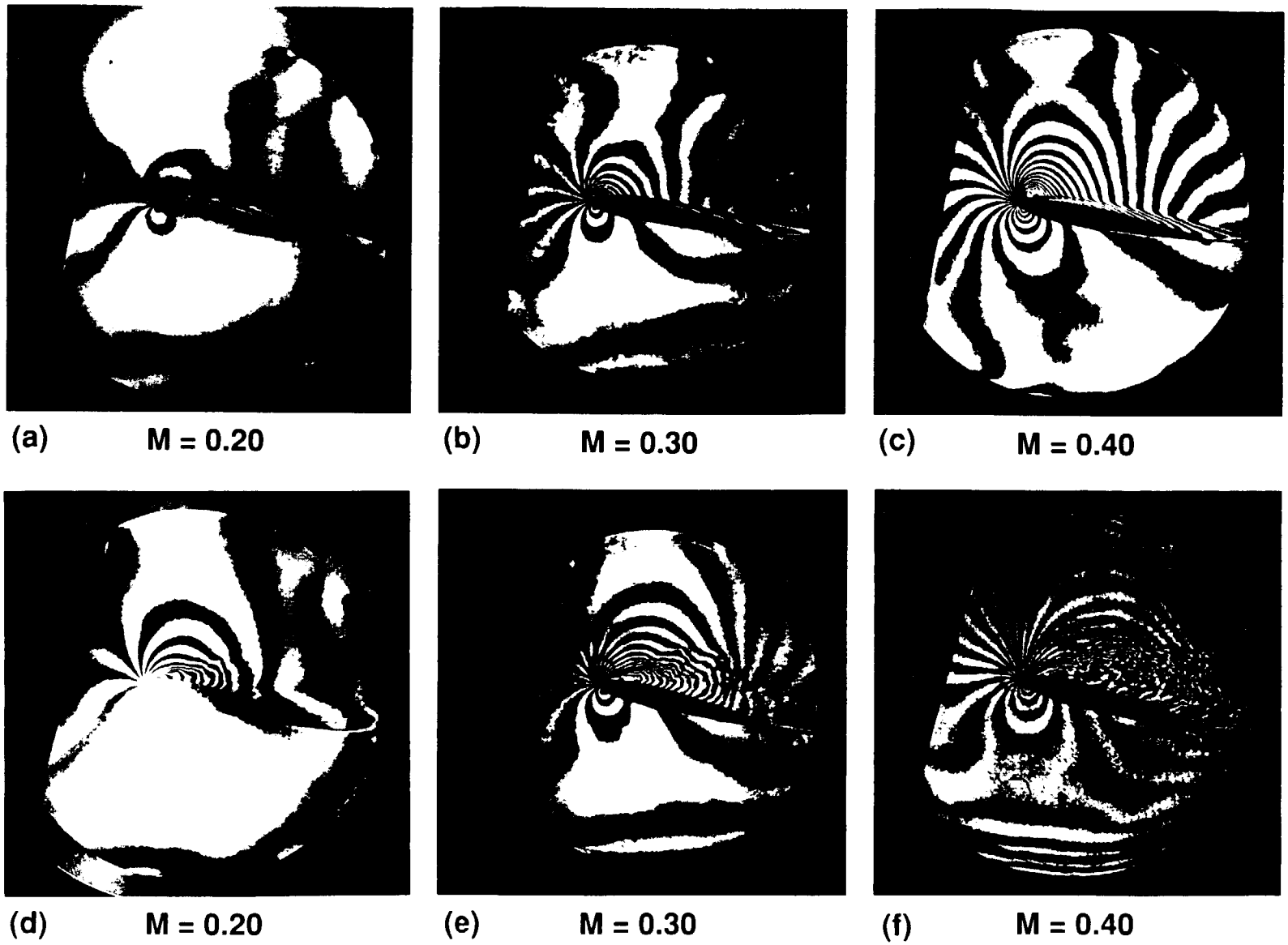

Fig. 7. Interferograms of Oscillating Airfoil Flow at Various Mach Numbers for Conditions Before and During Dynamic Stall: Top Row: $\alpha = 10.65^0$. Bottom Row: $\alpha = 14.28^0$.

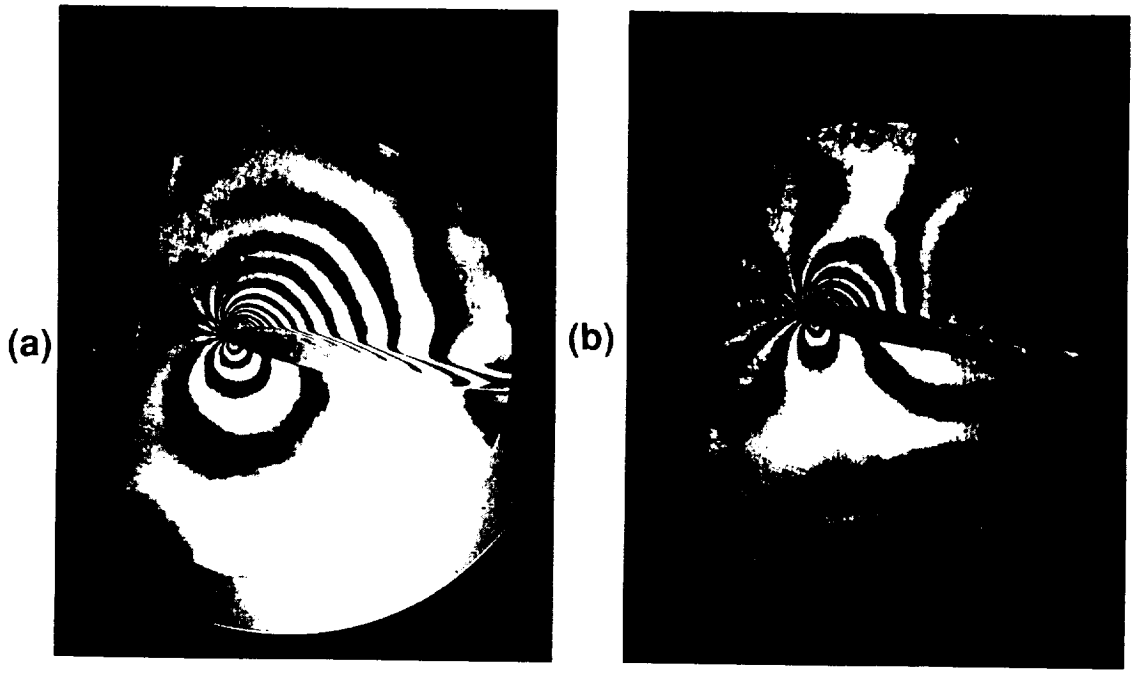

Fig. 8. Effect of Unsteadiness on Flow Field on Airfoil as Shown by Interferometry: M = 0.3, $\alpha = 10.78^0$, (a) k = 0.0, (b) k = 0.05

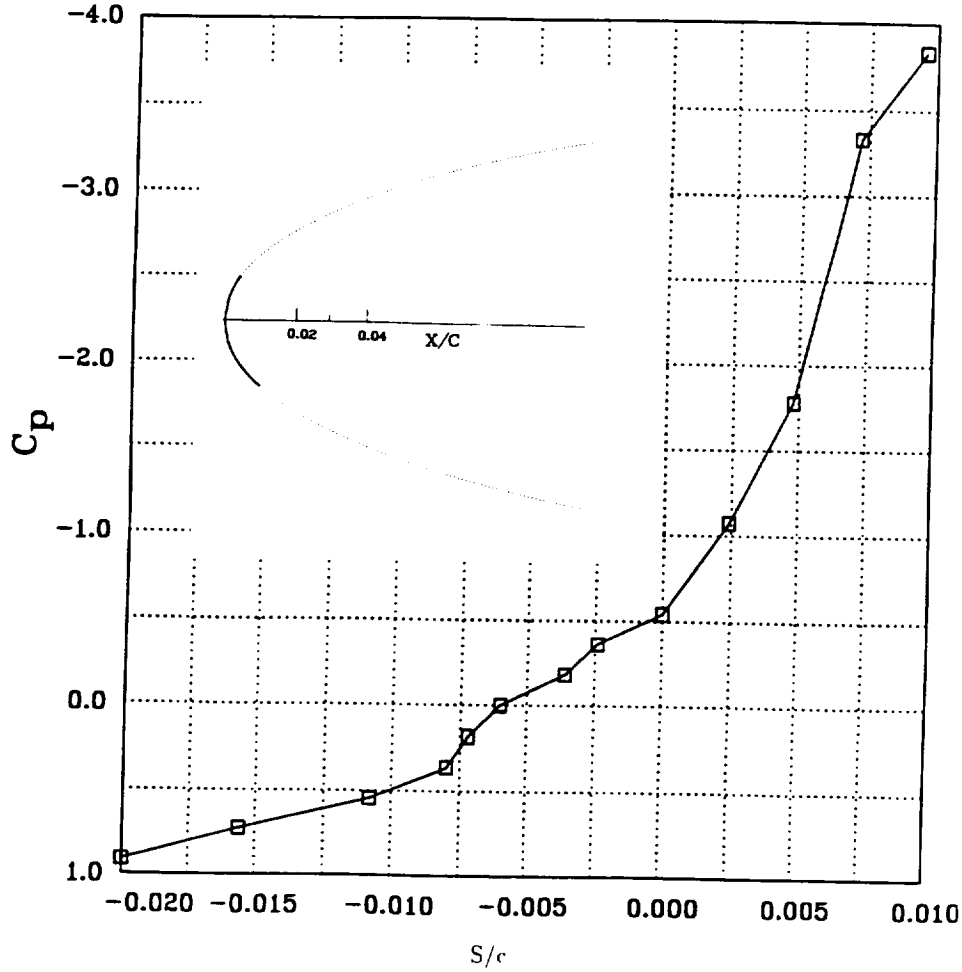

Fig. 9. Pressure Distribution Around the Leading Edge of an Oscillating Airfoil as Determined from Interferogram: M= 0.3, k=0.075, $\alpha = 12.83^o$.

Fig. 10. Comparison of Flow Development Over an Oscillating Airfoil. M=0.3, k=0.075, $\alpha = 14.72°$: (a) Schlieren Picture; (b) Interferogram.